5-2005

Morphological, textual, geochemical, and mineralogical properties of dolostone-derived residuum in Knox County, Tennessee

Bryan Scott Schultz

To the Graduate Council:

I am submitting herewith a thesis written by Bryan Scott Schultz entitled "Morphological, textual, geochemical, and mineralogical properties of dolostone-derived residuum in Knox County, Tennessee." I have examined the final electronic copy of this thesis for form and content and recommend that it be accepted in partial fulfillment of the requirements for the degree of Master of Science, with a major in Geology.

Steven Driese, Larry McKay, Major Professor

We have read this thesis and recommend its acceptance:

Edmund Perfect

Accepted for the Council:
Carolyn R. Hodges

Vice Provost and Dean of the Graduate School

(Original signatures are on file with official student records.)

To the Graduate Council:

We are submitting herewith a thesis written by Bryan Scott Schultz entitled "Morphological, Textural, Geochemical, and Mineralogical Properties of Dolostone-Derived Residuum in Knox County, Tennessee." We have examined the final paper copy of this thesis for form and content and recommend that it be accepted in partial fulfillment of the requirements for the degree of Master of Science, with a major in Geology.

Steven Driese, Major Professor

Larry McKay, Major Professor

I have read this thesis
and recommend its acceptance:

Edmund Perfect

Accepted for the Council:

Vice Chancellor and
Dean of Graduate Studies

Morphological, Textural, Geochemical, and Mineralogical Properties of Dolostone-Derived Residuum in Knox County, Tennessee

A Thesis Presented for the

Master of Science Degree

The University of Tennessee, Knoxville

Bryan Scott Schultz

May 2005

ACKNOWLEDGMENTS

First and foremost, I would like to extend my appreciation to my co-advisors, Drs. Steven Driese and Larry McKay, for their collaboration and establishment of inter-disciplinary research within the geosciences. Their guidance, feedback, encouragement and friendship throughout this project have made for a most memorable and positive experience at the University of Tennessee. I also thank my committee member, Dr. Ed Perfect, for his advice and sharing of facilities. Others deserving of recognition include Nathan Hartgrove at the N.R.C.S. for his help in locating a suitable study site, Dr. Jaehoon Lee from Biosystems Engineering for his assistance and input, Dr. Linda Kah for her continued friendship, input, and use of facilities, Bill Dean for assistance with running samples for XRF analysis, Jeremy Bennett for assistance in drill-core retrieval and field site reconnaissance, and Eric Ober for his willingness to help, whatever the task. Special thanks go to the Strong Farm property owners Martha Kern and John Nicely for their kindness, patience and support of scientific endeavors.

This project was supported by facilities and equipment within the University of Tennessee Department of Earth and Planetary Sciences. Additional financial aid was provided by Drs. Larry McKay and Steven Driese and a grant from the Geological Society of America. Additional funding was provided by the UT Center for Environmental Biotechnology and the UT Waste Management Research and Education Institute.

Family and friends also played a vital part in this project, and on many occasions helped to maintain my sanity during the more stressful times. Thanks to Rob "Hoytoe-Sauce" Vollbeer, Jimbo-Jangles, Mikey Katos, Kenstangers, Matty-G, Laine and the

Rhythm King for your friendship and tolerance to the many nicknames you all may have acquired to this point. Thanks to Dr. Colin Sumrall for his assistance, conversation, and dinnertime get-togethers. Special thanks goes to my sister, Kristen, for whose infinite support, wisdom and friendship I will forever be in debt. Most importantly I would like to thank my mother and father, Gerri and Bruce, for sparking, nurturing, and sharing all things wonderful.

ABSTRACT

This research concerns the weathering of carbonate bedrock and subsequent genesis and properties of carbonate-derived residuum in Knox County, Tennessee. The carbonate-derived residuum evaluated in this study is classified as an Ultisol, and comprises up to 11 m of regolith overlying Mascot Fm. dolostone bedrock within the Valley and Ridge Province of East Tennessee. Morphological, textural, geochemical, and mineralogical analyses were performed on entire soil profiles and subjacent bedrock from core samples retrieved from 7 boreholes. Findings of this research reveal that the regolith is derived primarily from extensive weathering of the parent bedrock, but with evidence of substantial reworking of materials by flowing water, slope movement and pedogenesis, and possible inputs of material from other sources that include the overlying bedrock (Chickamauga Group). The occurrence of at least one paleosol found near the base of borehole 1 further supports this assertion. Based upon data that include mass-balance calculations for strain (volume change), translocations of clay-constituent elements (relative to TiO_2), as well as physical characteristics of underlying Mascot Fm. bedrock that includes percentages of insoluble residues and estimated thickness of the bedrock at the study site, it is apparent that the Mascot Dolomite is a primary parent material for these soils. However, much clay has been introduced and translocated during soil genesis, and can only be accounted for by the addition of materials from outside (and stratigraphically overlying) sources in conjunction with the weathering of extensive thickness of dolostone bedrock. A multi-stage, 2-D conceptual model has been proposed to account for long-term Ultisol maturation within a dynamic geomorphic surface. Boundaries between genetic units within the soil residuum and overlying

colluvium have been homogenized by advanced Ultisol pedogenesis, however, they are still detectable upon close inspection. Furthermore, results suggest that pore structure and macroporosity occlusion is most dependent on illuviation of pedogenic clays and precipitation of mineral precipitates, which commonly extend from 2 m depth down to the bedrock contact.

TABLE OF CONTENTS

LIST OF TABLES

LIST OF FIGURES

1.0 INTRODUCTION

This research concerns the weathering of carbonate bedrock and subsequent development of physical and chemical properties of the carbonate-derived residuum. Traditionally, two major soil groups develop on carbonate-derived residuum: dark Rendzina-like soils, which are typically found in areas with relatively shallow depths to bedrock, and Terra Rossa-like soils which are characterized by red and yellow colors in the B horizons and commonly extend to depths exceeding several meters. The Terra-Rossa-like soils are common in the southern portions of the United States, including large areas in Tennessee, Kentucky, Virginia, and Missouri (Soil Survey Staff, 1994). Many of these soils are classified as Ultisols or Alfisols and are among the deepest and most clay-rich soils in the southeastern U.S. (Miller, 1972; Moneymaker, 1973). The carbonate-derived residuum evaluated in this study is typical of Terra-Rossa-like soils, and comprises up to 11 m of regolith overlying dolostone bedrock within the Valley and Ridge Province of East Tennessee.

The soil type present at the field site is classified at the order level as an Ultisol. In general, pedologists define Ultisols as mineral soils of temperate to tropical regions having a well-developed argillic horizon and low base saturation (FitzPatrick, 1983; Fanning and Fanning, 1989). Additional characteristics of Ultisols include geologically old landscapes and parent materials having developed in moisture regimes where precipitation exceeds potential evaporation during a portion of most years (Buol et al., 1997). The maturity of Ultisols often leads to extensive horizonization (A, B, B/C, and C) of the weathered material.

Studies have shown that soil formation and properties are closely related to their parent materials (Retallack, 2001). For most siliciclastic rocks, a transitional phase of soil development involves the formation of saprolite (Cr horizon). In general, saprolite is defined as rotten, friable, isovolumetrically weathered bedrock, having characteristics of both soil and rock. Saprolite has been found to retain original structure and sedimentary layering, while also containing soil features such as high matrix porosity, translocation or illuviation of clays, precipitation of Fe/Mn oxides, and bioturbation (Becker, 1895; Hatcher et al., 1992; Stolt and Baker, 1994; Smith, 2001; Driese et al., 2001). This differs markedly when compared to carbonate rock weathering, whereby insufficient quantities of insoluble residues are present for weathering processes to form saprolite. Instead, weathered material adjacent to carbonate bedrock is generally of two forms: discontinous thinly banded (< 1.5 cm) zones in the lowermost 1-2 m of residuum that somewhat resemble sedimentary relict bedding, or silty clay zones with no presence of banded material or relict bedding (Miller, 1972).

Genesis of Ultisols has been the subject of much debate. One view on Ultisol genesis suggests that they result from podzolization, which involves extensive acidic leaching, destruction of clay and additions of Fe-oxide and oxyhydroxide precipitates. Lessivage, or the downward translocation of clay-size particles derived from weatherable minerals in A and E horizons, is capable of producing argillic horizons (Bt) necessary for Ultisol development (Buol et al., 1997). Simonson (1949) argued that lessivage processes alone do not provide adequate explanations for horizon differentiation, and described Ultisol genesis in terms of clay mineral formation and destruction. The primary basis for his argument concerns the insufficient thickness of clay-poor A horizon material needed for development of clay-rich Bt horizons that dominate the soil profile. Furthermore, Simonson (1949) concluded that the dominant processes involved in soil development are the formation of silicate clay minerals from insoluble residues near the zone of rock disintegration, and hydrolysis-driven destruction of clay minerals in the upper horizons. A contradictory interpretation involves the alterations of minerals in-situ within the C horizon and throughout the solum, which is responsible for the majority of the total clay mineral content (McCaleb, 1959). Ballagh and Runge (1970) agree that in many cases the thickening of argillic horizons is due to illuviation of clays. However, they suggested that the source of the illuviated clays must be derived from parent materials other than the underlying carbonate bedrock. Their conclusion is based upon differences in clay mineralogy and clay size-fractions in both the limestone rock and overlying residuum.

Studies concerning the properties of carbonate-derived residuum provide information pertaining to soil morphology, texture, chemistry, and clay mineralogy. Unfortunately, the majority of research investigating Ultisol residuum properties is limited to the upper 2 m of the solum, and few studies include the subjacent carbonate bedrock. For example, Alexander et al. (1939) evaluated 10 soils developed from limestones in various southeastern states (as well as Pennsylvania and Maryland). Their research revealed an increase in clay and Fe_2O_3 with increasing depths (down to 2 m depth). In most profiles, the B horizon exhibit alumina ratios ranging from 1.88 to 2.43. Alexander et al. (1939) estimated the depth to bedrock in most places to be approximately 8 m. Morgan and Obenshain (1942) collected chemical data for 3 soils (Hagerstown, Clarksville, and Pisgah) developed from limestone and dolostone in

Virginia. Mass-balance measurements calculated for the parent rock and residuum samples indicate net losses of TiO_2, Fe_2O_3 and Al_2O_3 in the majority of the soil horizons. They also noted that the Hagerstown residuum contained up to 75% clay between 1-1.5 m depth.

Pearson and Ensminger (1949) documented the types of clay minerals present in the uppermost 1.2 m of limestone residuum classified as Decatur series in northeastern Alabama. Their results indicated that kaolinite was the dominant clay mineral, with lesser quantities of illite present in the clay fraction. In addition, they found that the percentages of kaolinite increased with depth, which was inversely correlated to the amount of quartz present at the same depths. Additional research concerning residuum properties of the uppermost 2 m of apparently carbonate-parented soils support the aforementioned findings, which indicate an increase in both overall clay and kaolinitic clay content, and in Fe-oxides concentrations with increasing depths (Simonson, 1949; Jeffries et al., 1953; Brydon and Marshall, 1958; Nash, 1963; Mubiru, 1994). Although rare, Ultisol studies that included carbonate bedrock samples revealed that the majority of the insoluble residues consist of significant amounts of illite and lesser quantities of HIV and kaolinite (Miller, 1971; Plaster and Sherwood, 1971).

Based upon previous literature, general characteristics of carbonate-derived soil residuum include low pH and base saturation, intense leaching, varying concentrations and types of clay minerals present throughout the solum and bedrock, and potential for significant soil thickness. Despite the widespread occurrence of these soils throughout the southeastern United States literature on the thickness and residuum properties at significant depths is scarce, as well as on relationships between the residuum and underlying carbonate rock. This deficiency is due, in part, to geologists typically ignoring residuum in their studies, and the majority of soils research being limited to < 2 m depth and rarely including the subjacent bedrock. Some of the major questions concerning carbonate soil development include the following: Does sufficient insoluble residue exist within the parent material (carbonate bedrock) to account for the thickness of overlying clay-rich residuum (if formed in-situ)? If not, are these soils polygenetic accumulations of residua derived from various parent materials? Do soil structure, texture, morphology, etc. reveal similar trends/properties at significant depths? Are there any features suggesting colluvial and/or alluvial additions to the soil profiles? If so, has the substantial maturation of these soils resulted in alteration and later homogenization of these materials, thereby complicating the ability to accurately identify their origin? Does slope position and proximity to prominent sinkholes affect the overall thickness and distribution of pedogenic clay?

The intent of this study is to gain information pertaining to these questions by evaluating and comparing the morphological, textural, geochemical, and mineralogical properties of dolostone-derived residuum and parent material. Two hypotheses for the origin of these Terra Rossa-like Ultisols, which are to be tested in this study are (Fig. 1):

1) The soils formed *in-situ* as simple residuum from carbonate bedrock, weathering from the top down.

2) The soils are polygenetic in origin, and formed from both carbonate-derived residuum as well as from overlying non-carbonate stratigraphic units and repeated inputs of colluvial- and/or alluvially-derived materials that weathered on a dynamic geomorphic surface.

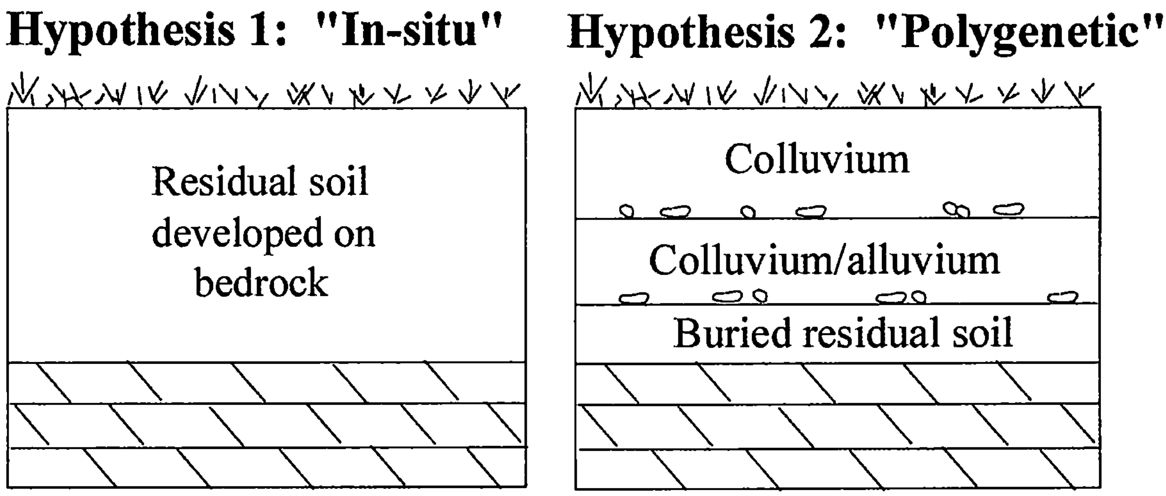

Figure 1: Conceptual model showing two possible modes of soil development. Hypothesis 1) In-situ clay formation and accumulation on dolostone parent material, and 2) Polygenetic assemblage representing multiple soils and inputs.

Corollary hypotheses for this study suggest that infilling of pedogenic clay and mineral precipitates in the subsurface along macropore walls, ped faces and fractures are extensive, and serve as a major control on macropore structure and size in areas with soils underlain by carbonate bedrock. Furthermore, the percentage of clay is expected to gradually increase with depth due to the illuviation of clay within the subsurface.

The principal objectives of this study are to document the overall weathering transition of dolostone bedrock to residuum from the measurement of physical and chemical properties of an entire profile of residuum and soil developed on dolostone bedrock, and to compare these properties to the conceptual models for genesis of carbonate-derived residuum and soils (Mascot Dolomite; Lower Ordovician). Evidence of a polygenetic origin for this residuum should include identifiable paleosols and colluvial/alluvial deposits, as well as micromorphological indicators of reworking of materials, such as clay papules, multiple zones of formation and deposition of pedogenic clay. Additional evidence for polygenetic assemblage may include geochemical discontinuities within the residuum profile indicative of exposure and/or deposition of materials not locally derived.

2.0 LOCATION AND PEDOLOGICAL / GEOLOGICAL SETTING

This study analyzed the residuum derived from the Mascot and Kingsport Dolomite (Lower Ordovician) at the Strong Farm site, in northeastern Knox County, Tennessee (Fig. 2). The site is approximately 9 km northeast of the junction of I-40 and Rutledge Pike (US-11W), and occurs on well-drained and clay-rich Ultisols within the humid and sub-tropical climate of the southeastern U.S., where optimal weathering and thickness of soil profile development occurs. The land cover is mostly pasture with a mixture of grasses and shrubs, but would have been dominated by hardwoods prior to European settlement. Wooded areas consisting of pines and hardwoods also occur in relatively close proximity to the study sites. Much of the site is dominated by karst topography and local drainages that empty into the nearby Holston River (Fig. 3). The soils (i.e., borehole locations) were sampled at the previously mentioned geomorphic positions (ridge top, toe of slope, etc.). The landscape consists of deforested, moderately (5 to 12%) dipping slopes near the coordinates N 36°03'02" latitude and W 83°47'13" longitude (Fig. 2). Soils at this site are mapped as Dewey Series, and are characteristically well drained and very deep (> 1.5 m; Soil Survey Staff, 1994). The taxonomic class of the soils is a fine, kaolinitic, thermic, Typic Paleudult. Soil surveys conducted on Dewey Series soils generally exhibit gradational boundaries between soil horizons. Below approximately 50 cm depth, soil horizons characteristically exhibit very high clay content. Other documented features for Dewey Series soils includes distinct clay films (illuviated clays) as pore linings and on ped faces at variable depths.

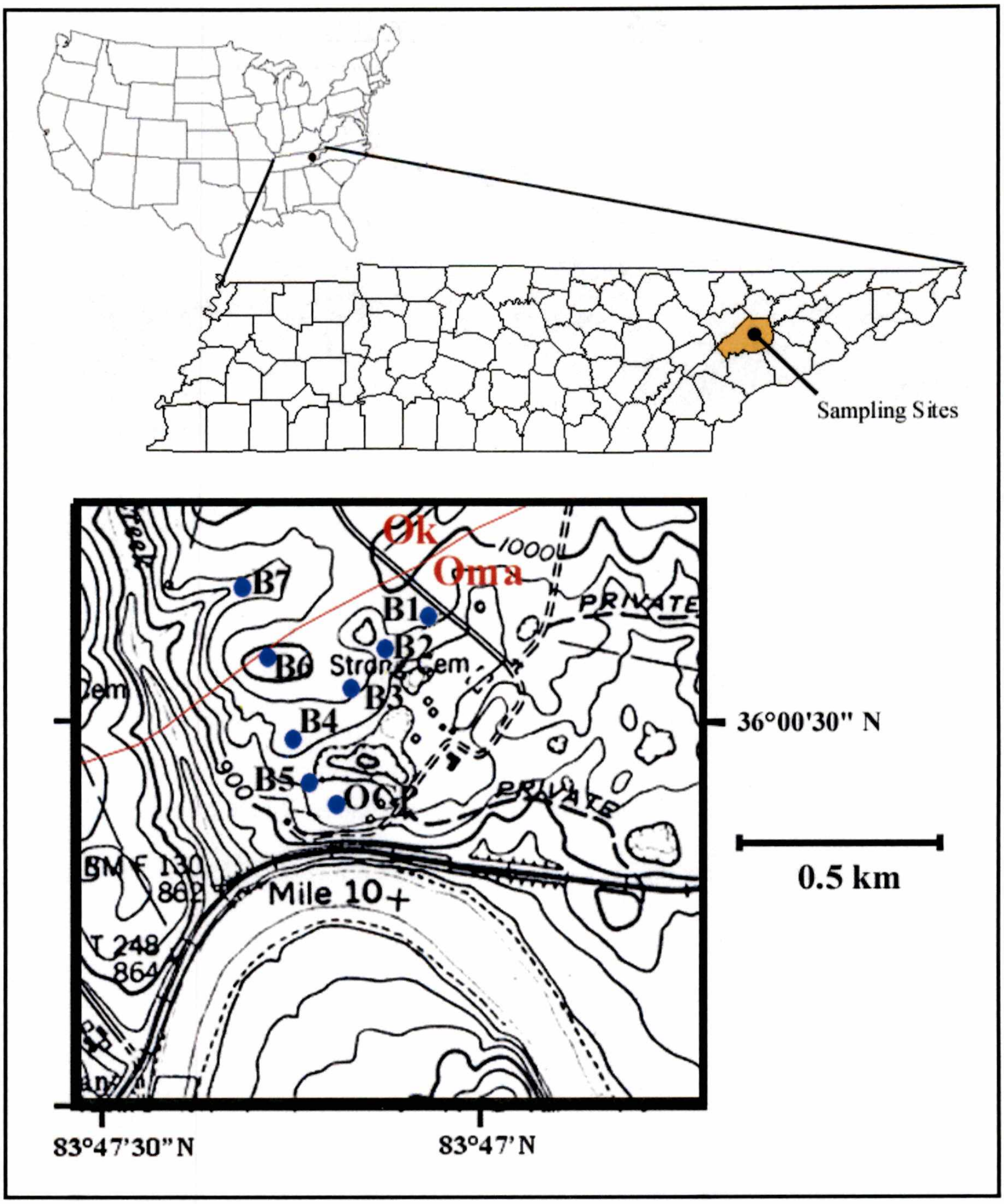

Figure 2: Topographic map of field site showing geological overlay in red (Ok = Kingsport Formation; Oma = Mascot Formation), and borehole locations in blue. Cross-dip slope transect: B1 through B4; Dip slope transect: B7 through OCP, outcrop.

Figure 3: A) Photograph taken from site near ridge-top location (B3) looking northeast. Note prominent sinkhole in background. B) Photograph taken from B3 looking west-northwest .

Originally described by Oder and Miller (1945), the presumed parent lithologies for soils at the study site are the Mascot and Kingsport Formations (Uppermost Knox Group), which consist of a light gray to grayish-brown, massively bedded fine-grained dolostone, with thin interbeds of chert and minor interbeds of shale, siltstone and sandstone (Walker, 1985). The thickness of this stratigraphic unit ranges from 75-203 m. The fine-grained lithofacies within the Mascot Fm. are interpreted to represent penecontemporaneous dolomitization in upper intertidal to supratidal environments (Walker, 1985). The Knox unconformity, which rests atop the Mascot Fm., marks a major break between the Knox Group and later Middle Ordovician carbonate/clastic sequences of the Chickamauga Group. Subaerial exposure, solution-collapse structures and development of a paleohydrologic system during the depositional hiatus (and prior to deposition of overlying Middle Ordovician carbonates) are well-documented distinguishing characteristics of the Mascot and Kingsport Formations (Harris, 1971).

3.0 METHODS

3.1 Soil Coring and Macromorphology

After the field site was chosen, a test borehole (B6) was hand-augered to a maximum depth of ~ 3 meters using a soil sampling field kit. Pedologic observations were made in the field, and soil cores were taken at various depths. Additionally, further sampling involved 6 boreholes along the previously mentioned transects at various slope positions (Fig. 2). The coring was conducted by GEOTEK Drilling Company, Inc., using a hydraulically driven, direct push technology (DPT) rig that provided continuous 2 inch diameter samples in 4 ft. acetate liners. The boreholes were advanced to refusal depths, which was assumed to be the top of bedrock. The macromorphology of the core material was logged using current Soil Survey Staff (1996) description/classification guidelines and Munsell charts during the summer of 2003 (Appendix A). Characterization included sub-sampling for determination of gravimetric water content (Appendix B), thin-section preparation, particle-size analysis using an X-ray disk centrifuge (XDC) method, elemental chemistry using an X-ray fluorescence (XRF) method, and clay mineralogy from X-ray diffraction (XRD).

3.2 Thin-Sections and Micromorphology

For laboratory analyses, 19 oriented samples were selected from the boreholes for professionally prepared thin-sections and micromorphologic observation. Soil cores were impregnated with boat resin and then dry-sawed in the laboratory in order to better preserve the internal structure and fabric, and provide detailed observations of the sampled residuum. The samples were selected to offer broad soil horizon coverage of boreholes 1 and 4, and also to target any significant horizon or potential alluvial or colluvial interbeds (Appendix C). Petrographic observations include a detailed description of macropore structure, texture, composition, cementation and alteration of grains. In addition, the distributions of pedogenic clays and mineral precipitates were petrographically "mapped" within the soil horizons based on color, relative age, and orientation (and concentration) within both macropores and matrix material. Estimations and percentages of petrographic features were performed using image-comparison charts.

3.3 Physical Characteristics

Soil physical measurements, including particle size analysis, bulk and particle density were performed on 23 to 25 sub-samples from boreholes 1 and 4 (Appendix D). Bulk density was determined by the paraffin clod method (Blake and Hartge, 1986; Appendix E). Gravimetric water content measurements (Scott, 2000) were conducted on sub-samples collected at 10 cm intervals for the uppermost core material, and then at 20 cm intervals for the lower subsoil material. Particle size analysis was carried out on 15 gram sub-samples using a Brookhaven Instruments X-ray disk centrifuge (XDC) system (Appendix D). This method allowed for the measurement of detailed particle size (mass/volume) distribution for samples containing very fine particles (as fine as 0.01 µm). It is based on the attenuation of X-ray beams passing through a 15 mL suspension of DI water and soil material that is being accelerated in a centrifuge.

3.4 Geochemistry and Mineralogy

Bulk geochemical analysis was performed on 25 sub-samples (including Mascot Dolomite bedrock) using an X-ray fluorescence (XRF) analyzer. Analyses were carried out on 5 gram samples that were powdered and dried at 60° C and then pressed into pellets. The pellets were analyzed for selected major, minor and trace elements using a

Philips MagixPRO wavelength-dispersive X-ray Fluorescence (XRF) Analyzer (Singer and Janitzky, 1986). The XRF analytical protocol utilized an appropriate clay soil standard, with major element abundances reported in oxide weight percent and trace element concentrations in ppm (Appendix E).

Whole-rock XRF chemical data were evaluated using a mass-balance approach to help characterize chemical variations in the soils due, in part, to closed-system effects of volumetric changes (strain, σ), residual enrichment of soil matrix, and open-system transport of material into or out of various horizons (translocation, τ) (Brimhall, 1991a,b; Driese et al., 2000). This protocol requires element concentration and bulk density of both parent and weathered material for characterization of these values. Furthermore, careful designation of an immobile element is important for translocation calculations, with titanium or zirconium most commonly used.

Clay mineral analysis of the <2, <0.5, and <0.1 μm size fractions was performed on 5 soil samples selected from boreholes 1 and 4. The samples were evenly spaced to provide maximum coverage with depth (Appendix F). Two additional samples included bulk bedrock and isolated chert material from HCl-acid reacted bedrock. Clay mineral analysis was performed using an automated Phillips XRG 3100 X-ray generator by Willamette Geological Service on elutriated mounts using Mg- and K-saturation, glycolation, controlled humidity and routine heat treatments (Moore and Reynolds, 1989).

4.0 MORPHOLOGY

4.1 Macromorphology

Two prominent sinkholes are present within 50-200 m of the boreholes (Figs. 2 and 3). Soil and residuum thickness measured in the boreholes range from 3.68 to 10.58 m (Table 1 and Fig. 4). Few outcrops of bedrock occur in the area, primarily due to the thick cover of clayey residuum. However, exposures along the back-slope (facing the Tennessee River) and along a gravel roadcut reveal near horizontal bedding in dolostone with appreciable chert nodules and chert-rich intervals. Strike-and-dip measurements taken from these available outcrops average about N55E /10° SE.

Residuum from the boreholes is mainly composed of strongly oxidized, dense clay that becomes heavily mottled, darker, and more concentrated with angular to subangular dolostone, chert, and siliciclastic lithorelicts with increasing depth (Appendix A). Thickness of the residuum and soils varies with proximity to sinkholes, with lesser thickness preserved in boreholes 2 and 5. During the coring process, recovery was often very high, with 28 out of the 40 core samples having >90% recovery and 12 of these samples having >100% recovery (Appendix H). Samples with >100% recovery (up to 230%) indicate the likely presence of very fine-grained, highly plastic, swelling clays.

There does not appear to be any relationship between the degree of weathering in chert and rock fragments with increasing depth. However, many chert fragments toward the base of the cores appear extremely weathered with white-gray clay rinds (< 5mm thick). It is likely that the high clay content, the occurrence of Fe/Mn-oxide lining macropores and ped faces, and increasing pore water content with depth primarily determine the various weathering states of the chert (Appendix E).

Table 1: Latitude/longitude, surface elevations and depth to refusal/bedrock for each borehole. All boreholes were collected using a truck-mounted rig with the exception of borehole 6, which was retrieved by hand-augering and did not encounter bedrock.

Borehole	Geomorphic Position	Latitude	Longitude	Surface Elevation (m)	Depth to Refusal (cm)
B1	toe-slope	N36 03 06.9	W83 47 04 7	299	1058
B2	dip slope escarpment	N36 03 04 6	W83 47 09.4	293	460
B3	upper dip slope	N36 03 02.2	W83 47 11 7	296	730
B4	cross-dip shoulder	N36 02 57.5	W83 47 16 5	291	880
B5	lower cross-dip slope	N36 02 55.8	W83 47 14.5	284	368
B6	ridge top	N36 03 03.5	W83 47 18 7	306	>295
B7	cross-dip foot slope	N36 03 09.2	W83 47 20.1	290	655

Note that surface elevations were estimated from topographic map.

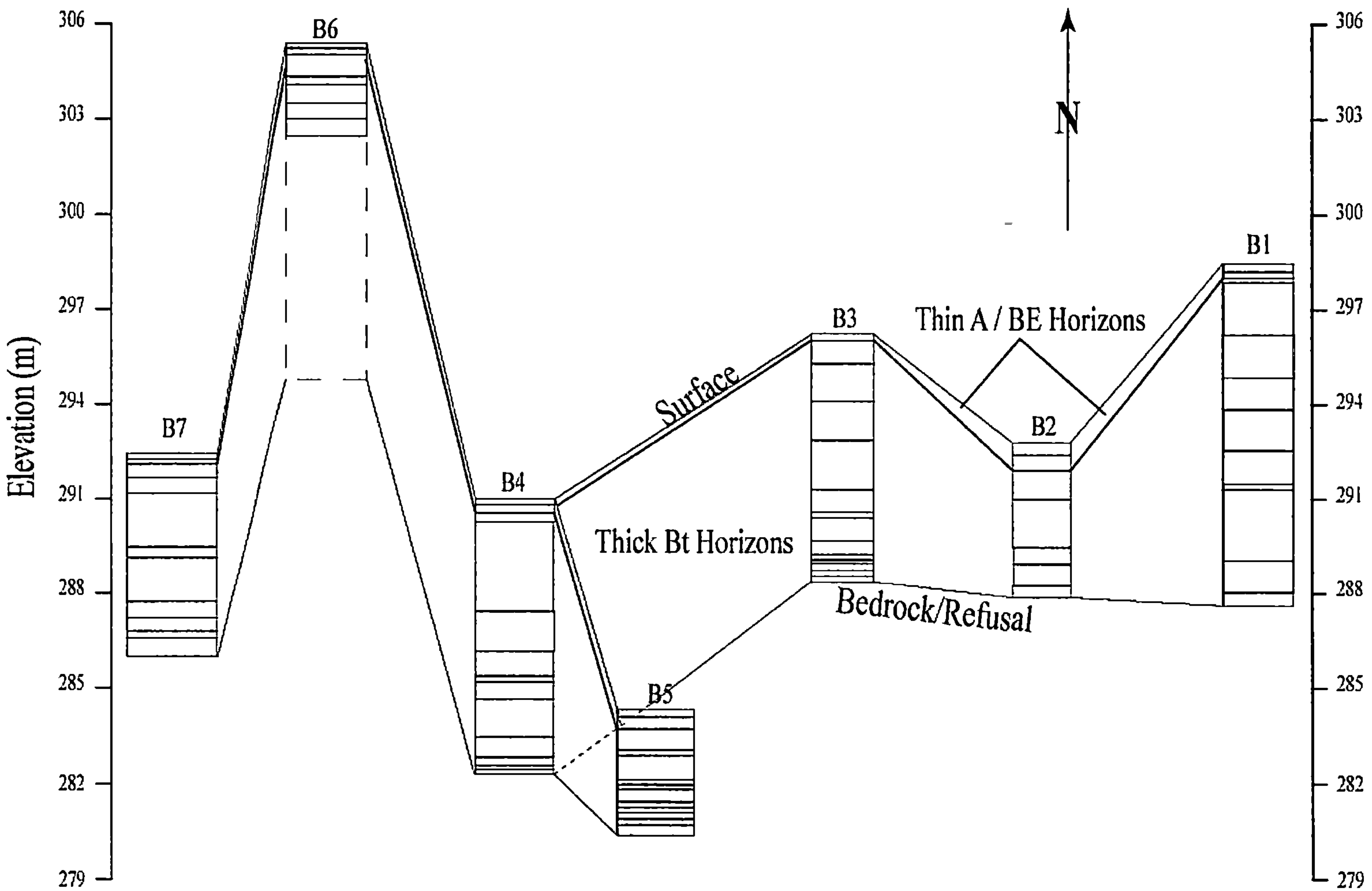

Figure 4: Fence diagram of dip slope and cross-dip slope transects showing borehole surface and bedrock elevations.

The AE / BE horizons in all boreholes were relatively thin (< 26 cm combined) and contained substantial chert fragments (Fig. 5A). Much of the chert within the A and BE zones is of the cauliflower variety, or small hollowed nodules. Many of these nodules are lined or entirely filled with Mn-oxide. Ped sizes and structures observed with the A and BE horizons consist of fine to medium, granular to subangular blocky. For most boreholes, dense, clay-rich Bt1 horizons are present at about 50 cm depth. At or near this depth, soil coloration abruptly grades from brown loam into a dark red, homogenous clay (Fig. 5B). Peds within the many Bt horizons present in this residuum exhibit mostly medium subangular blocky structure. The remaining core material below 50 cm depth is generally devoid of any sand-sized soil particles, with the exception of occasional fine- to medium-grained, sub- to well-rounded quartz sands (sometimes with the presence of dolostone silts that effervesce with HCl) comprising thin, discrete interbeds that occur only in boreholes 1, 3 and 4 (Fig. 5C). Some of the sandy interbeds are slightly cemented, however, most are friable to unconsolidated. It is not clear, based on macromorphological evidence whether the sandy interbeds are developed from in situ weathering of clastic layers in the parent bedrock, or whether they are from externally-derived alluvial materials deposited in the karst or on the residuum surface. Small (<1 mm), subangular to well-rounded red clay papules, or pedorelicts, are also present throughout and adjacent to the sandy layers, and are proposed by soil scientists as indicators of alluvial deposits (Fitzpatrick, 1993).

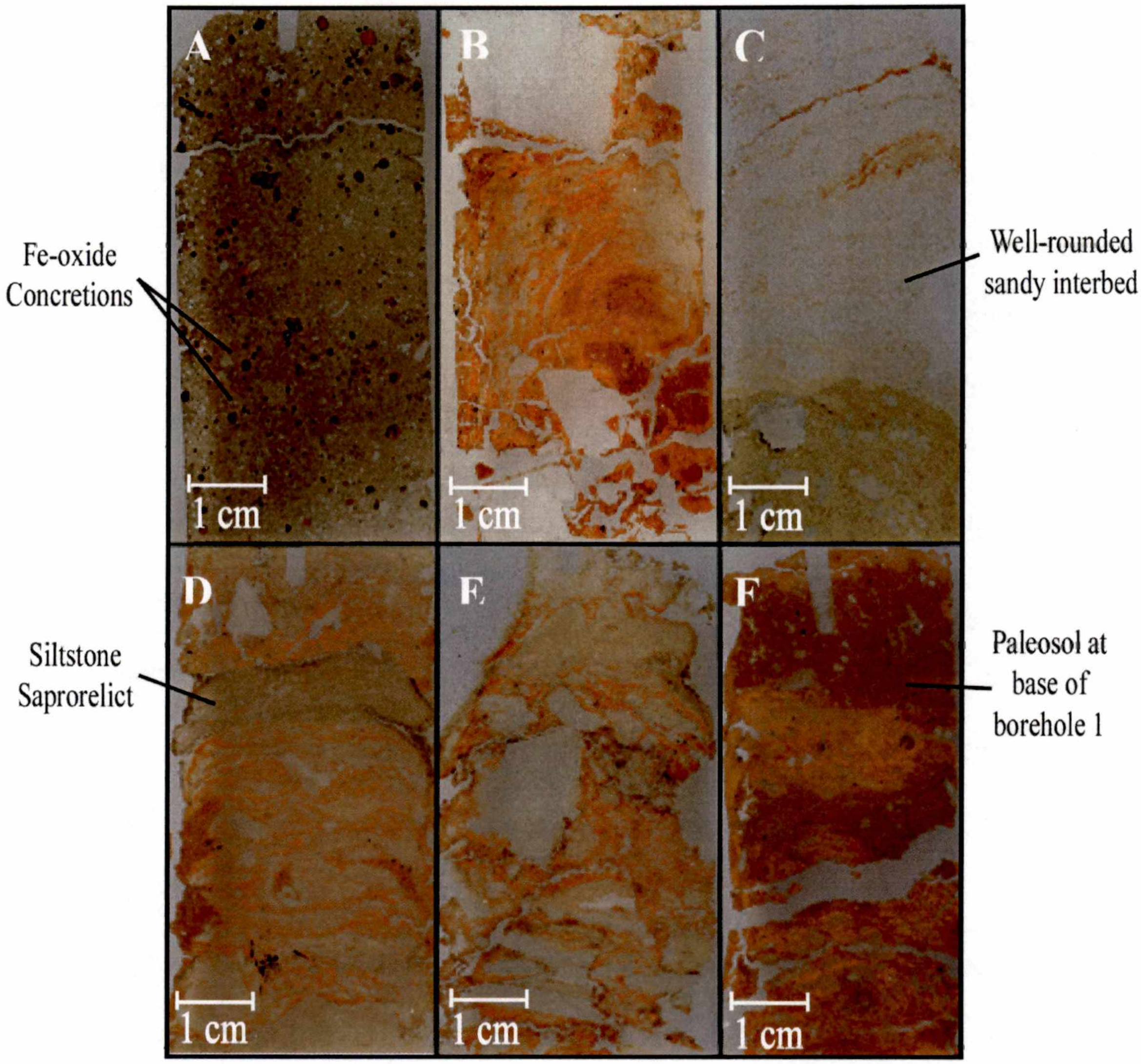

Figure 5: Large format thin-section photographs. A) surface loamy soil, B) mosaic of pedogenic clays, C) well-rounded sandy interbed, D) saprolite/saprorelict interbed, E) very deeply weathered dolostone rock fragments with pedogenic clay and Fe/Mn-oxide rinds, F) relict (deepest) soil at base of borehole 1.

The gradational nature of most soil horizon boundaries makes it difficult to distinguish soil-residuum from colluvium at a macromorphological scale (Fig. 6). Sharp contacts are present between dolostone bedrock and the soil-residuum, with the notable absence of a saprolitic (Cr horizon) transition. The only material that is saprolitic in nature within the residuum consists of lithorelicts/saprorelicts derived from siliciclastic interbeds within the Mascot Formation (Fig. 5D).

4.2 Micromorphology

4.2.1 Soil Matrix- Microscopic examination of the epoxy-impregnated thin-sections indicates that the majority of the material from the 7 boreholes are dominated by sepic-plasmic matrix (clay re-alignment due to shrink/swell and pedogenic alteration of clays), with the exception of A horizons and rare, thin siliciclastic interbeds. Sepic-plasmic fabrics observed in the samples can be subdivided into specific categories based on clay content and orientation within the matrix. Five morphologies of sepic-plasmic fabric are identified in the dolostone-derived residuum: skelsepic (highly birefringent plasma around skeletal grains), mosepic (one direction of preferred clay orientation), bimasepic (two directions), trimasepic (three directions), and omnisepic (multi-directions). Samples within A-horizons and siliciclastic zones (with mostly sand and silt fractions) reveal a silasepic fabric (silt/sand size grains lacking highly birefringent streaks). Most BE horizons contain matrix with skelsepic fabric that grades into a weakly bimasepic fabric. Bt horizons generally reveal bimasepic microfabric with more strongly-bimasepic, trimasepic, and omnisepic patterns demonstrated by Bt horizons

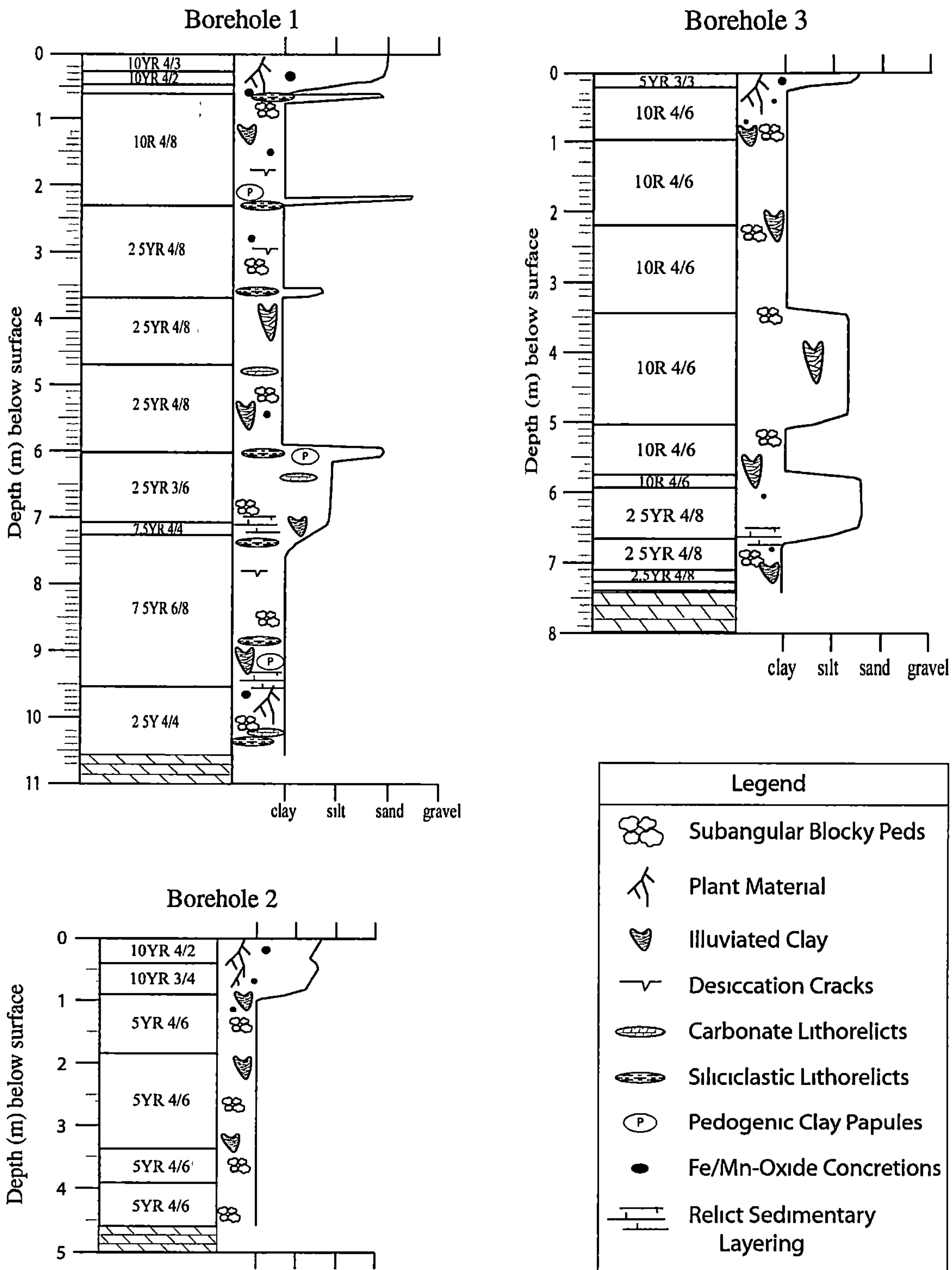

Figure 6: Stratigraphic columns showing size-fraction distributions and morphological features in boreholes 1-7.

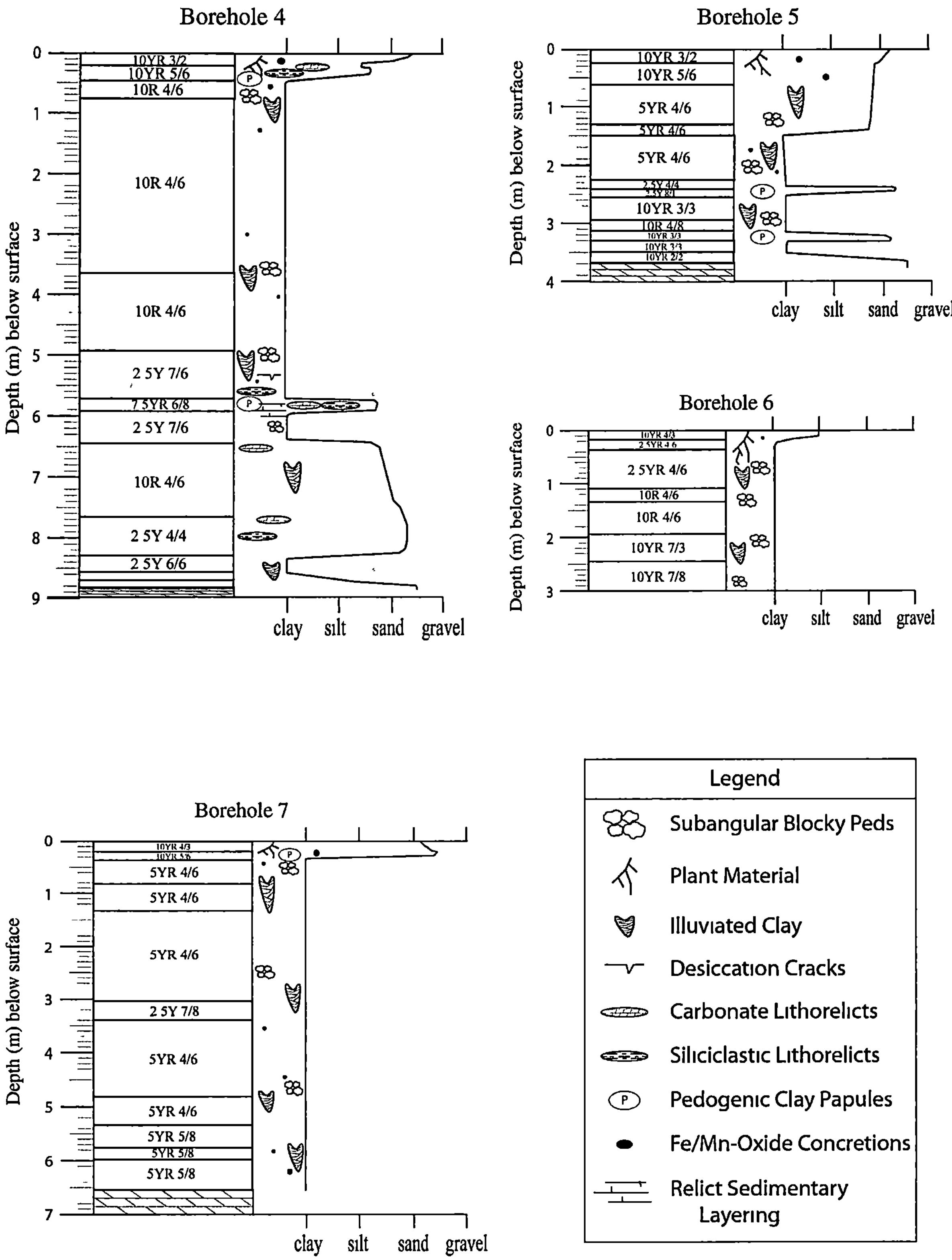

Figure 6 continued.

with increasing clay content (Fig. 7A). Mosepic fabrics are observed only within deeply weathered shale litho/saprorelicts, which are best exhibited in borehole 4 at approximately 815 cm depth. Generally, sampling regions with higher concentrations of Fe/Mn-oxide observed in the clayey matrix corresponds to plasma with weaker birefringent patterns. It is important to note, however, that the various sepic-plasmic fabrics observed in these samples are generally not characteristic of Ultisols (too kaolinitic and leached) and may have been at least partly induced by stress changes from the coring process.

4.2.2 Borehole 1 -- The matrix of borehole 1 residuum is dominated by bimasepic fabrics, with skelsepic fabrics occurring within the BE horizon and siliciclastic interbeds. The samples range from 15-25% macroporosity, as determined by visual estimation. Actual in-situ values are likely much lower because of shrinkage and cracking during sample drying and thin-section preparation. Most macropores are characterized as having dendritic to planar pore structures, which become more discontinuous with increasing depth, and occurs mainly as desiccation cracks and weathering rinds encircling/coating some dolostone fragments. Two conspicuous organic-rich zones occur at 233-239 cm and 367-373 cm depths (Fig. 7E). Both sand and silt fractions show a marked increase within these zones and are characterized by fine- to medium-grained, subrounded to well-rounded quartz sand grains. The sand and silt grains appear to have been derived from adjacent deeply weathered, fine- to medium-grained sandstone, calcareous siltstone, and

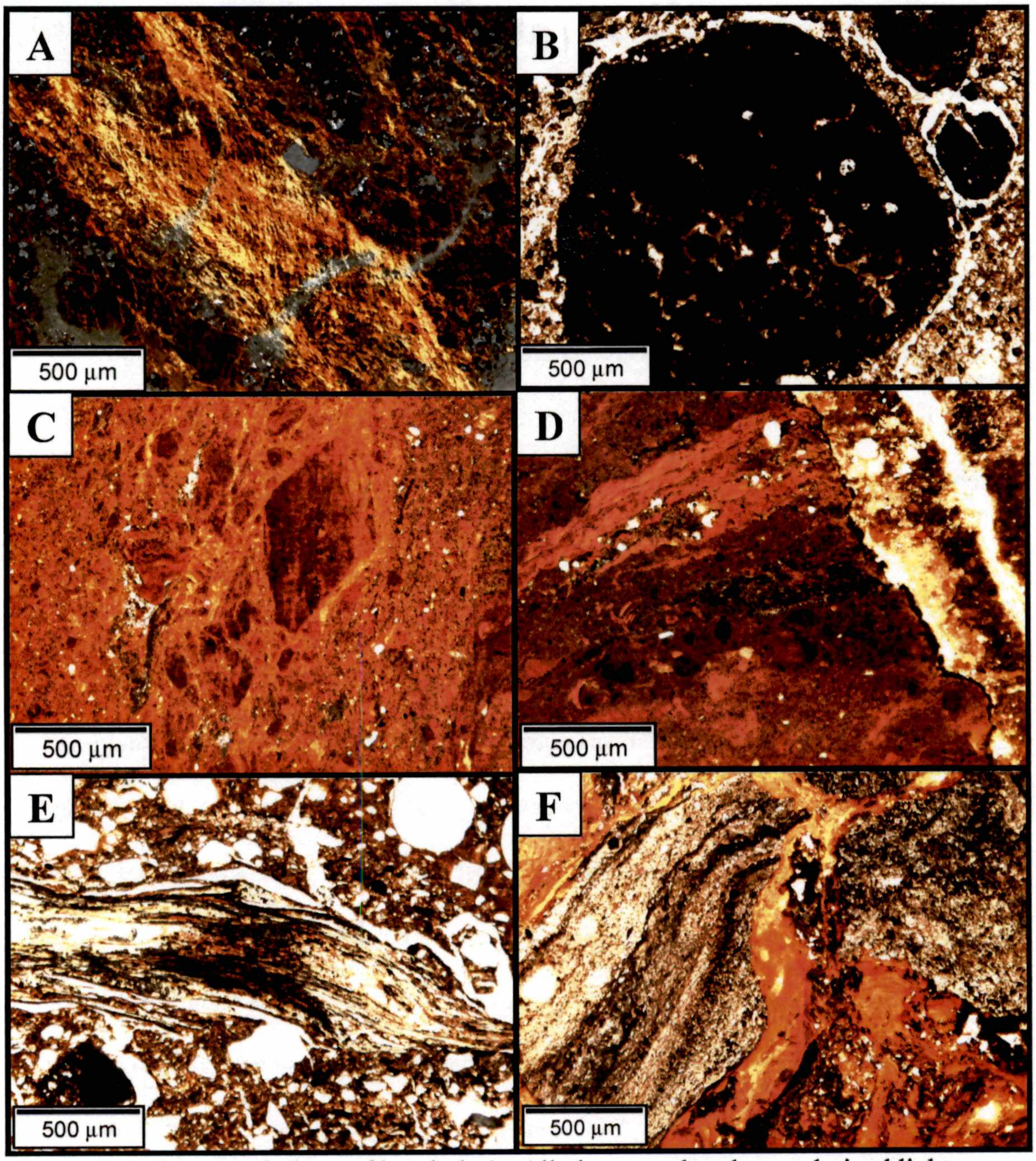

Figure 7: Micromorphology of borehole 1. All photos under plane polarized light, except for A which is under cross-polarized light. A) Typical strongly bimasepic plasmic fabric, 675 cm depth. B) Large multi-generation banded Fe-oxide concretions and nodules, 45 cm depth. C) Subrounded, oxidized pedogenic clay papules in thick clayey matrix at 367 cm depth. D) Thick, oxidized pedogenic clay matrix with redox-depleted macropores at 238 cm depth. E) Organic material (root) with surrounding loamy soil matrix occurring within Bt1 interbed at 234 cm depth. F) Deeply weathered siltstone litho/saprorelicts with pores completely occluded with multi-generation pedogenic clays and Mn-oxide seams, 600 cm depth.

shale litho/saprorelicts that also occur in the organic-rich zones (similar to Fig. 8A). Also within this sand- and silt-enriched zone are fine- to medium-grained limestone rock fragments with brachiopod, mollusc, and bryozoan fossil allochems, as well as coarse-grained limestone rock fragments with coarse calcite rhombs. Two other silt- and sand-rich interbeds occur at 600 cm and 708 cm depth. Although most of the sand fraction throughout the borehole is composed of fine-grained monocrystalline quartz (>95%), greater concentrations of polycrystalline quartz sand grains are present in the lowermost BC horizon. Few feldspar grains (2-5%) are present only within the siliciclastic interbeds, and are common within the silt fraction. Minor amounts of muscovite also occur in the siliciclastic-rich zones.

Throughout the borehole, increases in silt fraction are common with increasing depth, and the silt may have been partly derived from rinds of deeply weathered dolostone rock fragments. Where deeply weathered, these rock fragments exhibit pervasive dolomite ghosts occluded with silt infillings. Dolostone rock fragments, siliciclastic litho/saprorelicts and gravel-sized chert fragments appear scattered at various depths, however, they tend to increase with increasing depth (Figs. 7F and 8C). Varieties of dolostone fragments observed within borehole 1 include fine- to medium-grained dolomite similar to Mascot Fm. bedrock and oolitic/pelloidal varieties. Root material is common in the upper 25 cm of soil, then is absent until 964 cm depth (Fig. 7E). Below this depth, fine to medium (mostly < 2mm), very deeply weathered root material and root traces, as well as possible few animal burrows with dolomite silt infillings are visible, indicating the presence of a paleosol (Fig. 8E). Most notably, below 964 cm depth

Figure 8: Micromorphology of borehole 1: Image 2. All photos under plane polarized light except for B and F which are under cross-polarized light. A) Fine-grained monocrystalline quartz grains within deeply weathered, Fe-oxide cemented litho/saprorelict, 800 cm depth. B) Silicified oolitic/pelloidal dolostone fragment with interstitial chert/chalcedony with thick Fe-oxide rich pedogenic clay coatings, 800 cm depth. C) Deeply weathered siltstone litho/saprorelict with thick Mn-oxide coats and masses embedded in silty clay matrix, 800 cm depth. D) Banded silts and pedogenic clays adjacent to desiccation crack lined with Fe-oxide, 980 cm depth. E) Deeply weathered plant material, fine-grained limestone rock fragments, shaley-siltstone litho/saprorelicts, and fine-grained monocrystalline quartz grains possibly representing original soil residuum, 980 cm depth. F) Thin chert seam near base of borehole revealing near-horizontal bedrock, with thick, Fe-rich pedogenic clays persisting at maximum borehole depths, 1025 cm depth.

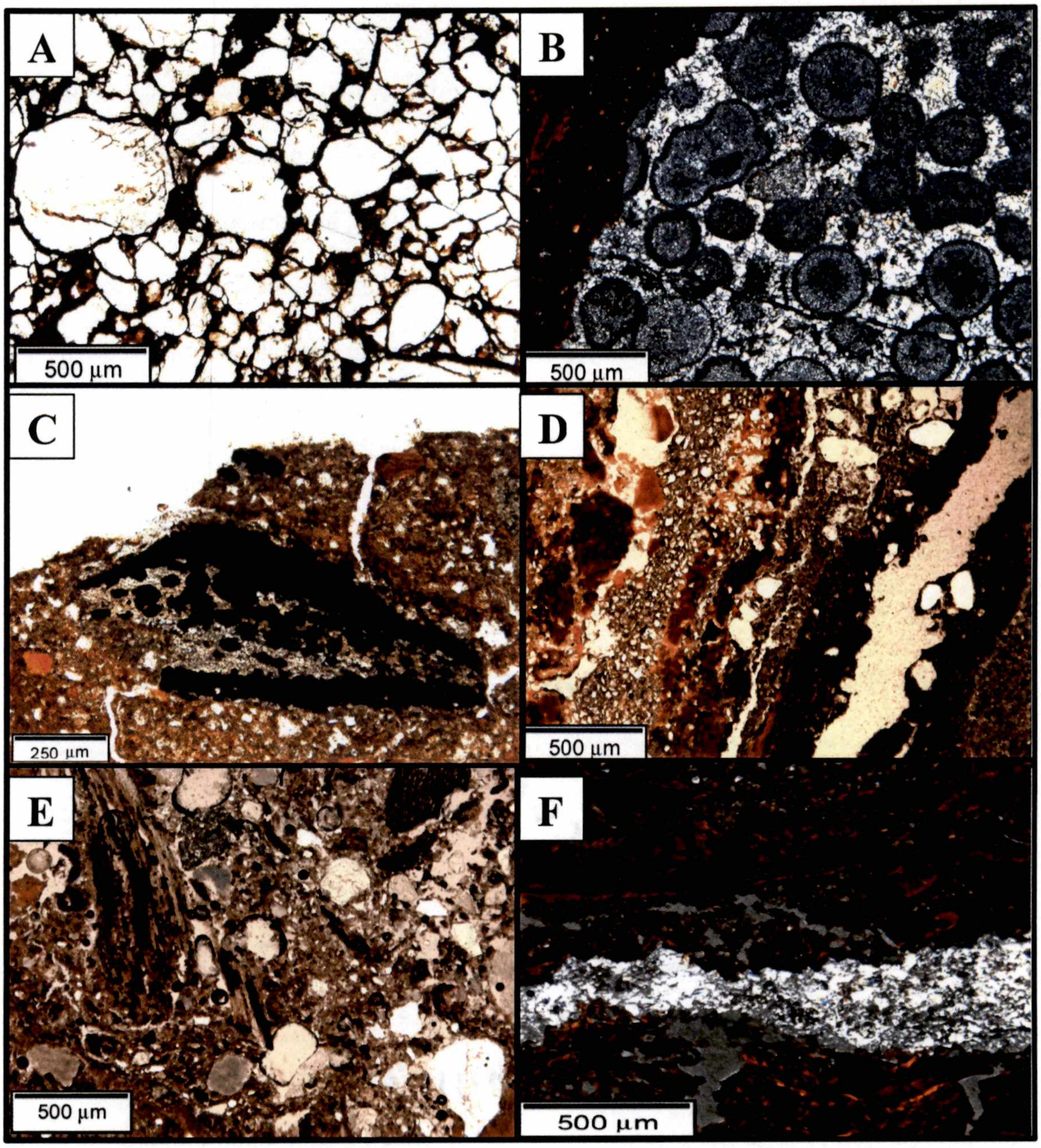
A
500 µm
B
500 µm
C
250 µm
D
500 µm
E
500 µm
F
500 µm

the residuum is slightly size-graded and becomes sandier down to 981 cm depth. Below 981 cm, the residuum smoothly grades into very high clay content material with both slickensides and desiccation cracks present. Root traces diminish in size and abundance below this depth. The base of borehole one consists of thin, horizontal chert layers embedded in extensive pedogenic clay that directly overlies Mascot Fm. bedrock (Fig. 8F). Overall pedogenic features of horizon BC strongly resemble those observed within the BE and Bt1 horizons (Table 2).

Redoximorphic features that include concretions, coatings/hypocoatings and cements all exhibit textural and morphological trends with depth. Fe-oxide, present as concretions, nodules, masses, coats, and hypocoats, is most concentrated within the upper 4 m (< 20% of soil matrix; Fig. 7B). Large (< 4mm wide), commonly cracked, multi-generation Fe-oxide nodules occur throughout this depth interval, with the largest near active macropores and within the more porous BE horizon. Many areas of soil matrix adjacent to these concretions show Fe-redox depletions (Fig. 7D). Fe-oxide content decreases with depth and is primarily expressed as Fe/Mn-oxide coats along macropore walls and ped/grain faces between 4-10 m depth (Fig. 8D). Subrounded to well-rounded pedogenic clay papules, or pedorelicts (< 1 mm across), occur within horizons Bt1, Bt5 interbed, and Bt6 (Fig. 7C). Volumetrically, the residuum is dominantly composed of fine, multi-generation pedogenic clays that constitute the bulk soil matrix material. Aureoles, vadose pendants, wavy convoluted and laterally convex bands of these clays suggest slow horizontal and vertical migration of soil pore-water. The pedogenic clays extensively line macropores, grain/ped faces, and serve to occlude macropore channels.

Table 2: Micromorphological features of borehole 1. Note that macroporosity, particle size and percent mineral composition were determined using image comparison charts.

Sample I.D	Horizon	Depth (cm)	Texture	Ped Size / Structure	Pore Structure	% Macro-Porosity	Particle Size			Composition		
							% Sand	% Silt	% Clay	% Qtz	% Clay	% RF
B1-P1	BE + Bt1	43-51	sandy-loam > clay	fine to medium granular to subangular blocky	planar-dendritic	25	35	20	45	20	45	15
B1-P2	Bt2 Interbed	233-239	sandy-clay	moderate-medium subangular blocky	planar-sinuous	15	20	20	60	27	60	13
B1-P3	Bt3 Interbed	367-373	silty-clay	moderate-medium subangular blocky	dendritic-sinuous	15	15	25	>60	25	60	15
B1-P4	Bt4	554-562	gravelly-clay	moderate-medium subangular blocky	dendritic-sinuous	20	3	15	82	7	80	10
B1-P5	Bt4 + Bt5	595-602	silty-sand	N/A N/A	dendritic	23	55	25	20	>55	25	>5
B1-P6	Bt5	671-678	gravelly-sandy-clay	fine-medium subangular blocky	wavy-planar	20	35	25	40	>35	40	25
B1-P7	Cr + Bt6	707-714	gravelly-sandy-clay	N/A N/A	discontinous-dendritic	17	35	30	35	>40	35	20
B1-P8	Bt6	796-803	gravelly-silty-clay	medium-coarse subangular blocky	sinuous-dendritic	15	28	25	47	>35	47	18
B1-P9	BC	979-986	gravelly-silty-clay	fine-medium subangular blocky	dendritic-planar	15	35	30	35	>35	35	25
B1-P10	BC	1023-1030	clay	fine subangular blocky	discontinuous-dendritic-planar	20	10	20	70	15	70	15

Note that all characteristics in this table are based on visual estimates/inspection of thin-sections using a petrographic microscope.

Table 2 continued.

Sample I D.	Horizon	Depth (cm)	Ped Clay Mottles	Matrix	Concretions/Nodules	Coatings
B1-P1	BE + Bt1	43-51	5% orange	skelsepic	10-12% multigen. Fe-oxide (<4mm)	Red illuviated clay lining grains, Fe-oxide concretions, and as aureoles
B1-P2	Bt2 Interbed	233-239	75% dark-red 15% orange 5% yellow-orange 5% tan-yellow	strongly bimasepic	5-8% Fe-Mn oxide (<3mm) 10% in organic-rich zone Red pedogenic clay nodules	Fe/Mn cements lining grains and pore faces , pervasive multigen pedogenic clays
B1-P3	Bt3 Interbed	367-373	65% dark-red 20% orange 15% yellow-orange	moderately bimasepic	12-14% Fe-oxide masses (<3mm) 2-5% Mn-oxide disseminated	Pervasive multigen ped. clay coats and vadose pendents
B1-P4	Bt4	554-562	60% dark red 15% orange 15% yellow-orange 10% orange-yellow	weakly bimasepic	5% Fe/Mn-oxide masses (<1mm)	8% Fe-oxide coatings on peds, pore faces, and b/w dolomite silt grains, well-developed multi-gen ped. clay + Fe-oxide coats
B1-P5	Bt4 + Bt5	595-602	55% orange 35% dark-red 5% yellow-orange 5% tan-yellow	skelsepic	8% Red ped. clay papules (<1mm) <5% Fe/Mn-oxide nodules (<1mm)	Pervasive multigen ped. clay often completely occluding pores. Fe/Mn-oxide coats + hypocoats
B1-P6	Bt5	671-678	40% dark-red 35% orange 15% orange-yellow 10% yellow	moderately bimasepic	3% Fe/Mn-oxide masses (<1mm)	Pervasive multigen ped. clay, 5% Fe/Mn-oxide coats
B1-P7	Cr + Bt6	707-714	50% dark-red 25% orange 15% orange-yellow 5% tan-yellow	skelsepic	3% Fe/Mn-oxide masses (<1mm)	Pervasive multigen ped. clay, 5-7% Fe/Mn-oxide coats
B1-P8	Bt6	796-803	55% brown-red 20% dark-red 5% orange 5% orange-yellow	skelsepic-bimasepic	5-7% Fe-oxide masses and glaebules (<2mm)	Pervasive Fe-oxide + ped. clay coats often with convoluted wavy bands (Fe-oxide ~8%)
B1-P9	BC	979-986	30% orange-red 20% pale yellow 20% dark-red 20% red-brown 10% orange	skelsepic-mosepic	Common Fe-rich ped. clay papules (<0 5mm), 3% Fe-oxide nodules	Extensive ped. clay coats, 8% Fe-oxide coats
B1-P10	BC	1023-1030	35% brown-orange 30% brown-red 20% orange 15% red	bimasepic-trimasepic	10% Fe-oxide 3% ped. clay papules near top	Pervasive multigen. ped. clay coats, few kaolinite/dickite cement coats along sandstone/siltstone lithorelicts, extensive Fe-rich coats + hypocoats

These clays are most strongly oxidized within the upper 5 m and become increasingly mottled with depth. Coats of kaolinite/dickite cement are present below 981 m in and around sandstone and siltstone litho/saprorelicts, and between wavy bands of illuviated pedogenic clay. Few, thick hematite cements occur at various depths within sandstone saprorelicts. Feldspars, where present, commonly contain authigenic overgrowths. Minor occurrences of authigenic quartz overgrowths occur around quartz grains at variable depths.

4.2.3 Borehole 4 – Similar to borehole 1, the matrix of borehole 4 residuum is dominated by bimasepic fabrics, with skelsepic fabrics characteristic of the BE horizon and siliciclastic interbeds. Macroporosity in the samples range from 13-22% exhibit sinuous-dendritic pore structure that, as was the case with borehole 1, becomes more discontinous with increasing depth (Fig. 9C). Also similar to borehole 1, actual in-situ values for macroporosity are likely much lower due to drying encountered during thin-section preparation. The highest macroporosity is observed within the BE horizon, and associated with desiccation cracks and rinds around deeply weathered dolostone fragments. However, such porosity does not occur along less intensely weathered dolostone fragments. Two thin (< 1 cm) siliciclastic interbeds occur at 60 cm and 78 cm depths, within the Bt1 horizon, and are composed of very fine-grained sandy silt without micas (Table 3). The sand grains are very well rounded and well sorted. Another unusually sandy region occurs between 863 cm and 874 cm depth, and these sands are almost entirely composed of monocrystalline quartz (minor deeply weathered chert), and are moderately well-sorted and well- to very well-rounded. Minor amounts of feldspar

Figure 9: Micromorphology of borehole 4 and Mascot bedrock. All photos under cross polarized light except for C and D. A) Silicified dolostone rock fragment with chert-lined elongate polycrystalline quartz inclusion at 5 cm depth. B) Close-up of polycrystalline quartz grain bearing strong resemblance to inclusion observed in A (50 cm depth). C) Dendritic, sinuous pore structure with successive pedogenic clay and Mn-oxide coats along pore walls in silty matrix surrounding numerous siltstone litho/saprorelicts at 600 cm depth. D) Macropore at 600 cm depth showing silt infillings along pore walls (note former pore walls marked by dendritic Mn-oxide lining former pore wall). E) Deeply weathered Mascot-like dolostone rock fragment with extensive multi-generational pedogenic clays filling dolomite crystal dissolution voids. F) Fine to medium-grained, slightly to moderately weathered, tan-brown dolomite with calcite and dolomite spar fill cements. Some pores and intergranular pore spaces lined with Fe-oxide. Bedrock outcrop sampled from approximately 40 m downslope (west) of borehole 4.

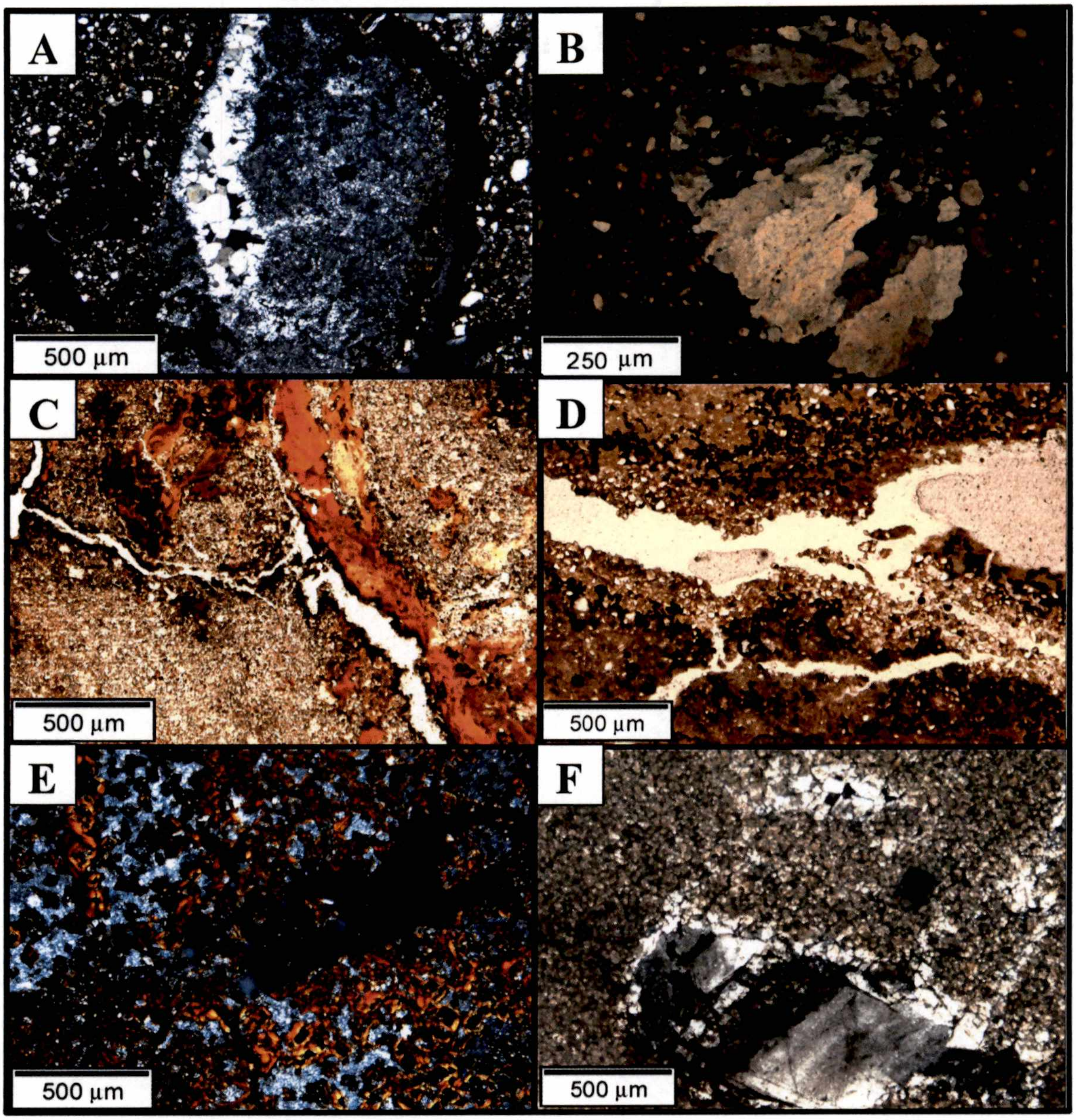
A
500 µm
B
250 µm
C
500 µm
D
500 µm
E
500 µm
F
500 µm

Table 3: Micromorphological features of borehole 4.

Sample I.D.	Horizon	Depth (cm)	Texture	Ped Size / Structure	Pore Structure	% Porosity	Particle Size			Composition		
							% Sand	% Silt	% Clay	% Qtz	% Clay	% RF
B4-P1	A	3-10	sandy-loam	fine-medium granular	sinuous-dendritic	21	25	42	33	55	37	8
B4-P2	BE + Bt1	44-52	silty-clay	fine- mod medium subangular blocky	sinuous-dendritic	19	15	30	55	30	60	5
B4-P3	Bt5	572-580	gravelly-sandy-clay	moderate-medium subangular blocky	dendritic-sinuous	22	25	20	55	35	45	20
B4-P4	Bt6	598-606	vfg sandy-clay	medium subrounded to subang.	discontinuous-dendritic	18	30	35	35	55	33	12
B4-P5	Bt8	813-820	gravelly-clay	no defined structure	discontinuous-dendritic	14	3	10	55	8	55	37
B4-P6	Bt10 + Bt11	873-880	silty-sand	N/A N/A	discontinuous-planar	~18	40	29	31	60	30	10

Table 3 continued

Sample I.D.	Horizon	Depth (cm)	Ped. Clay Mottles	Matrix	Concretions/Nodules	Coatings
B4-P1	A	3-10	2% orange-red	loamy	5-8% multigen. Fe-oxide (<5mm)	Few ped clays near base, some diffuse Fe-oxide hypocoats
B4-P2	BE + Bt1	44-52	40% red 30% red-brown 15% orange 15% orange-yellow	skelsepic-bimasepic	Some red ped clay papules, 3% Fe-oxide (<4mm)	Extensive multigen. ped. clay coats, some macropores coated w/ Fe-oxide cements + mild hypocoatings
B4-P3	Bt5	572-580	35% brown-red 35% red 30% orange	skelsepic-bimasepic	4% Fe-oxide (<1 5mm), common ped clay papulles	Convoluted + criss-crossing network of multigen. ped clays + Fe-oxide coats
B4-P4	Bt6	598-606	45% red-brown 25% brown 13% red-orange 7% tan-yellow	skelsepic-bimasepic	3% Fe-oxide masses (<1mm), very minor ped clay papules (<1mm)	10-15% Fe/Mn-oxide seams (<3mm), Extensive multigen. ped clay coats
B4-P5	Bt8	813-820	40% orange-red 25% brown-red 15% orange 15% brown	skelsepic-mosepic		Some pores/grains/shale lithorelicts coated w/ kaolinite cement, significant ped clay coats, thick Fe-oxide coats
B4-P6	Bt10 + Bt11	873-880	65% green-brown 10% orange-red 10% red	skelsepic	Few fine Fe-oxide masses	Significant ped clay coats Fe-oxide coats (6%)

(mostly perthite) occur scattered throughout the borehole, and are dominantly silt-sized. The greatest concentration of feldspar occurs at approximately 600 cm depth (8%), where slightly convoluted relict bedding (saprolite ?) occurs in association with deeply weathered shale litho/saprorelicts and Mascot-like silicified dolostone (Appendix C). Silt infillings are present within various types of macropores at this interval (Fig. 9D). Up to 7% muscovite is also present at this depth. Trace heavy minerals scattered throughout the borehole include zircon and ilmenite.

Sharp increases in silt fraction (and subsequent decrease in clay fraction) occur near the base of the core within the lowermost 50 cm of residuum. Similar to borehole 1, dolostone and cherty gravel tend to increase with depth with many deeply weathered dolostone fragments displaying weathered exteriors containing pervasive dolostone “ghost” rhombs. Close inspection of many dolostone fragments throughout borehole 4 reveals inclusions and/or seams of polycrystalline quartz, commonly lined with fine-grained chert (Fig. 9A). The polycrystalline quartz grains exhibit features consistent with hydrothermal alteration such as near-perfect undulatory extinction and slightly elongated and sutured grains (Fig. 9B). Two additional features of the polycrystalline quartz inclusions include the absence of other minerals (e.g., feldspar or muscovite) and diagenetically coarsened quartz grains, which results in a strong resemblance to chalcedony/banded agate. Other rock fragments observed within borehole 4 include fine to medium-grained dolomite similar to Mascot Fm. bedrock, and deeply weathered shale and Fe-cemented, fine-grained sandstone litho/saprorelicts.

As was the case for borehole 1, Fe-oxide concretions, nodules and masses are most common and best-developed within the loamy A and BE horizons. Many multi-generation concretions reveal successive growth bands that envelop smaller Fe-oxide concretions and their occurrences correlate with low clay content horizons. At and below 5.8 m, most Fe-oxide is present as coatings along open macropores. Many areas of soil matrix adjacent to these Fe-oxide coats contain thin (< 3 mm) redox-depleted mottles. Well-rounded, red pedogenic clay papules (< 1 mm across) occur within the BE, Bt1, Bt5 and Bt6 horizons. Multi-generational pedogenic clays are substantial, with significant pore occlusion developed just below the contact between the BE and Bt1 horizons. Multi-generation pedogenic clay pedorelicts and vadose pendants occur adjacent to, or partially filling macropores and desiccation cracks, whereas wavy convoluted and laterally convex bands of these clays are typically present along/between grain boundaries, within dissolution voids (in dolostone fragments) and relict bedding planes (where siliciclastic litho/saprorelicts occur; Fig. 9E). These illuviated clays are strongly oxidized with reddish colors throughout the majority of the core, which grade into reddish-brown colors at 6.5 m depth, and then to greenish-brown colors in the basal 10 cm of core material. A rare form of kaolinite/dickite cement occurs at variable depths, but mostly in association with deeply weathered shale litho/saprorelicts, and along few grains faces and macropore walls. As was the case with borehole 1, hematite cements are rare at various depths within deeply weathered sandstone saprorelicts. Feldspars, which appear limited to siliciclastic saprorelicts and silt fractions, commonly display authigenic feldspar overgrowths.

4.2.4 Mascot Dolomite -- The Mascot Fm. bedrock is composed of fine- to medium-grained, tan-brown dolostone, with some coarse dolomite spar-fill cements (Fig. 9F).

Few small fractures (< 500 µm thick) have a planar-sinuous structure and extend sub-horizontally along bedding planes and chert layers. Fe-oxide cements and fine Fe masses (< 100-200 µm) commonly fill these fractures, as well as intergranular pores. Minor amounts of oxidized pedogenic clay are observed near the top of the bedrock thin-section.

5.0 TEXTURE (PARTICLE SIZE DISTRIBUTION) AND BULK POROSITY

Particle size analysis was performed on 23 total samples taken from boreholes 1 (11) and 4 (12). Samples were selected to span the different soil horizons, and also included various sandy or silty interbeds (Table 4). The uppermost 50 cm in both boreholes (A/BE horizons) is composed of clay loam, with common chert and dolostone rock fragments. At approximately 1 m depth a marked increase in clay content occurs, which extends to depths greater than 8 meters (Figs. 10 and 11). Although both boreholes exhibit similar particle-size distribution trends with depth, borehole 1 contains greater overall clay content. The clay fraction generally reaches a maximum at depths of 1 to 5 meters. Although a few sandy/silty interbeds are present within the core material, they are volumetrically insignificant within the 1-8 m interval. Much of what constituted the very fine sand fraction in this clay-rich zone was observed, during the dry-sieve process, to be fragmented and disseminated chert. Below 8 m, the core material becomes increasingly silty, and gravel-size rock fragments, which include dolostone and lithorelicts from siliciclastic interbeds, become more common.

Particle-size analysis using an X-ray disk centrifuge technique provided detailed information about size-fraction distributions for the < 2 μm range. The analyses indicate that the residuum is dominantly composed of pedogenic clay (clays finer than 0.1 μm; Fitzpatrick, 1993). Up to 66% of the clays are pedogenic in nature, with the greatest concentrations within 1-8 meters depth (Fig. 11). A sharp decrease in pedogenic clays occurs toward the base of each of the cores near the bedrock interface, which corresponds to a gradual increase in the silt fraction. Detailed clay distribution data also reveal varying bimodal size

Table 4: Selected samples for particle size determination using an X-ray disk centrifuge.

I.D.	DEPTH (cm)	HORIZON
B1-1	10	A
B1-4	40	BE
B1-5	58	Sandy Interbed
B1-9	140	Bt2
B1-17	305	Bt2
B1-22	407	Bt3
B1-28	527	Bt4
B1-31	595	Sandy Interbed
B1-34	655	Bt5
B1-41	815	Bt6
B1-50	1050	BC
B4-1	10	A
B4-3	30	BE
B4-5	60	Sandy silt int. w/ Bt1
B4-11	180	Bt2
B4-23	425	Bt3
B4-27	510	Bt4
B4-32	610	Bt6
B4-36	690	Bt7
B4-42	810	Bt8
B4-44	850	Bt9
B4-45	870	Bt10
B4-46	880	Bt11

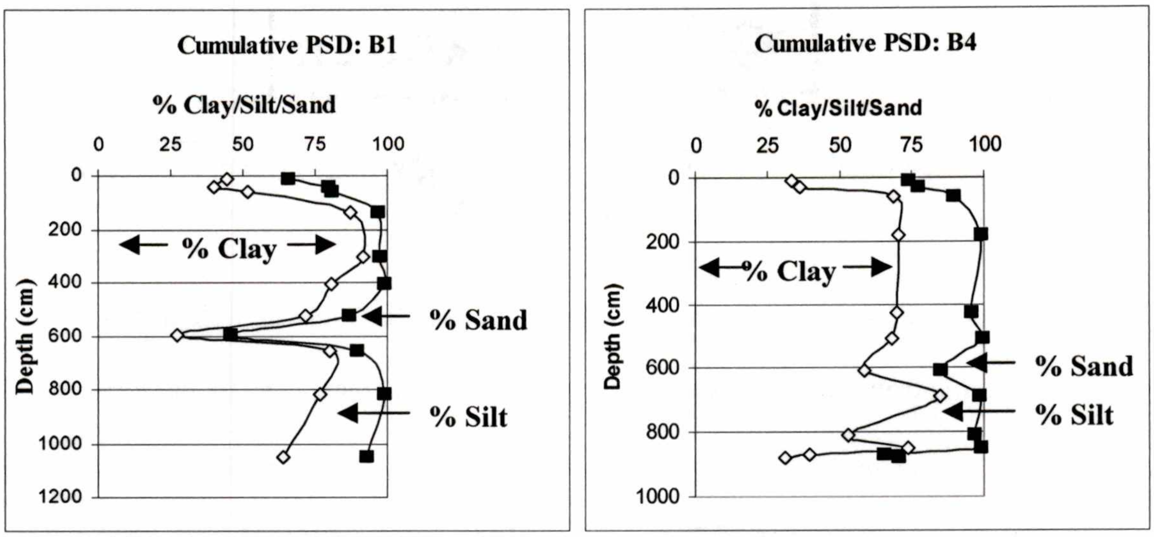

Figure 10: Cumulative particle size distributions versus depth for boreholes 1 and 4.

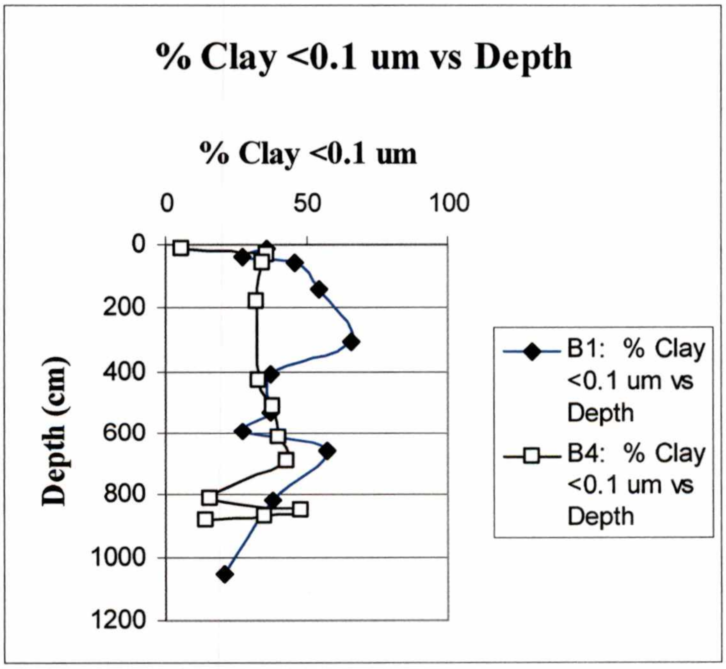

Figure 11: % Clay and % clay <0.1 μm versus depth for boreholes 1 and 4.

distributional patterns within the samples (Fig. 12). The trends generally indicate a subtle bimodal distribution of fine silt and pedogenic clays. At 3 m depth, there is about 98% clay in the < 53 μm fraction. Overall, more total clay and pedogenic clay is present within B1.

Bulk porosity measurements were calculated from bulk and particle density values, and range from 28-50% (Appendix E). Horizons characterized by greater porosity typically exhibit high clay content, while the loamy A / BE horizons were found to contain the lowest porosities (Table 5). It should be noted that the coring process may have distorted actual bulk densities of the sampled material, thereby introducing potential error in the calculated bulk porosities. This distortion due to coring was observed by the swelling (>100% recovery) and possible compaction (<100% recovery) of soil material (Appendix H).

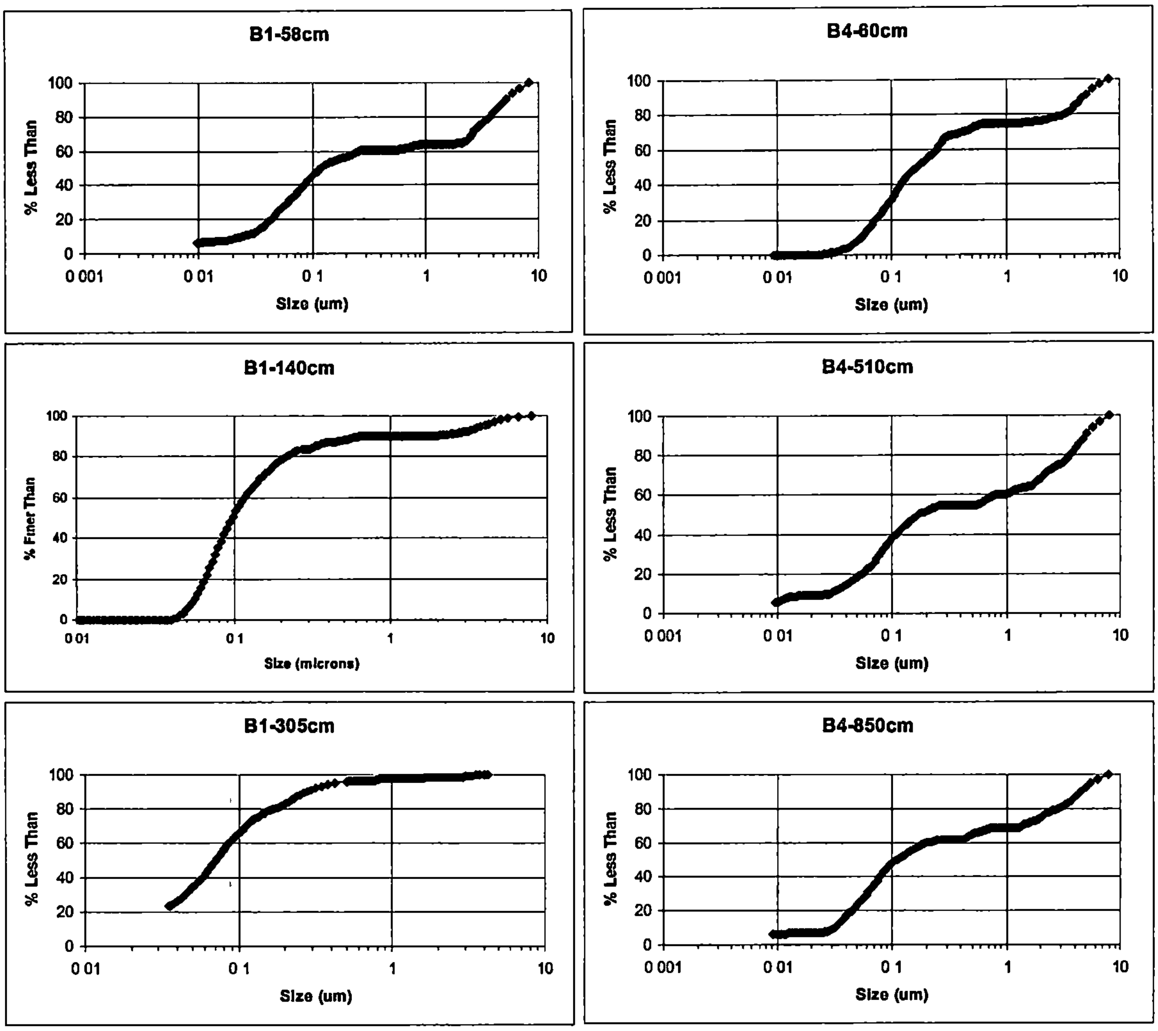

Figure 12: Examples of detailed cumulative clay distribution curves for boreholes 1 and 4. Note the subtle/weak fine silt and pedogenic clay bimodal distribution.

Table 5: Bulk porosity calculations

Sample I.D.	Depth (cm)	Pb	Ps	% Clay	Bulk Porosity (%)
B1-4	40	1.77	2.73	40	35
B1-5	58	1.83	2 63	52	30
B1-9	140	1.74	2 72	87	36
B1-17	305	1.56	2 78	92	44
B1-22	407	1 67	2.77	81	40
B1-28	527	1.47	2.74	72	46
B1-31	595	1.48	2.56	27	42
B1-34	655	1.48	2.71	80	45
B1-41	815	1.46	2.90	77	50
B1-50	1050	1.58	2.69	64	41
B4-1	10	1.89	2.64	34	28
B4-3	30	2.09	2.91	37	28
B4-5	60	1.86	2.65	68	30
B4-11	180	1.73	2.72	70	36
B4-23	425	1.73	3.09	70	44
B4-27	510	1.65	2.67	68	38
B4-32	610	1.84	2 94	58	37
B4-36	690	1.64	2 75	85	40
B4-42	810	1.9	3.12	53	39
B4-44	850	1.73	2 81	74	38
B4-45	870	1.75	2.74	40	36
B4-46	880	1.70	2.66	31	36

Note that Pb = bulk density as measured from wax clod method, Ps = particle density as measured from pycnometer method.

6.0 GEOCHEMISTRY AND MINERALOGY

6.1 Geochemistry

Whole-rock geochemical analysis was performed for major soil horizon and sandy interbed intervals, for boreholes 1 and 4 (Fig. 13). Chemical variations in the residuum were evaluated by measuring and plotting molecular ratios, which qualitatively provide approximations of weathering reactions and status of the soils (Retallack, 2001). Molecular-ratio calculations used to demonstrate common pedogenic reactions (see Retallack, 2001) show an overall uniform oxidized signature of the residuum that is higher near the surface and decreases with depth, and ranges from 0.35-0.10 (Fig. 14). Slight anomalies observed within the boreholes responsible for these ranges occur at ~500 cm depth, where a small increase exists for borehole 1 (0.35) and a minor decrease is present in borehole 4 (0.10). Within approximately the lowermost 50 cm of core material in both boreholes, substantial decreases in oxidation ratios occur, decreasing from 0.0 to 0.15. Ba/Sr ratios in the residuum show nearly identical trends for both boreholes (Fig. 15). Ratios show generally uniform increases from 0.6 at the surface to maximum values <1.0 around 5 m depth. Below 5 m depth and down to the bedrock contact, Ba/Sr ratios decrease uniformly back to 0.6, thereby suggesting that optimal leaching occurs in the upper 5 m of residuum. Other indicators of hydrolysis-driven reactions using the ratio of Al / bases reveal the same trends, which correlate well with the translocation and distribution of clays, as measured by Al_2O_3 (Fig. 16). Hydration ratios of silicon to sesquioxides also show a major decrease from near 20 within the uppermost 50 cm of residuum, to < 5 in the lowermost 50 cm depth (Fig. 17).

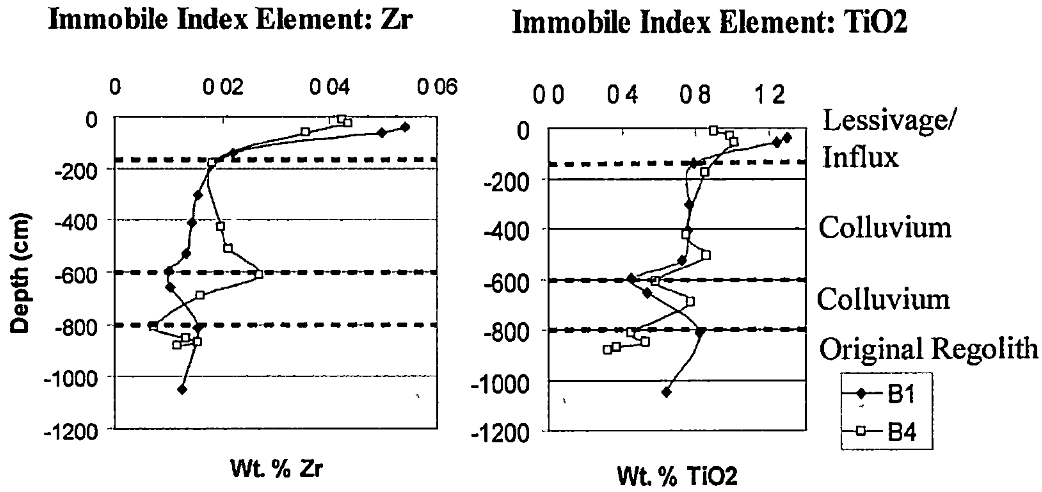

Figure 13: Distributions of immobile elements Zr and TiO2 vs. depth for boreholes 1 and 4 and interpretations for origins of weathered materials. Note that the concentration of TiO2 shows less variation with depth.

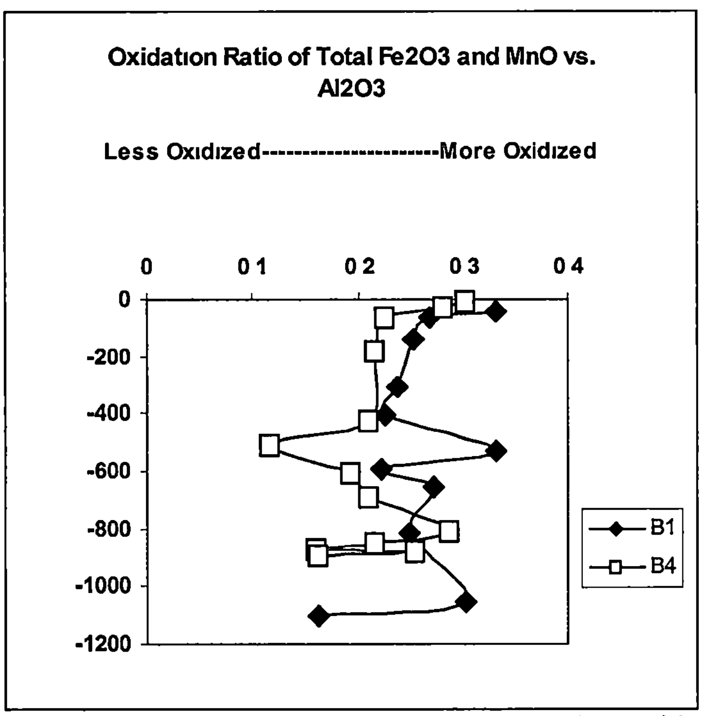

Figure 14: Whole-rock XRF data, expressed as oxidation ratios for boreholes 1 and 4.

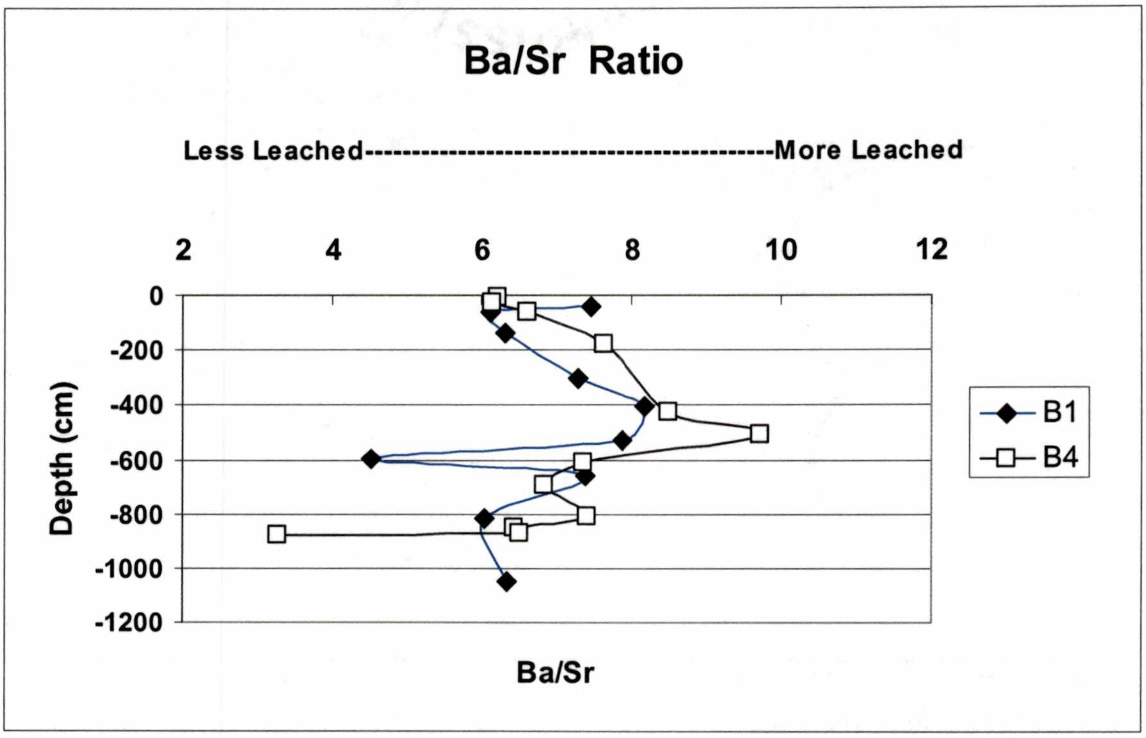

Figure 15: Whole-rock XRF data for Ba/Sr ratios for boreholes 1 and 4. Note that soils are less leached near the surface, and have maximum leaching at 400-500 cm depth

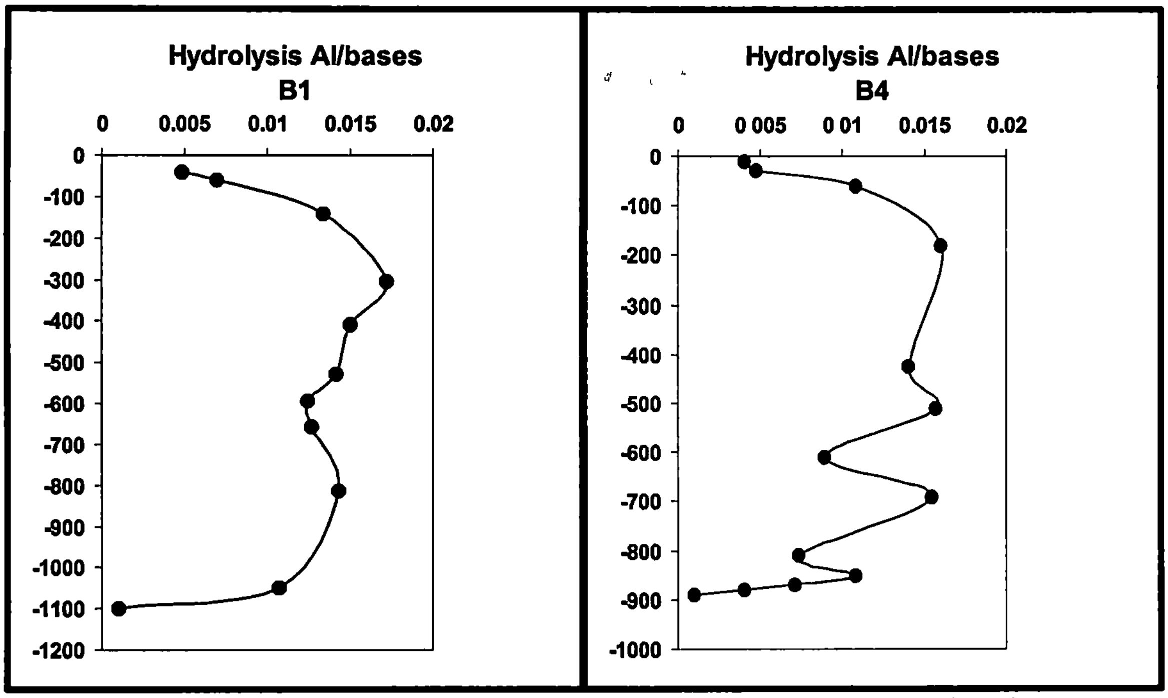

Figure 16: Whole-rock XRF data for Al / bases ratios revealing hydrolysis-driven weathering reactions in boreholes 1 and 4. Note that greater values indicate more weathered.

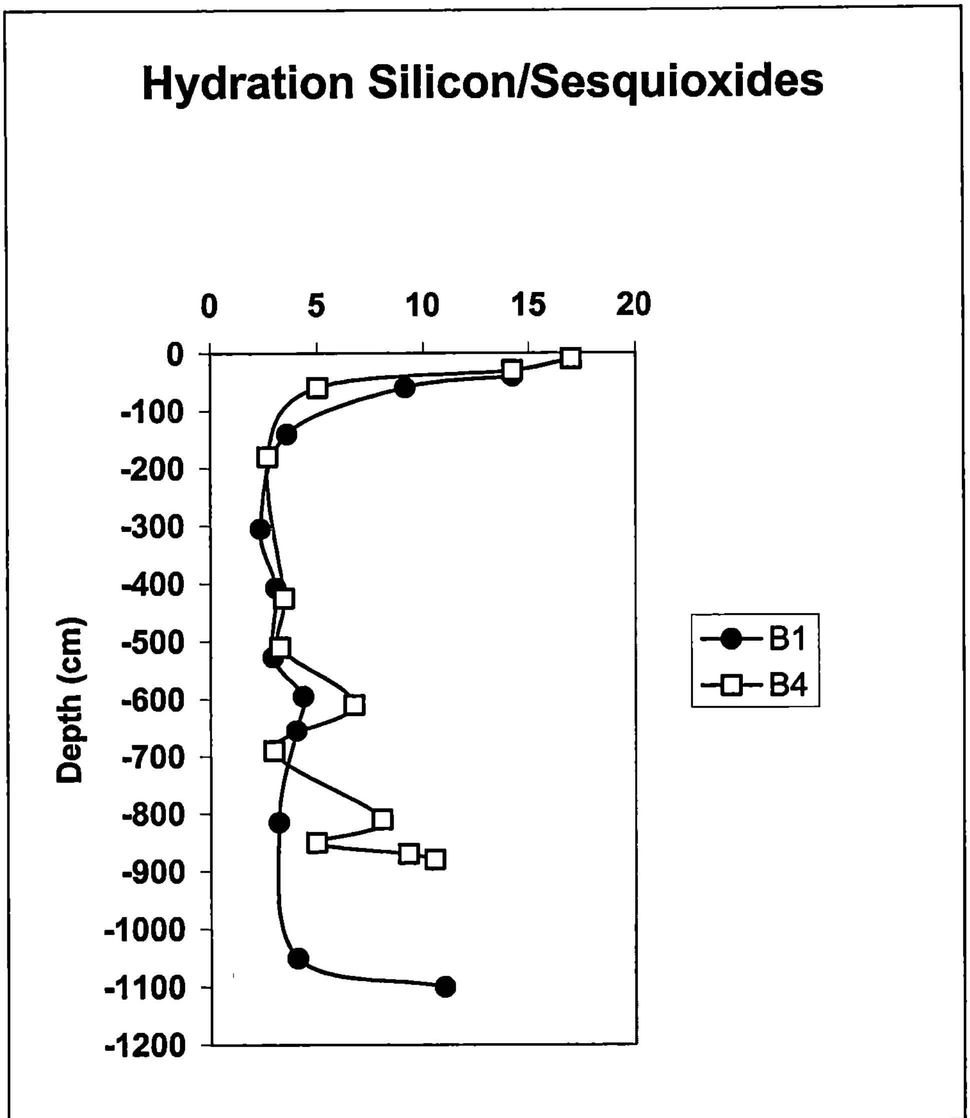

Figure 17: Whole-rock XRF data for Silicon / Sequioxides ratios exemplifying hydration-driven weathering reactions in boreholes 1 and 4.

Mass-balance calculations utilized TiO_2 as the immobile index element because of its more uniform distribution in both boreholes (Fig. 13). Geochemical plots used insoluble residue of Mascot Fm. bedrock as a parent material for all mass-balance calculations in this study. Plots illustrating volumetric changes within the profiles suggest a negative strain approaching –1.0, indicating complete collapse of soil material during weathering (Fig. 18). Mass-balance calculations of elements incorporated into the residuum via detrital influx show an overall loss of SiO_2 within both boreholes (Fig. 19). Additions of Zr occur above 1.5 m depth, with values generally decreasing with greater depths. A small net gain inflection occurs within one of the siliciclastic interbeds in both boreholes at 6 m depth. A similar prominent increase in Zr occurs at 8.7 m depth in borehole 4, which is not present in borehole 1. In addition to these trends observed for immobile Zr and TiO_2, plots of Nb versus depth reveal strong similarities in inflections for both boreholes 1 and 4 (Appendix F).

Transport calculations for alkali elements indicate overall net losses in each borehole. Translocation of elements comprising clay minerals show, overall net losses of Si, K, and Na, and net gains of Al throughout the boreholes (Fig. 20). A prominent net increase in Na and Al occurs in borehole 1 at 6 m depth. Net Al gains correlate well with clay bulges of Bt horizons. Extensive leaching of the Ultisols has likely driven the transport and removal of these alkali elements, as well as the enrichment of Al as indicated previously by the particle-size data. Appreciable net gains in Ca and Mg are present at 6 m depth (primarily in borehole 1), however, sharp increases of one to two orders-of-magnitude occur in the lowermost soil horizons of both boreholes (Fig. 21). Translocations of redox-sensitive elements vary significantly with depth, with Co and Cr

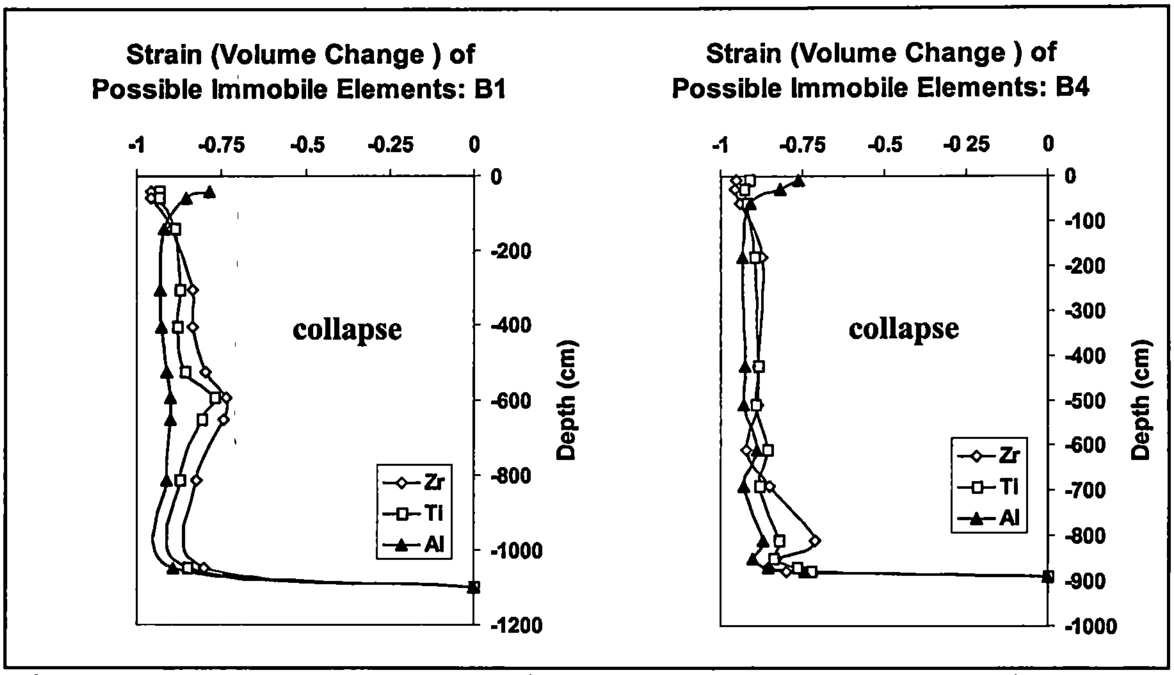

Figure 18: Whole-rock XRF data showing negative volumetric changes (strain), or collapse, for boreholes 1 and 4 calculated assuming either immobile Zr, Ti, or Al. Negative values represent net loss of constituent relative to parent material with –1 equivalent to 100% loss, and +1 is 100% net gain.

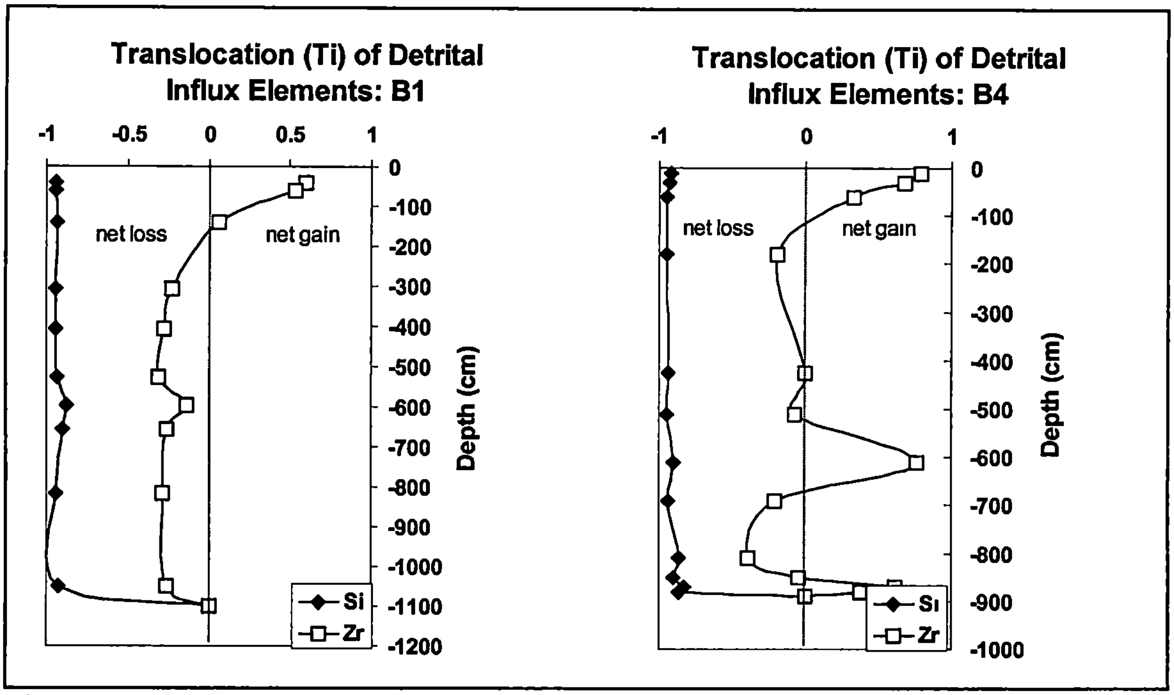

Figure 19: Transport functions (translocation) for detrital influx elements in boreholes 1 and 4 calculated assuming immobile Ti. Negative values represent net loss of constituent relative to parent material with –1 equivalent to 100% loss, and +1 is 100% net gain.

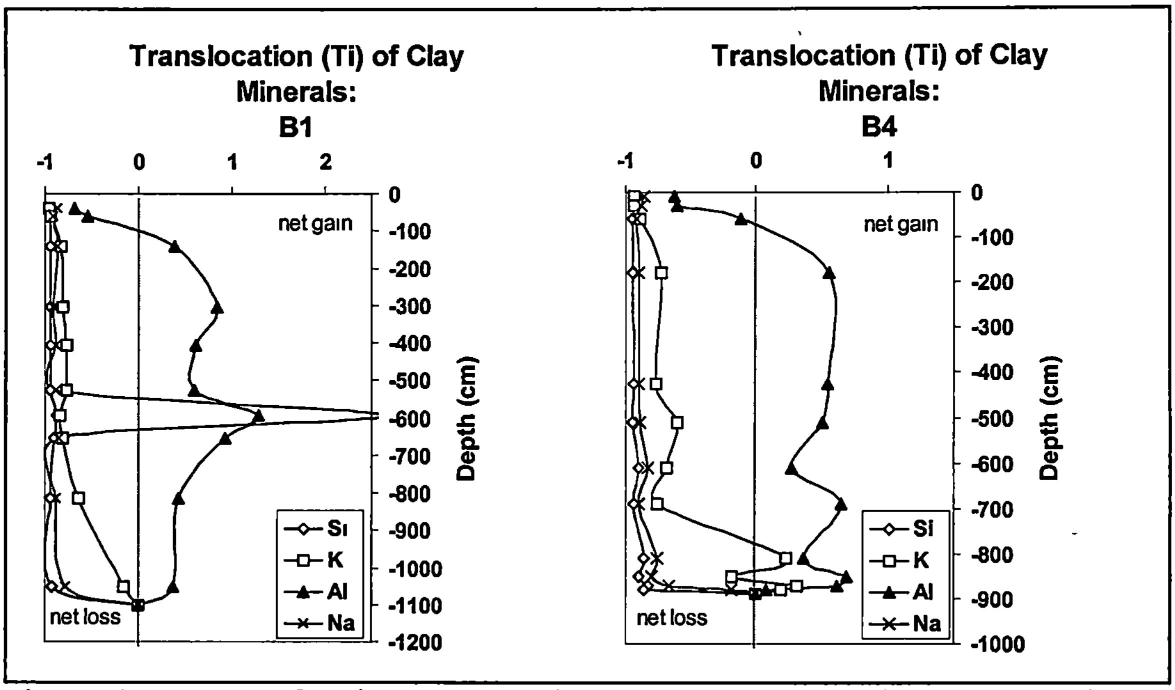

Figure 20: Transport functions (translocation) for alkali and clay mineral elements in boreholes 1 and 4 calculated assuming immobile Ti. Negative values represent net loss of constituent relative to parent material with -1 equivalent to 100% loss, and +1 is 100% net gain.

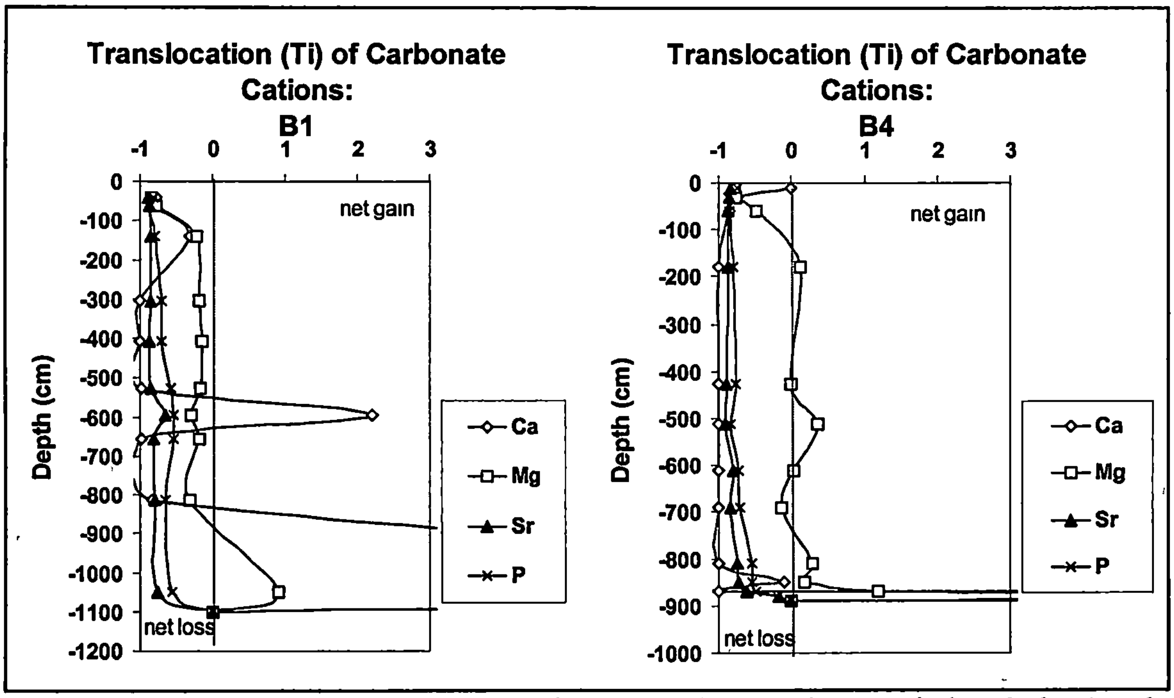

Figure 21: Transport functions (translocation) for carbonate elements in boreholes 1 and 4 calculated using immobile Ti. Negative values represent net loss of constituent relative to parent material with -1 equivalent to 100% loss, and +1 is 100% net gain.

generally decreasing, and Fe and Mn increasing towards the surface. Increases in Fe and Mn correlate well with the more clay-rich horizons, and commonly show an increase of over 200% (Fig. 22). Values for Mn show the most variability and anomalous losses occurring within siliciclastic interbeds. Relative enrichments of Mn generally correlate with horizons containing thick MnO_2 stained coats.

6.2 Mineralogy

In all five soil samples, the matrix is primarily composed of illite and kaolinite with significant amounts of goethite (Fig. 23 and Fig. 24). Lesser quantities of dehydrated halloysite (bellpine), Fe-Mg chlorite, and smectite (hydroxyl Al-Fe interlayer smectite = HIV) comprise the other clay species. Generally no carbonate is present in the clay samples. Minor amounts of quartz occur in the 2-0.5 μm fraction. The quartz diminishes with decreasing grain size and is absent in the <0.1 μm fraction. Illite becomes increasingly disordered in the finer fractions, which is exemplified by increasing peak width and slight shifts in d-spacings to the left (lower 2-theta). The kaolinite component appears to be highly disordered and in some cases demonstrates peak character associated with dehydrated halloysite. The most significant trends revealed by clay mineralogical analysis includes significant increases in illite with increasing depth, and decreases in kaolinite with increasing depth. Goethite tends to increase in the finer fractions (Fig. 23).

Two 100 g samples of Mascot Fm. bedrock were pulverized and reacted with HCl to determine the amount of insoluble residues in the dolostone. The samples ranged

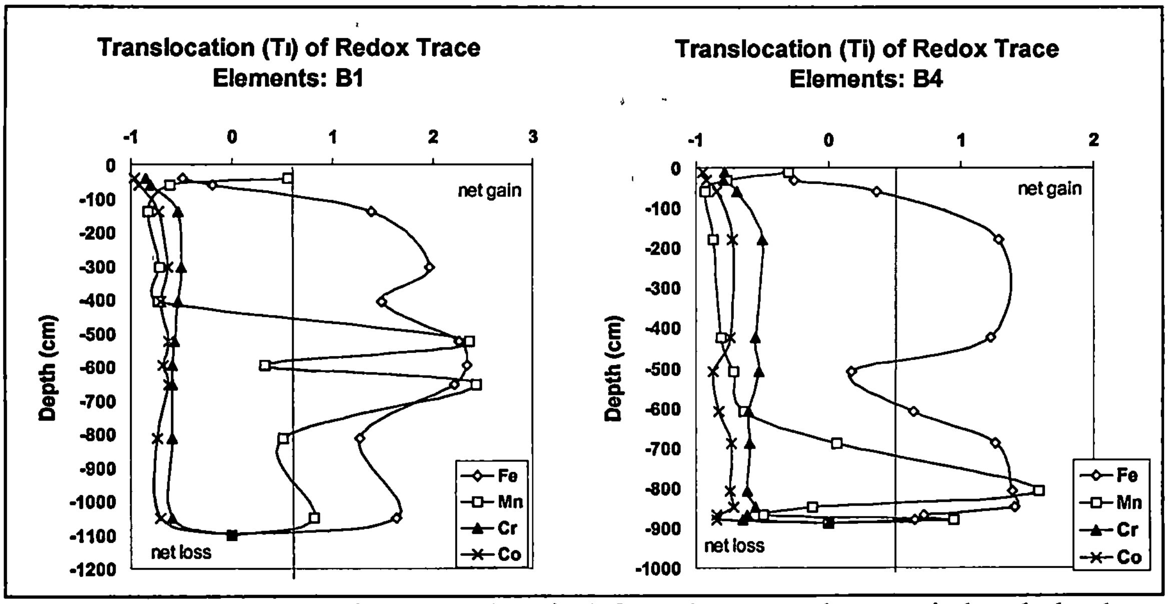

Figure 22: Transport functions (translocation) for redox trace elements in boreholes 1 and 4 calculated assuming immobile Ti. Negative values represent net loss of constituent relative to parent material with -1 equivalent to 100% loss, and vice versa for positive values.

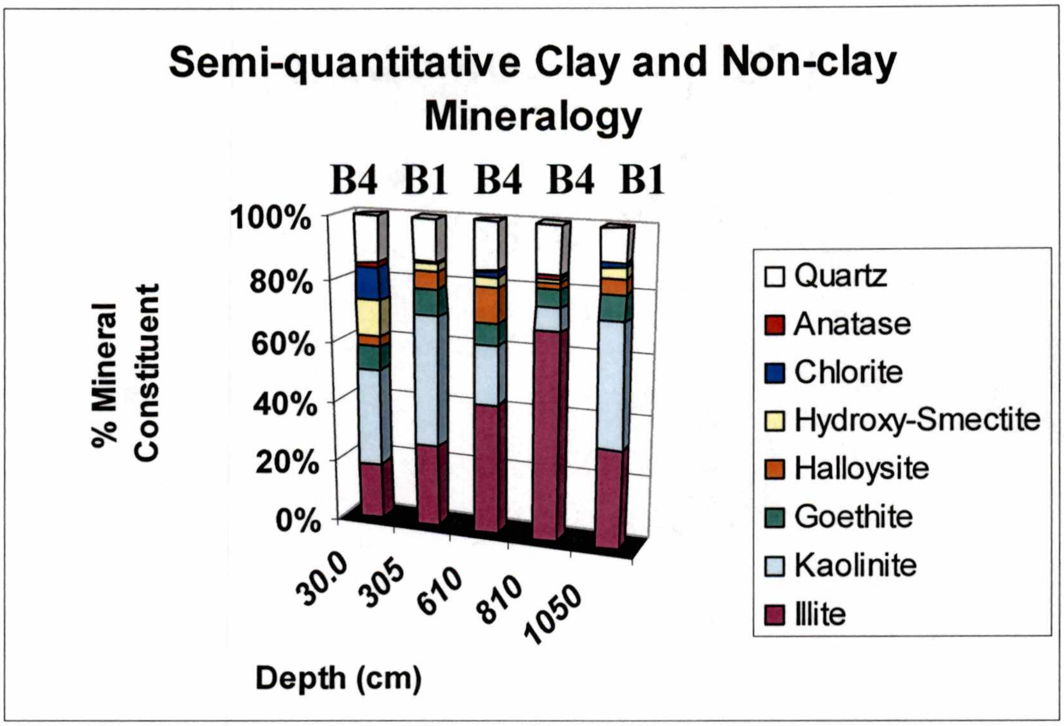

Figure 23: Semi-quantitative clay and non-clay mineralogy versus depth (data from boreholes 1 and 4). Note that samples from 305cm and 1050cm depths were sub-sampled from borehole 1, whereas samples from 30cm, 610cm and 810cm depths were sub-sampled from borehole 4.

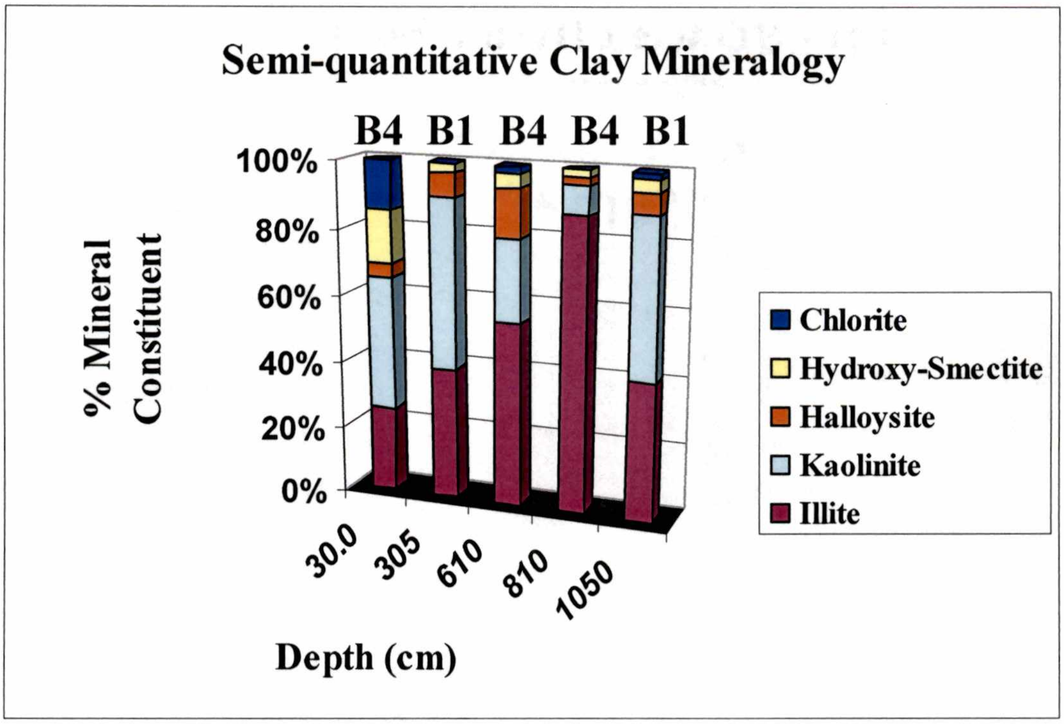

Figure 24: Semi-quantitative clay mineralogy versus depth without additions from quartz, anatase and goethite (data from boreholes 1 and 4). Note that samples from 305cm and 1050cm depths were sub-sampled from borehole 1, whereas samples from 30cm, 610cm and 810cm depths were sub-sampled from borehole 4.

from 7 to 15% of insoluble material consisting of appreciable amounts of brown-colored silts and cherty residue. The samples analyzed for XRD included a whole rock Mascot Dolostone sample and a subsample of chert that was isolated by treating additional bedrock sample with HCl acid. Whole-rock mineralogical data indicate that the rock is almost entirely dolomite with subordinate quartz, calcite, microcline, and albite. The chert sample contained mostly quartz, with minor dolomite and traces of calcite, microcline, and albite.

7.0 INTERPRETATIONS AND DISCUSSION

7.1 Soil genesis and comparison of physical/chemical properties to conceptual models

This study has provided important information on the genesis of soil and residuum derived from relatively flat-lying dolostone. One hypothesis is that Ultisols form in-situ as a single residuum from the long-term weathering of underlying carbonate bedrock. The estimated thickness of the Mascot Dolostone in the vicinity of the study site is 180 m, with at least 90 m of Kingsport Dolostone occurring stratigraphically below the Mascot Fm. (U.S.G.S., 1966). Based on the recovery of approximately 10% insoluble residue from the Mascot Fm. bedrock samples, and assuming this bedrock as the sole parent material for the residuum, 18 m of insoluble residue/material would result from the weathering of the carbonate bedrock. The thickest residuum observed at the site (borehole 1) is at least 11 m. To satisfy the thickness of residuum developed at this borehole, it would require a minimum of 5% insoluble residue in the bedrock. However, of the recovered 10% insoluble residue mentioned above, less than half of this material is comprised of micaceous clays and silts (~40%), with the remaining material consisting of chert in various size-fractions. If one assumes that about 100 of the 180 total meters of underlying Mascot Fm. bedrock has weathered away (these values are estimated due to the thick coverage of residuum and discontinuous outcrops of Mascot Fm. bedrock), soil thickness should average 5 m, assuming an insoluble residue content of 5% and no erosion or relocation of insoluble material. However, mass-balance geochemical plots for strain reveal >90% volume loss of the insoluble residue, suggesting that in-situ genesis of Ultisols plays only a subsidiary role in soil formation.

It is important to note that these extremely low values for strain may have been partly induced by the coring method, whereby compaction or expansion of core material from the drilling process changed the bulk density of the soil, possibly distorting calculations for strain. Furthermore, although the role of erosion throughout the time of development for this residuum cannot be directly quantified, it certainly relocated much of the above-mentioned insoluble materials thereby supporting an alternate mode of soil development. As seen by extensive pedogenic clay illuviation in thin-section, lessivage and translocation of clays from the thin (<50 cm) A and BE horizons at the study site also play a secondary role in the development of thick, clay-rich Bt horizons.

An alternative hypothesis tested in this study is that these soils are formed as a polygenetic assemblage of reworked parent materials. Insufficient thickness through the in-situ formation of these Ultisols as a single residuum (based on mass-balance calculations), in conjunction with the occurrence of very deeply weathered plant roots within the upper part of horizon BC at 965 cm depth (no other plant material was observed below 1 m depth in other boreholes) supports a polygenetic mode of residuum and soil formation. Additional micromorphological features that include, common, well-rounded, Fe-rich pedogenic clay papules (< 1mm wide), fine-grained limestone rock fragments, shaley-siltstone saprorelicts, and fine-grained monocrystalline quartz grains found scattered above 965 cm depth in borehole 1 provide further evidence for a polygenetic origin. Although undetected in the other boreholes, micromorphological and geochemical evidence suggest that the lowermost 1 m of residuum at this geomorphic position was at one time exposed to the atmosphere and a soil profile (now paleosol) developed on the surface and was subsequently buried by colluvium and alluvium. It is possible, based on morphological similarities between boreholes 1, 3 and 4 that paleosols may occur near the bases of other boreholes, however further investigation using thin-sections and geochemical analysis is needed to confirm this.

Additional potential evidence for the assertion that a paleosol occurs at the base of borehole 1 is indicated by the gradual decrease of kaolinite with increasing depth, followed by a sharp enrichment of this clay below 964 cm depth. Furthermore, illite concentrations increase with depth, and Miller (1972) and Monger (1986) found illite to be the dominant phyllosilicate constituent of the unweathered Paleozoic carbonate rock. Similar to the trend observed in kaolinite with depth, a significant decrease in illite concentration occurs at 1050 cm depth (Fig. 24). The significant thickness of overlying residuum appears to consist of colluvial additions of mostly weathered Mascot Fm. material (e.g., rock fragments, litho/saprorelicts). Geochemical evidence may support this interpretation based on at least three major discontinuities for plots of immobile Zr and TiO_2 at 6 m depth for both boreholes 1 and 4 (Fig. 13). These same trends and discontinuities are also demonstrated by trace element data for Nb with depth, which may mark periods of landscape instability and inputs of colluvial/alluvial material (Appendix F). It is unclear, however, if this discontinuity is inherited from the siliciclastic saprorelicts that are concentrated at this depth or from the above-mentioned colluvial additions, perhaps derived from multiple parent lithologies.

Soil morphology and genesis at the Strong Farm site are likely affected by the karstic, and likely brecciated nature of the underlying Mascot and Kingsport Dolomite bedrock. In contrast to residua formed from weathered siliciclastic rock (e.g. Graham et al., 1990; Driese et al., 2001; McKay et al., in press), the soils have little to no saprolite

(Cr horizon) transition between bedrock and soil residuum, but, instead, a sharp contact between pedogenic clay or dolomite silt and the underlying dolostone bedrock. Thin (< 10 cm thick), scattered siliciclastic interbeds constitute the only observed saprolite, however, these interbeds increase with depth and in places show relict, near horizontal bedding (Fig. 5D). Based on morphological/ textural data and supported by literature (Miller, 1972; Walker, 1985), the saprolitic material (which constitutes saprorelicts when intermittently occurring in residuum) is interpreted as derived from both alluvial/colluvial additions and siliciclastic interbeds within the Mascot Formation.

Some intervals within boreholes 1 and 4 contain well-rounded, fine- to medium-grained quartz sands (commonly with thick pedogenic clay coats) in addition to fossiliferous limestone fragments. It should be noted that these sand grains and fossil allochems bear strong resemblance to siliciclastic-rich zones of the underlying Chepultepec dolomite and fossil assemblages of the overlying Chickamauga Group (Cummings, 1959). Based upon the occurrences of these grains at variable depths and their absence in boreholes 2, 5, 6, and 7, these grains are interpreted as having been derived from the above-mentioned units through: 1) additions of colluvium derived from residuum developed from the Chepultepec and Chickamauga units that were weathered away, as well as from 2) infilling of large dissolution voids during karstification throughout the span of geologic time known as the Knox Unconformity. Mapping of the Mascot-Jefferson City zinc district and surrounding areas of eastern Tennessee suggests that there are extensive solution-collapse structures and brecciated zones with the Mascot and Kingsport units, which would have provided sinks for the deposition of eroded

Chepultapec sands (and sandstone lithorelicts) and Chickamauga Group residuum (Harris, 1971; Matlock, 1987).

Another concern for interpreting regolith genesis concerns one's ability to confidently distinguish between the multiple colluvial and/or alluvial deposits. It is probable that the long-term maturation of the regolith has homogenized these deposits, with variations in mottling, PSD and geochemical/mineralogical data primarily due to soil pore-water availability and macropore flow pathways. Evidence such as the lack of steep scarps on modern hill slopes, and features consistent with intense weathering and pedogenic development for the dolostone-derived residuum, such as highly disordered kaolinite, whole-rock XRF molecular ratios, and strain, or volume change of the residuum, suggest a long-term and gradual accumulation of mostly pedogenic clays. Slow, imperceptible soil creep appears to be the primary and current method for down slope movement of colluvium.

7.2 Pore structure and porosity occlusion due to illuviated clays and mineral precipitates

Comparison of particle size data with bulk porosity measurements indicates that the relatively higher porosities correspond to clay-rich horizons (up to 50%), and conversely, lower porosities are typical of loamy A / BE horizons (28-30%; Appendix E). Petrographic observations indicate that the greatest macroporosity exists in the A and BE horizons (upper 50 cm of residuum), with sizes ranging from 50 μm to 1.5 mm in diameter. Dendritic to sinuous pore structure is ubiquitous for all soil horizons, but becomes more discontinuous with increasing depth. Below 50 cm depth, zones of relatively greater porosity occur confined to preferred pathways that include deeply weathered rims of dolostone rock fragments. Macroporosity is also enhanced within intervals of grain-size increases and from the decementation of fine to medium-grained quartz sandstone lithorelicts.

Below approximately 50 cm depth, the soil residuum in all geomorphic positions has extensive accumulations of multi-generational pedogenic clay and lesser amounts of Fe/Mn-oxides, which together comprise the bulk of the soil matrix; these are also present as coatings and infillings along macropore walls, grain/ped faces, within dolomite dissolution voids, and as hypocoatings within both silty and clayey matrices. The extensive occurrence and cross-cutting nature of pedogenic clay within the subsurface suggest that multi-generational illuviation of these clays have significant impact on soil-pore water pathways. Morphological and geochemical translocation data show that significant pedogenic clay accumulation persists down to the bedrock contact.

7.3 Conceptual model for carbonate-derived soil genesis

Based on the findings of this research, a conceptual model was developed for the formation of carbonate-derived soils (Fig. 25). This model identifies a polygenetic pathway and at least five stages of residuum development:

Stage 1: Development of residual soil on non-Mascot Fm. bedrock (possibly stratigraphically overlying Chickamauga Group) begins, which is characterized by lowering of the bedrock due to chemical weathering and in-situ clay formation.

Stage 2: Disruption of original soil formation due to erosion. Landscape

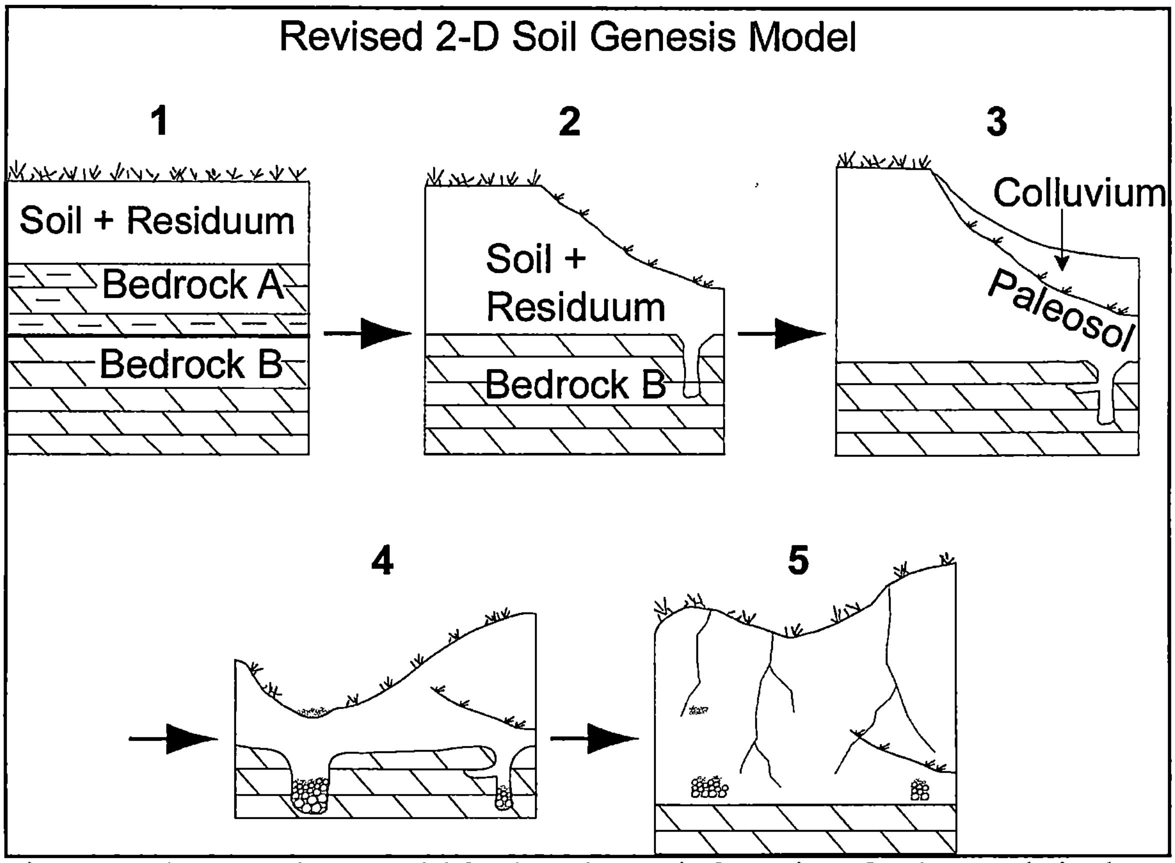

Figure 25: Conceptual 2-D model for the polygenetic formation of carbonate-derived residuum and soil genesis based on the finding of this research. At least 5 stages of soil development are proposed: 1) onset of in-situ residual soil development on non-Mascot Bedrock, 2) erosion and incorporation of residual soil with Mascot-derived residuum, 3 burial of residual soil by colluvial material, 4) dynamic geomorphic surface with alluvial deposits, and 5) advanced Ultisol pedogenesis.

instability and subsequent development of sinkholes within parent bedrock exacerbates erosion rates in areas of close proximity to active sinks, resulting in the incorporation of residual soil with Mascot-derived followed by soil development.

Stage 3: Continued disruption of original soil formation due to erosion and later influx of colluvial material, fillıng in topographic lows and burying the residual soil. Soil development begins again and early stages of thick, clayey Bt horizons gradually accumulate.

Stage 4: Continued chemical weathering, in-situ clay formation and lowering of bedrock work in tandem with illuviation and lessivage of pedogenic clay derived from uppermost horizons, which are replenished by additions of colluvium and alluvium. Later stages of thick soil development and significant pore occlusion occur at depths below 2-3 m.

Stage 5: Modern pedogenesis overprinting, or "blurring" of boundaries between genetic units resulting from advanced Ultisol development and maturation during the Middle to Late Holocene.

8.0 CONCLUSIONS

Morphological, textural, geochemical and mineralogical data indicate a polygenetic origin for the genesis of Ultisols and carbonate-derived residuum. Based upon data that include mass-balance calculations for strain (volume change) and translocations of clay-constituent elements, relative to TiO_2, it is apparent that the Mascot Dolomite is the primary parent material for these soils. However, much clay has been introduced and translocated during soil genesis that would require weathering of very significant thickness of dolostone bedrock. It is interpreted that illuviation and lessivage of pedogenic clay from multiple colluvial additions, in conjunction with in-situ clay formation, cooperatively govern the genesis of soils developed on carbonate bedrock. Boundaries between genetic units within the soil residuum and overlying colluvium have been blurred by advanced Ultisol pedogenesis, but are still detectable upon close inspection.

Related studies on advanced Ultisol pedogenesis suggest hundreds of thousands to millions of years required for their development (Birkeland, 1984; Retallack, 2001). The significant maturation of this residuum may have allowed for soil genesis to span intervals of dynamic landscape changes. Recent literature has proposed that periods of landscape instability characterized by colluvial/alluvial activity was common during the Early Holocene, with the landscape becoming more stable and accompanied by intense pedogenesis throughout the Middle to Late Holocene (Driese et al., in press).

9.0 SUGGESTIONS FOR FUTURE RESEARCH

In order to better quantify the time for development of Ultisols, ^{14}C age dating should be performed on a sample at or slightly below 964 cm depth within borehole 1. If the age of the organic material exceeds the range for ^{14}C, then the horizon is clearly a paleosol, and furthermore confirms that the residuum is almost entirely derived from polygenetic inputs of parent materials. Another suggestion for future research includes the possibility of advanced provenance fingerprinting using neodymium isotopes of possible source rocks, such as the stratigraphically overlying Chickamauga Group. To better identify relict surfaces, total organic carbon (TOC) could be measured and plotted with depth. Because the Ultisols present at the Strong Farm are relatively low in organic content, subtle increases in TOC may be easily recognizable. Additionally, entire micromorphological, geochemical, and clay mineralogical analyses should be performed on the remaining core material.

REFERENCES

Alexander, L.T., Beyers, H.G., and Eddington, G., 1939. A chemical study of some soils derived from limestone. USDA Tech. Bull. 678, 28 pp.

Anjos, L.H., Fernandes, M.R., Pereira, M.G., and Franzmeier, D.P., 1998. Landscape and pedogenesis of an Oxisol-Inceptisol-Ultisol sequence in southeastern Brazil. Soil Science Society of America Journal 62, p. 1651-1658.

Arnseth, R.W., and Turner, R.S., 1988. Sequential extraction of iron, manganese, Aluminum, and silicon in soils from two contrasting watersheds. Soil Science Society of America Journal 52, p. 1801-1807.

Ballagh, T.M. and Runge, E.C.A., 1970. Clay-rich horizons over limestone- Illuvial or residual?. Soil Sci. Soc. of America Proc., vol. 34, p. 534-536.

Becker, G.F., 1895. A reconnaissance of the gold fields of the southern Appalachians. U.S. Geol. Surv. 16th Annu. Rep., Part 3. U.S. Gov. Print. Office, Washington DC.

Birkeland, Peter, 1984. Soils and Geomorphology: New York, Oxford University Press, 372 p.

Blake, G.R., and Hartge, K.H., 1986. Bulk density, in Klute, A. (ed.), Methods of soil analysis part I. Physical and mineralogical methods: Soil Sci. Soc. of America Monograph 9 (2nd ed.), p. 363-375.

Brimhall, G.H., Lewis, C.J., Ford, C., Bratt, J., Taylor, G., Warin, O., 1991a. Quantitative geochemical approach to pedogenesis: importance of parent material reduction, volumetric expansion, and eolian influx in laterization. Geoderma, v. 51, p. 51-91.

Brimhall, G.H., Chadwick, O.A., Lewis, C.J., Compston, W., Williams, I.S., Danti, K.J., Dietrich, W.E., Power, M., M., Hendricks, D., Bratt, J., 1991b. Deformational mass transfer and invasive processes in soil evolution: Science, v. 255, p. 695-702.

Brydon, J.E. and Marshall, C.E., 1958. Mineralogy and chemistry of the Hagerstown soil in Missouri. Missouri Agr. Exp. Sta. Res. Bull. 655, 56 pp.

Buol, S.W., Hole, F.D., McCracken, R.J., Southard, R.J, 1997. Soil genesis and classification. Iowa State University Press, Iowa. 527 pp.

Cummings, D., 1959. A study of the basal Chepultepec Sandstone (Cambrian-Ordovician Boundary) in the Ridge and Valley province of Tennessee. Masters thesis Publication, University of Tennessee, 47 pp.

Dreier, R.B., Solomon, D.K., and Beaudoin, C.M., 1987. Fracture characterization in the unsaturated zone of a shallow land burial facility. In Evans, D.D. and Nicholson, T.J. (eds.), Flow and transport through unsaturated rock. Geophysical Monograph 42, 51-59.

Driese, S.G., Mora, C.I., Stiles, C.A., Joeckel, R.M., Nordt, L.C., 2000, Mass-balance reconstruction of a modern Vertisol: implications for interpreting geochemistry and burial alteration of paleoVertisols: Geoderma, v. 95, p. 179-204.

Driese, S.G., McKay, L.D., and Penfield, C.P., 2001. Lithologic and pedogenic influences on porosity distribution and groundwater flow in fractured sedimentary saprolite: an application of environmental sedimentology. Journal of Sedimentary Research 71, p. 843-857.

Fanning, D.S. and Balluff-Fanning, M.C., 1989. Soil morphology, genesis, and classification. John Wiley & Sons Ltd., New York. 395 pp.

Fitzpatrick, E.A., 1983. Soils. Longman, New York. 353 pp.

Fitzpatrick, E.A., 1993. Soil microscopy and micromorphology. John Wiley & Sons Ltd., New York. 304 pp.

Graham, R.C., Daniels, R.B., and Buol, S.W., 1990. Soil-geomorphic relations on the Blue Ridge Front:I. Regolith types and slope processes. Soil Sci. Soc. Am. Journal 54, p. 1362-1367.

Graham, R.C., and Buol, S.W., 1990. Soil-geomorphic relations on the Blue Ridge Front: II. Soil characteristics and pedogenesis. Soil Sci. Soc. Am. Journal 54, p. 1367-1377.

Harris, L.D., 1971. A Lower Paleozoic paleoaquifer- the Kingsport Formation and Mascot Dolomite of Tennessee and southwest Virginia: Economic Geology, v. 66, pp. 735-743.

Hatcher, R.D., Jr., Lemiszki, P.J., Dreier, R.B., Ketelle, R.H., Lee, R.R., Leitzke, D.A., McMaster, W.M., Foreman, J.L., and Lee, S.Y., 1992. Status report on the geology of the Oak Ridge Reservation: Oak Ridge National Laboratory (ORNL/ TM-12074) Environmental Sciences Division, Publication 3860, 244 pp.

Hoover, M.T. and Ciolkosz, E.J., 1988. Colluvial soil parent material relationships in the Ridge and Valley physiographic province of Pennsylvania. Soil Science, vol. 145, no. 3, p. 163-171.

Jacobs, P.M., West, L.T., and Shaw, J.N., 2002. Redoximorphic features as indicators of seasonal saturation, Lowndes County, Georgia. Soil Sci. Soc. Amer., vol. 66, p. 315-323.

Jardine, P.M., Wilson, G.V., Luxmoore, R.J., and McCarthy, J.F., 1989. Transport of inorganic and natural organic tracers through an isolated pedon in a forested watershed. Soil Science Society of America Journal 53, p. 317-323.

Jardine, P.M., Wilson, G.V., and Luxmoore, R.J., 1990. Unsaturated solute transport through a forest soil during rain storm events. Geoderma 46, p. 103-118.

Jeffries, C.D., Rolfe, B.N., and Kunze, G.W., 1953. Mica weathering sequence in the Highfield and Chester soil profiles. Soil Sci. Soc. Proc., vol. 17, p. 337-339.

Jenny, H., 1941. Factors of soil formation. McGraw-Hill Inc., 281 pp.

Luxmoore, R.J., and Ferrand, L.A., 1993. Towards pore-scale analysis of preferential flow and chemical transport. In Russo, D., and Dagan, G. (eds.), Water Flow and Solute Transport in Soils. New York, Springer-Verlag, p. 45-60.

McCaleb, S.B., 1959. The genesis of the red-yellow Podzolic soils. Soil Sci. Soc. Amer. Proc., vol. 23, p. 164-168.

McKay, L.D., Driese, S.G., Smith, K.H., and Vepraskas, M.J., 2002. Hydrogeology and pedology of saprolite formed from sedimentary rock parent material, eastern TN, U.S.A. In Press, 40 pp.

Miller, B.J., 1972. Relationship of soil properties to transformation of carbonate rocks into soil. Doctoral dissertation, University of Tennessee.

Moneymaker, R.H., 1973. Geology of Knox County, Tennessee. Tennessee Division of Geology Bulletin 70, p. 94-101.

Monger, H.C., 1986. Geochemical and mineralogical properties of Copper Ridge and Chepultepec regolith at the Oak Ridge National Laboratory Reservation-West Chestnut Ridge site. Masters thesis publication, University of Tennessee, 112 pp.

Moniz, A.C., and Buol, S.W., 1982. Formation of an Oxisol-Ultisol transition in Sao Paulo, Brazil: I. Double-water flow model of soil development. Soil Science Society of America Journal 46, p. 1228-1233.

Moniz, A.C., Buol, S.W., and Weed, S.B., 1982. Formation of an Oxisol-Ultisol Transition in Sao Paulo, Brazil: II. Lateral dynamics of chemical weathering. Soil Science Society of America Journal 46, p. 1234-1239.

Moore, D.M. and Reynolds, R.C., 1997. X-Ray diffraction and the identification and analysis of clay minerals, 2nd ed.: New York, Oxford University Press, 379 p.

Moore, G.K., 1988. Concepts of groundwater occurrence and flow near Oak Ridge National Laboratory, TN: ORNL/TM-10969, Oak Ridge National Laboratory, Oak Ridge, TN.

Moore, G.K., 1989. Groundwater parameters and flow systems near Oak Ridge National Laboratory, TN: ORNL/TM-11368, Oak Ridge National Laboratory, Oak Ridge, TN.

Morgan, C.G. and Obenshain, S.S., 1942. Genesis of three soils residual from limestone. Soil Sci. Soc. Amer. Proc., vol. 7, p. 441-447.

Mubiru, D.N. and Karathanasis, A.D., 1994. Loess rejuvenation effects on intensely weathered soils of south-central Kentucky. Soil Science, vol 157, no. 4, p. 244-251.

Nash, V.E., 1963. Chemical and mineralogical properties of an Orangeburg profile. Soil Sci. Soc. Proc., vol. 27, p. 688-693.

O'Brien, E.L. and Buol, S.W., 1984. Physical transformations in a vertical soil-saprolite Sequence. Soil Science Society of Amenca Journal 48, p. 354-357.

Oder, C.R. and Miller H.M., 1945. Stratigraphy of the Mascot-Jefferson City zinc district, Tennessee. American Institute of Mining, Metallurgical, and Petroleum Engineers, Technical Publication, 9 p.

Pearson, R.W. and Ensminger, L.E., 1949. Types of clay minerals in Alabama soils. Soil Sci. Soc. Proc., vol. 13, p. 153-156.

Plaster, R.W. and Sherwood, W.C., 1971. Bedrock weathering and residual soil formation in Central Virginia. Geol. Soc. Amer. Bull., vol. 82, p. 2813-2826.

Schoeneberger, P.J., Amoozegar, A., and Buol, S.W., 1995. Physical property variation of a soil and saprolite continuum at three geomorphic positions. Soil Science Society of America Journal 59, p. 1389-1397.

Scott, H.D., 2000. Soil physics: Agricultural and environmental applications. Iowa State Univ. Press, Ames. 421 p.

Simonson, R.W., 1949. Genesis and classification of red-yellow Podzolic soils. Soil Sci. Soc. Proc., vol. 14, p. 316-319.

Singer, M.J., Janitzky, P., 1986, Field and laboratory procedures used in a soil chronosequence study: United States Geological Survey Bulletin, v. 1648, 49 p.

Smith, K., 2001. Influence of illuviated clays and soil cements on hydraulic conductivity in sedimentary saprolite. Masters thesis publication, University of Tennessee, 111 pp.

Soil Survey Staff, 1994, Keys to soil taxonomy: Blacksburg, Virginia, Pocahontas Press, 328 p.

Stolt, M.H., and Baker, J.C., 1994. Strategies for studying saprolite and saprolite genesis. In Cremens, D.L., Brown, R.B., and Huddleston, J.H. (eds.), Whole regolith pedology. Soil Science Society of America Special Publication 34, 1-19.

Stolt, M.H., Ogg, C.M., and Baker, J.C., 1994. Strongly contrasting redoximorphic patterns in Virginia Valley and Ridge paleosols. Soil Sci. Soc. Amer., vol. 58, p. 477-484.

U.S.G.S., 1966. Geologic map: John Sevier Quadrangle, Knox County, Tennessee.

Walker, K.R., 1985. The geologic history of the Thorn Hill Paleozoic section (Cambrian-Mississippian), eastern Tennessee. SE-GSA Field Trip Guide. p. 43-50.

Watson, K.W., and Luxmoore, R.J., 1986. Estimating macroporosity in a forested watershed by use of a tension infiltrometer. Soil Science Society of America Journal 52, p. 325-329.

Wharton, C.F., 1965. Relationship of the characteristics of some Ultisols on the Western Highland Rim in Tennessee to parent material, relief, and time of formation. Doctoral dissertation, University of Tennessee.

Wilson, G.V., Alfonsi, J.M., and Jardine, P.M., 1989. Spatial variability of saturated hydraulic conductivity of the subsoil of two forested watersheds. Soil Science Society of America Journal 53, p. 679-685.

Wilson, G.V., Jardine, P.M., and Luxmoore, R.J., 1990. Hydrology of forested watershed during storm events. Geoderma 46, p. 119-138.

Wilson, G.V., Jardine, P.M., O'Dell, J.D., and Collineau, M., 1993. Field-scale transport from a buried line source in variable saturated soil. Journal of Hydrology 145, p. 83-109.

APPENDICES

Appendix A: Macromorphology

Borehole 1

BOREHOLE	DEPTH (cm)	HORIZON	COLOR (moist)	COLOR (mottles)	TEXTURE	DESCRIPTION
B1	0-14	Ap	10YR 4/2		gcl	grass and fine roots, chert gravel are 1 to 5 cm (< 30%), abrupt surface boundary (anthropogenic fill)
B1	14-26	AE	10YR 4/3		sl	fine (<1cm) and disseminated chert fragments (<15%)
B1	26-47	BE	10YR 4/2		scl	Mn-oxide concretions (<1cm), gradational boundary to Bt1
B1	47-57	Bt1	10R 4/6		c	Mn-oxide concretions (mostly <1mm, some <0 5cm), sharp contact with very fine-grained sandy zone, vf-f and disseminated chert fragments
B1	57-59	Bt1 Interbed	5Y 8/1	5Y 6/6	vfs	enigmatic origin, possible fluvial or pedogenic origin, mottled region 1-2 cm surrounding fine-med grained sands
B1	59-233	Bt2	10R 4/8	10YR 7/6 (10%)	c	disseminated Mn-oxide concretions/particles, highly weathered chert fragments at 101 & 125 cm (<1mm 75%, <1cm 25%), yellowish-orange mottles ~2-5cm & concentrated at 115-118 cm & 145-155 cm, presence of Mn-oxide fades out and is lost at ~110 cm, sharp contact with organic-rich layer
B1	233-239	Bt2 Interbed	10YR 4/3	5YR 6/8 (15%)	mosc	med grained sands are well-sorted with some organic matter, vf roots, Mn-oxide concretions (<3mm), chert fragments (<2-3cm), minor mottles (~5%), sand grains are concentrated at base of organic matter
B1	239-367	Bt3	2 5YR 4/8	7 5YR 6/8 (20%)	c	minor to no chert except at 286-290 cm (mod weathered fragments <4 cm across), mottled region with redox features surrounding (<1cm) chert fragments, wavy sharp contact with underlying organic-rich zone
B1	367-370	Bt3 Interbed	10YR 4/3		vfol	silty-fine grained sands are mixed dolomite & well-rounded qtz, presence of angular dolostone/limestone (<15%), fine-subangular blocky ped structure, black chert (minor), possible fragipans
B1	370-470	Bt3	2 5YR 4/8	7 5YR 6/8 (20%)	c	minor to no chert until 418 cm and lower (<1 cm and concentrated in thin bands <2 cm), mottles scattered throughout, Mn-oxide lining ped faces
B1	470-591	Bt4	2 5YR 4/8	7 5YR 6/8 (20%) 10R 3/4 (10-15%)	c	similar to above but also contains red mottles & overall more pervasive mottling, chert fragments (<5-10%) and Mn-oxide concretions (~5%) are < 1 cm (rare chert ~3cm), some chert and ped faces lined with Mn-oxide, sharp contact with underlying sandy layer
B1	591-602	Bt4 Interbed	2 5Y 7/4		vfs	fine-med grained sands, unconsolidated to very weakly cemented, enigmatic origin, possible fluvial or pedogenic origin, also possible sandstone interbed origin
B1	602-707	Bt5	2 5YR 3/6	10YR 8/8 (25%) 7 5YR 6/8 (15%) 2 5Y 5/3 (10%)	sic	heavily mottled, black chert (<10%, <1 cm), minor Mn-oxide concretions (<3 mm), ~625 cm possibly showing convoluted bedding (saprolite interbed-?), sharp contact w/ underlying sands
B1	707-709	Cr	7 5YR 4/4		f-msc	presence of micaceous material, friable to slightly cemented, enigmatic origin
B1	709-964	Bt6	7 5YR 6/8	7 5YR 4/4 (20%) 2 5YR 3/6 (20%) 10YR 8/8 (20%)	c	similar to Bt5 but with major gray chert fragments/interval at 715-722 cm (< 4 cm), white-gray kaolinitic (?) clay on ped faces and surrounding chert, Mn-oxide pervasively lining ped faces (~5%), convoluted bedding (saprolite interbed- ?) with kaolinitic zones 2-5 mm thick
B1	964-1058	BC	2 5Y 4/4	7 5YR 6/8 2 5YR 3/6	c	slightly greenish-brown moist clay, minor angular chert, some chert with silty rinds, minor dolostone/limestone (<1 cm), disseminated Mn-oxide (<2%), surface of core plug at 1056-1058 cm depth contain thin coat of sitly-vfg dolomitic/lime sands (effervesces with acid)

Key to textural classes: vf- very fine-grained, f- fine-grained, m- medium-grained, c- clay, si- silt, s- sand, g- gravel, l- loam, o- organic.

Borehole 2

BOREHOLE	DEPTH (cm)	HORIZON	COLOR (moist)	COLOR (mottles)	TEXTURE	DESCRIPTION
B2	0-12	Ap	10YR 4/2		sl	grass and fine roots present, minor chert (< 5 cm), gradational contact with underlying Ae horizon
B2	12-41	AE	10YR 3/3		cl	fine roots present, minor chert (< 5 cm), gradational contact with underlying Be horizon
B2	41-92	BE	10YR 3/4		sicl	fine roots present, minor chert (<2 cm & some diss-emminated), Mn-oxide lining ped faces & disseminated (2-5%), gradational change to silty clay (10YR 4/6) with slightly higher chert & Mn-oxide (5-10% each), gradational contact with under-lying Bt horizon
B2	92-182	Bt1	5YR 4/6		c	chert fragments present (5%, light gray to white, mostly diss-emminated, <1 cm, mod.-deeply weathered), Mn-oxide lining ped & chert faces also found as small concretions (<5%, <2 mm)
B2	182-336	Bt2	5YR 4/6	7 5YR 6/8 (15%) 10R 3/4 (10%)	c	similar to Bt_1 but with associated mottles, 7 5YR 6/8 mottles quickly grades into more reduced color (10YR 6/6), significant chert zones at 251-254, 264-267, 298-300, & 307-310 cm (<2 cm) , minor Mn-oxide lining ped faces, overall gradational contact with Bt_3
B2	336-390	Bt3	5YR 4/6	10YR 6/6 (25%) 10R 3/4 (15%)	c	similar to Bt_2 but with different mottling, chert fragments similar to above but only mod. weathered, gradational contact with Bt_4
B2	390-460	Bt4	5YR 4/6	10YR 6/6 (40%) 10R 3/4 (20%)	c	similar to Bt_3 but with different mottling, significant chert zone at 392-396 cm (<2 5 cm)

Borehole 3

BOREHOLE	DEPTH (cm)	HORIZON	COLOR (moist)	COLOR (mottles)	TEXTURE	DESCRIPTION
B3	0-20	Ap/AE	5YR 3/3		csl	grass and fine roots present, chert fragments (rounded & sub-angular with some occurring as cauliflower chert, up to 1 cm across), Mn-oxide present as infillings within cauliflower chert & as concretions (< 4 mm), gradational contact with under-lying Bt_1 (no obvious BE horizon)
B3	20-98	Bt1	10R 4/6	7 5YR 6/6	c	very fine roots present, mostly disseminated chert (minor; <2 mm), Mn-oxide concretions (minor; < 2mm), clay gradationally becomes denser, significant chert layer at 98-101 cm (<2 cm , 20%, mod. weathered) with mottles surrounding zone, Mn-oxide gradationally not present at 98 cm)
B3	98-220	Bt2	10R 4/6	5Y6/4 (20%) 7 5YR 6/6 (10%) 2 5YR 3/4 (10%)	c	similar to Bt_1 but with mottles present, 5Y 6/4 mottles shows evidence of redox depleted conditions
B3	220-344	Bt3	10R 4/6	5Y 6/4 (35%) 7 5YR 6/6 (10%) 2 5YR 3/4 (10%)	c	similar to Bt_2 but with different mottling, cherty zones at 250-254 (mod.-deeply weathered, <1 5 cm), 302-307(slightly-mod. weathered, same size), & 315-338 cm (mod. weathered, <3 cm), red illuviated clay (mottle 2 5YR 3/4) up to 20% at ~250cm
B3	344-504	Bt4	10R 4/6	2 5YR 3/4 (25%) 5Y 6/4 (25%) 7 5YR 6/6 (10%)	c	similar to Bt_3 but with different mottling, minor Mn-oxide con-cretions & lining ped faces (<3mm) occurring mostly adjacent to deeply weathered chert fragments (<2mm), cauliflower chert fragments at 437-441 & 456-459 cm (<2 cm across, one with drusy quartz crystals), sharp contact at 504 with illuviated red clay "plume" heavily concentrated above contact
B3	504-505	Bt4 Interbed	10YR 4/3		sl	wavy contact with over/underlying horizons, brown loamy material appears slightly cemented and contains subrounded "soil" clasts, clasts left undisturbed for future petrographic analysis (B3-P1)
B3	505-575	Bt4	10R 4/6	2 5YR 3/4 (25%) 5Y 6/4 (25%) 7 5YR 6/6 (5%) 10YR 7/3 (5%)	c	similar to Bt_4, major chert fragments/comminuted interval at 545-558 cm (<2 cm , mod.-deeply weathered) with presence of fine qtz sand within surrounding 1 cm clay matrix (10YR 7/3)
B3	575-586	Bt5	10R 4/6		sc	zone of f-m grained, rounded qtz sandy clay is same color as dominant clay, no mottling is present around region
B3	586-665	Bt6	2 5YR 4/8	2 5YR 3/4 (15%) 10YR 7/6 (15%)	sc	sandy clay pockets present (similar to above, ~2 cm wide, 10-15%) , chert frag- ments scattered (5%, mod. weathered), Mn-oxide concretions (<1 cm) & lining ped faces, chert fragments, & sandy pockets
B3	665-710	Bt7	2 5YR 4/8	10YR 6/8 (50%)	c	thin (1-3 mm) wavy-concentric bands of mottles, mottling is more organized/structured with increasing depth (possibly showing convoluted bedding (saprolite interbed- ?), Mn-oxide same as above
B3	710-724	Bt8	2 5YR 4/8	5YR 2 5/1 (30%)	c	overall browner, much wetter clay, Mn-oxide lining ped faces/ mottled surfaces (15%), gradational contact with underlying clay
B3	724-730	Bt9	5YR 2 5/1	2 5YR 4/8 (30%)	c	increasingly brown color; Mn-oxide lining ped faces/ mottled surfaces (10%)

Borehole 4

BOREHOLE	DEPTH (cm)	HORIZON	COLOR (moist)	COLOR (mottles)	TEXTURE	DESCRIPTION
B4	0-9	Ap	10YR 3/2		gsl	gravelly silt loam, grass and fine roots, chert gravel < 1 5 cm across (cauliflower chert also present), gradational contact with Ae
B4	9-18	AE	10YR 4/4		sl	fine & very fine roots, disseminated chert (< 1mm), gradational contact w/ BE
B4	18-46	BE	10YR 5/6		sc	very fine roots (near top), chert fragments include cauliflower type (< 0 5 cm, mostly disseminated, deeply weathered, <5%), Mn-oxide present as concretions (<2mm, < 5%) and as complete infillings w/in cauliflower chert, gradational contact with Bt_1 (onset of very high concentration of red illuviated clays)
B4	46-60	Bt1	10R 4/6		c	clay, homogenous and dense, minor chert fragments (<3mm, deeply weathered)
B4	60-61	Interbed	7 5YR 5/6		vfgssi	no presence of micas, vfg sands are very well-rounded & sorted
B4	61-78	Btl	10R 4/6		c	same as Btl
B4	78-79	Interbed	7 5YR 5/6		vfgssi	no presence of micas, vfg sands are very well-rounded & sorted
B4	79-363	Bt2	10R 4/6	10YR 6/6 (10%) 10R 3/4 (5%)	c	similar to Bt1, but with minor disseminated chert, minor Mn-oxide concretions (<2mm , mostly disseminated), mottles are scattered, chert fragments mostly limited to 231-232 cm, 315-317 cm, and 331-333 cm (mod -deeply weathered, <1cm), Mn-oxide gradationally not present @ 185 cm)
B4	363-494	Bt3	10R 4/6	7 5YR 6/8 (20%) 2 5Y 7/6 (15%) 10R 3/4 (5%)	c	similar to Bt2, significant chert interval marks contact w/ Bt_2 & may suggest colluvial deposit due to presence & signature of Mn-oxide (most Mn-oxide found in BE + Bt1 horizons in other cores, <4mm , 5-10% near base of 363-376 cm chert interval), other chert fragments are scattered (<0 5cm , mostly disseminated), sharp contact with Bt_4 clay gradually becoming wetter w/ depth
B4	494-572	Bt4	2 5Y 7/6	7 5YR 6/8 (15%) 10R 4/6 (10%) 10R 3/4 (10%) 2 5Y 8/3 (10%)	c	clay with thick (<1cm) wavy zones of kaolinitic-like clays, Mn-oxide present as thin linings on ped faces & also disseminated, clay gradually becoming wetter w/ depth
B4	572-590	Bt5	7 5YR 6/8	5YR 4/6 (25%) 10R 4/6 (20%) 2 5Y 7/6 (20%) 10R 3/4 (10%)	vfsc	sandy clay, vfg highly oxidized quartz sands, significant chert interval from 590-593 cm (<2cm , slightly weathered), sands only occur as pockets or disseminated within horizon (25% of horizon is vfg sands), < 5% Mn-oxide concretions (<2mm) and lining ped faces, sharp contact with Bt6, sands are well-sorted and rounded
B4	590-645	Bt6	2 5Y 7/6	7 5YR 6/8 (35%)	c	Similar to Bt5, lacks kaolinite, 5-10% Mn-oxide lining peds and concretions (<3mm) & disseminated, lacks vfg sands, sharp contact w/ chert frags /interval @ 645 cm
B4	645-765	Bt7	10R 4/6	10R 3/4 (20%) 2 5y 4/4 (20%) 7 5YR 6/8 (10%)	sc	Transition into darker/redder colors overall, kaolinitic zone @ 677-680 cm mixed with brown clay and w/ rind of vfg-sandy clay (same as 572-590 cm) and an outermost rind of Mn-oxide (<2mm), chert fragments (<0 5cm, mostly disseminated, very deeply weathered), Mn-oxide present lining peds and pore walls (<3mm thick) and as concretions (<3mm), wavy-sharp contact w/ Bt8
B4	765-831	Bt8	2 5Y 4/4	10R 4/6 (15%) 5Y 6/2 (10%)	gcs	Much browner overall, thick (<0 5cm) seam of kaolinite @ contact, scattered chert fragments (10-15%, deeply weathered) often containing coat of kaolinite (<2cm), sharp contact w/ Bt9
B4	831-863	Bt9	2 5Y 6/6	2 5YR 4/6 (10%) 10R 3/4 (10%) 10YR 7/6 (10%) 5YR 5/8 (5%)	c	Significant chert interval from 831-838 cm (slightly-mod. weathered, <3cm), gradational sandy contact w/ Bt10
B4	863-874	Bt10	2 5YR 4/6	5YR 5/8 (25%) 2 5Y 6/6 (20%) 10YR 7/6 (15%)	cs	Clayey-sand, sands are med -grained (80% sands, 20% clay) and well sorted +rounded, sands show oxidized color (red/orange), minor Mn-oxide as seam w/in sands (<1mm thick), no micas
B4	874-880	Bt11	2 5Y 6/6	2 5Y 3/3 (10%) Gley 2 6/10B (10%)	gc	Sharp contact w/ overlying Bt10, Blue-gray chert (<0 5cm) with presence of bluish-white kaolinite, minor Mn-oxide lining ped faces

Borehole 5

BOREHOLE	DEPTH (cm)	HORIZON	COLOR (moist)	COLOR (mottles)	TEXTURE	DESCRIPTION
B5	0-11	Ap	10YR 3/2		gsl	Grass and fine roots, sub-angular blocky peds, disseminated chert (< 5%), gradational contact with AE
B5	11-23	AE	10YR 3/3		s	Fine-med. roots, disseminated chert, gradational contact w/ BE
B5	23-63	BE	10YR 5/6		sc	Very fine roots near top, mostly disseminated chert w/ some cauliflower variety w/ inside completely filled w/ Mn-Oxide, reg chert (< 1 cm) w/ 3 mm Mn-oxide rinds, Mn-oxide also present as concretions (<2mm), minor red (Fe) concretions (10R 4/8, <2mm), gradational contact w/ Bt_1
B5	63-131	Bt1	5YR 4/6	2 5Y 8/2 (10%) 10R 3/4 (5%)	sc	Disseminated chert, Mn-oxide concretions (< 1cm, 5%), Bt_1 not as "red" as other cores' Bt_1, wavy-sharp contact w/ Bt_2
B5	131-148	Bt2	5YR 4/6		sc	Silty-clay similar to Bt_1, fragments of vfg-sandstone/siltstone (10YR 8/4) w/ NO micas and NO effervescence (<1cm), disseminated Mn-oxide / concretions (<1mm) w/in silty clay, sharp contact w/ chert interval (148-150 cm, mod. weathered)
B5	148-229	Bt3	5YR 4/6	5YR 5/8 (10%) 10R 3/4 (5%)	c	Scattered chert frags (<1cm, mod.-deeply weathered, 5-10%), Mn-oxide concretions (<0 5cm, 5%) and disseminated, sharp contact w/ mottled brown clay below
B5	229-237	Bt4	2 5Y 4/4	5YR 4/6 (40%) 10R 3/4 (10%)	c	Greenish-brown clay, disseminated chert and Mn-oxide, sharp contact w/ underlying weathered dolostone frags. + silts (tan-white, 2 5Y 8/1)
B5	237-251	Cr	2 5Y 8/1		gs	Mod.-deeply weathered dolostone fragments (<3mm) and silts, effervesces w/ HCl acid, sharp contact w/ Btg
B5	251-294	Bt5	10YR 3/3	2 5Y 4/4 (15%) 5YR 4/6 (10%)	c	Greenish-brown clay, mostly disseminated chert (some <3mm), clay becoming more moist w/ depth, minor red clay concretions (10R 4/8), mottles are scattered and irregular, sharp contact w/ Bt_5
B5	294-312	Bt6	10R 4/8	10YR 3/3 (30%) 10R 3/4 (20%)	c	Dense clay, minor deeply weathered dolostone (almost clay-like, <5mm, whitish-gray), minor Mn-oxide concretions (<3mm), sharp contact with Bt_6
B5	312-330	Bt7	10YR 3/3	10YR 3/3 (10%) 2 5Y 4/4 (20%)	gsc	Scattered dolostone (slightly-deeply weathered, grayish-white, <1cm), wavy-clear contact with Bt_7
B5	330-350	Bt8	10YR 3/3	10YR 3/3 (30%) 10R 3/4 (10%)	c	Similar to Bt_5, but with 5-10% deeply weathered bedrock, 5% Mn-oxide, sharp contact with 2Cr
B5	350-368	Cr2	10YR 2/2		gs	Whitish-tan, deeply weathered dolostone bedrock w/ dolostone silts, fragments are <4cm diameter, dense dark clay rind bordering contact (<0 5cm thick, 10YR 2/2)

Borehole 6

BOREHOLE	DEPTH (cm)	HORIZON	COLOR (moist)	COLOR (mottles)	TEXTURE	DESCRIPTION
B6	0-15	Ap	10YR 4/3	5YR 4/6 (15%)	l	Fine-med. roots, moderate-fine granular ped fabric
B6	15-35	Bt1	2 5YR 4/6	7 5YR 6/8 (30%)	c	Fine roots, moderate-fine subangular blocky peds,distinct clay films on faces of peds and lining pores, chert fragments (white-gray, mod.-deeply weathered, 5%)
B6	35-110	Bt2	2 5YR 4/6	7 5YR 6/8 (40%)	c	Few very fine roots, subangular blocky peds, distinct clay films on faces of peds, chert gravel, and lining pores, ~2% chert (same as above), gradational boundary w/ Bt_3 (including color variation)
B6	110-138	Bt3	10R 4/6	10YR 7/8 (10%)	c	Subangular blocky peds, minor mottling; < 5% chert gravels (mod.-deeply weathered)
B6	138-196	Bt4	10R 4/6	10YR 7/8 (30%)	c	Subangular blocky peds, more prominent yellowish mottles, ~5% chert towards bottom (mod. Weathered, < 1 cm)
B6	196-243	Bt5	10YR 7/3	2 5Y 4/4 (20%) 10R 4/6 (20%)	c	Subangular blocky peds, more dynamic mottling present, minor disseminated chert
B6	243-295	Bt6	10YR 7/8	10R 4/6 (25%)	c	Subangular blocky peds, chert fragments (mod. Weathered, < 1 5 cm), saprolitic signature present from 250-260 cm

Borehole 7

BOREHOLE	DEPTH (cm)	HORIZON	COLOR (moist)	COLOR (mottles)	TEXTURE	DESCRIPTION
B7	0-9	Ap	10YR 4/3		gs	Sub -angular blocky peds, grass + fine roots, scattered chert chert fragments (<10%, <1cm) and disseminated, Mn-oxide lining chert fragments, some chert w/ red clay coats
B7	9-16	AE	10YR 3/3		gsl	Sub -angular blocky peds, very fine and fine roots, scattered chert (<20%), Mn-oxide same as above, clear-gradational contact w/ BE
B7	16-37	BE	10YR 5/6		gsc	Very fine roots near top, significant chert interval @ 24-33 cm (<3cm), scatterered chert fragments (<1 5cm) w/ some as cauli-flower w/ Mn-oxide and red clay infillings, minor red clay concretions (<3mm, 10R 4/8), gradational contact w/ Bt_1
B7	37-82	Bt1	5YR 4/6		c	Scattered chert fragments (<1cm, 10%) and disseminated, significant chert interval @ 82-86cm (<3cm, white, deeply weathered, Mn-oxide concretions (<0 5cm, <5%) and disseminated
B7	82-133	Bt2	5YR 4/6	5YR 6/8 (10%)	c	Similar to Bt_1, but without Mn-oxide, minor disseminated chert
B7	133-302	Bt3	5YR 4/6	10R 3/4 (25%) 10YR 6/8 (15%)	c	Significant chert intervals @ 133-136 cm and 151-158 cm (<2cm, grayish-white, mod -deeply weathered), chert fragments @ 270-272 <1cm), clear-gradational boundary w/ Bt_4
B7	302-341	Bt4	2 5Y 7/8	5YR 4/6 (30%) 10R 3/4 (5%)	c	Clay showing more reduced colors, no chert fragments or Mn-oxide, one small zone of kaolinite (1cm^2), clear boundary w/ Bt_5
B7	341-481	Bt5	5YR 4/6	10R 3/4 (15%) 2 5Y 7/8 (5%)	c	Minor disseminated chert, Mn-oxide concretions (<3mm, <5%) and lining ped faces
B7	481-536	Bt6	5YR 4/6	10YR 4/3 (35%) 10R 3/4 (5%) 7 5YR 6/8 (5%)	c	Scattered chert fragments (<1cm, 10%, tan, deeply weathered), Mn-oxide lining ped faces (<3mm thick), sharp contact w/ Bt_7
B7	536-574	Bt7	5YR 5/8		c	Significant chert interval @ 536-538 cm, no mottling, very minor disseminated chert, homogenous dense clay; gradational contact with Bt_8
B7	574-599	Bt8	5YR 5/8	10YR 4/3 (30%)	c	Scattered and disseminated chert (<0 5cm, 5-10%, very deeply weathered, Mn-oxide concretions (<2mm, <5%) and lining peds, sharp contact with Bt_9
B7	599-655	Bt9	5YR 5/8	10R 3/4 (15%) 10YR 4/3 (10%) 2 5Y 6/8 (10%)	c	Significant chert interval @ 599-602 (<0 5cm), minor scattered & disseminated chert (<0 5cm, very deeply weathered), Mn-oxide concretions (<3mm, 10%) and lining ped faces, no bedrock at base of core

Appendix B: Gravimetric Water Content for Boreholes B2-B3, B5-B7

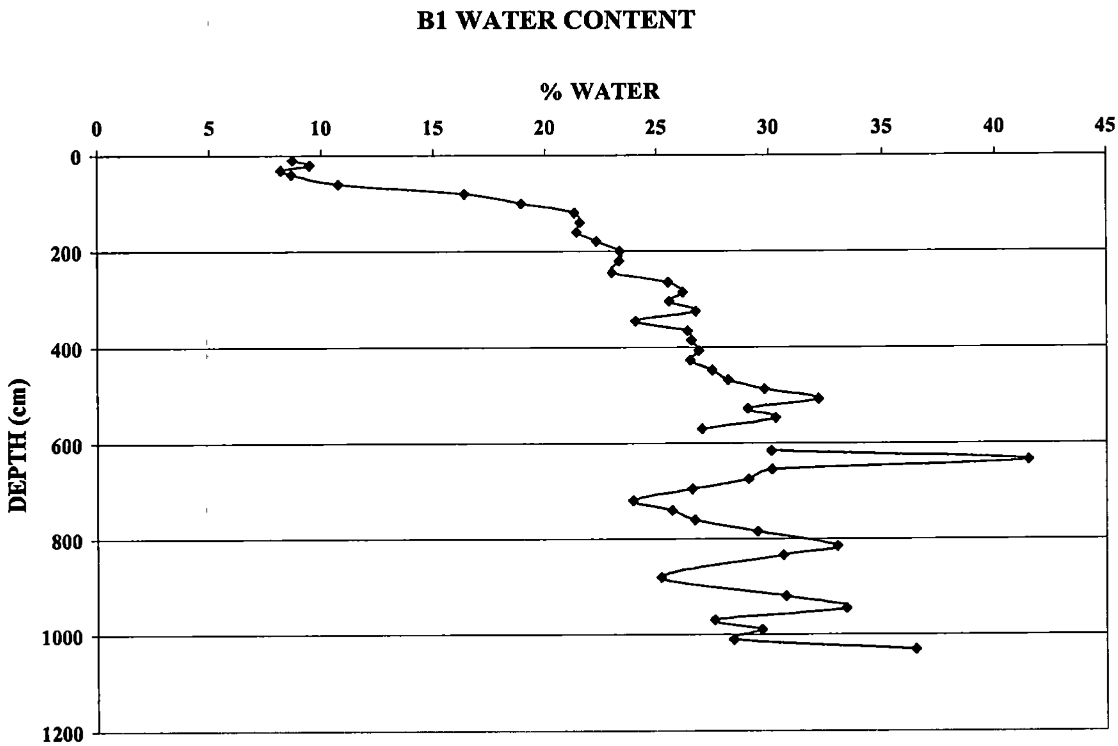

B2 WATER CONTENT

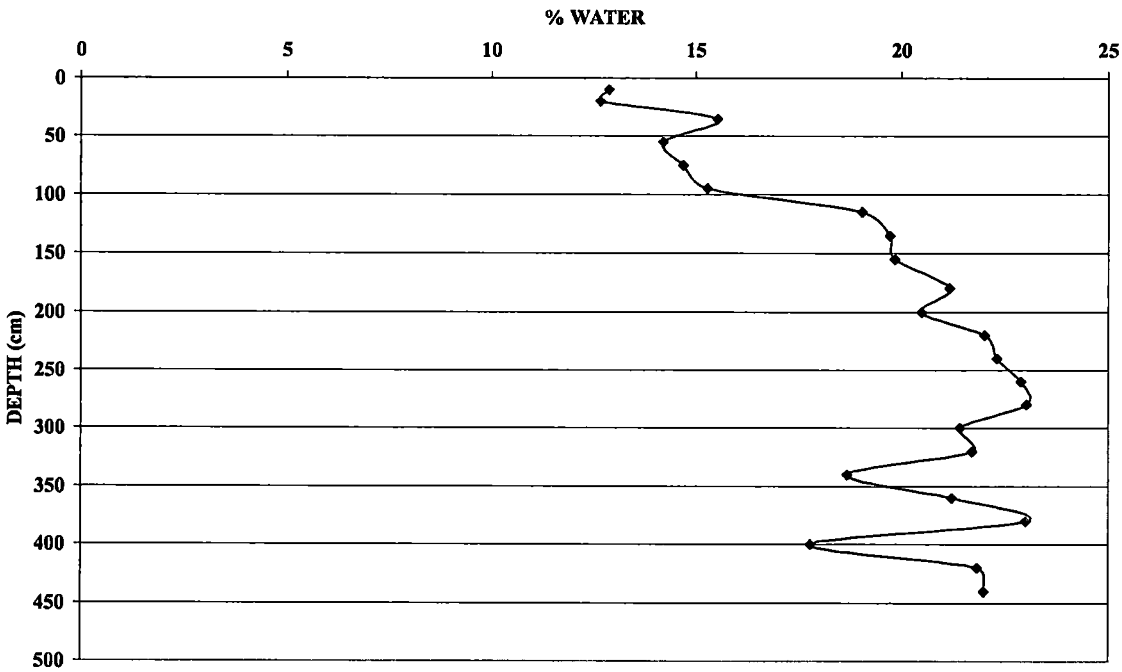

B3 WATER CONTENT

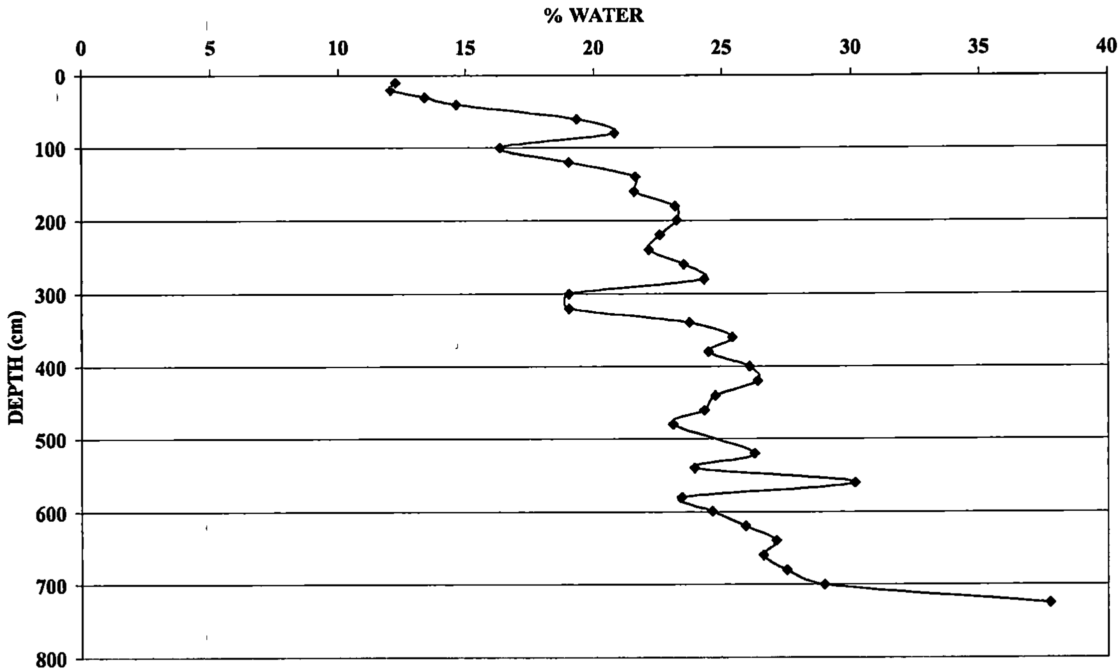

B4 WATER CONTENT

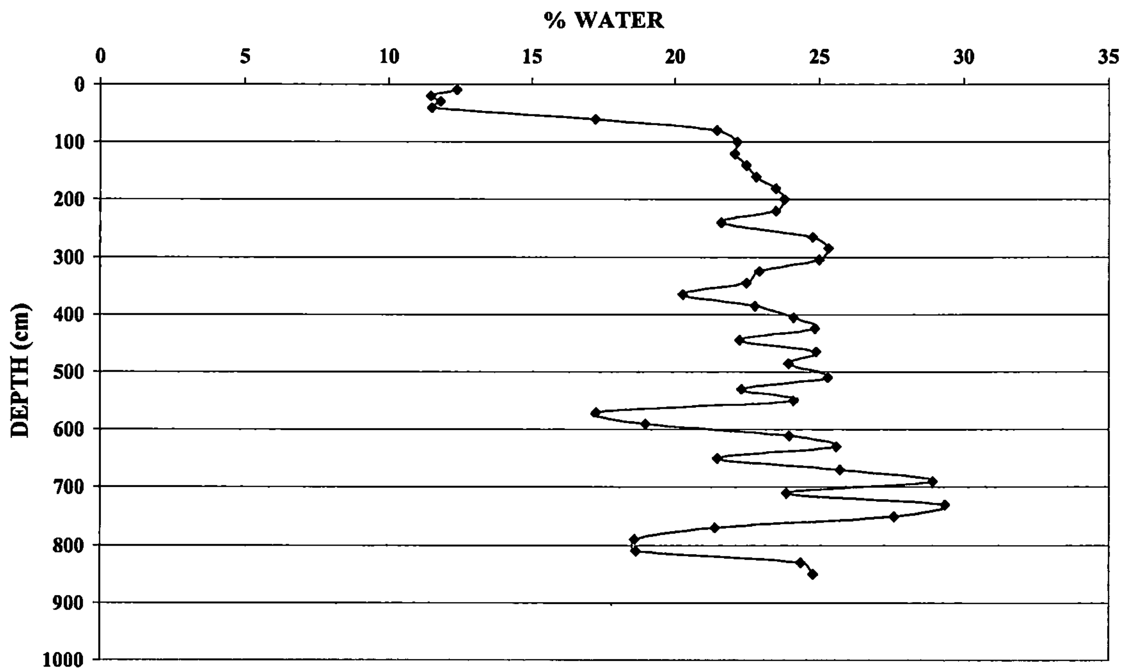

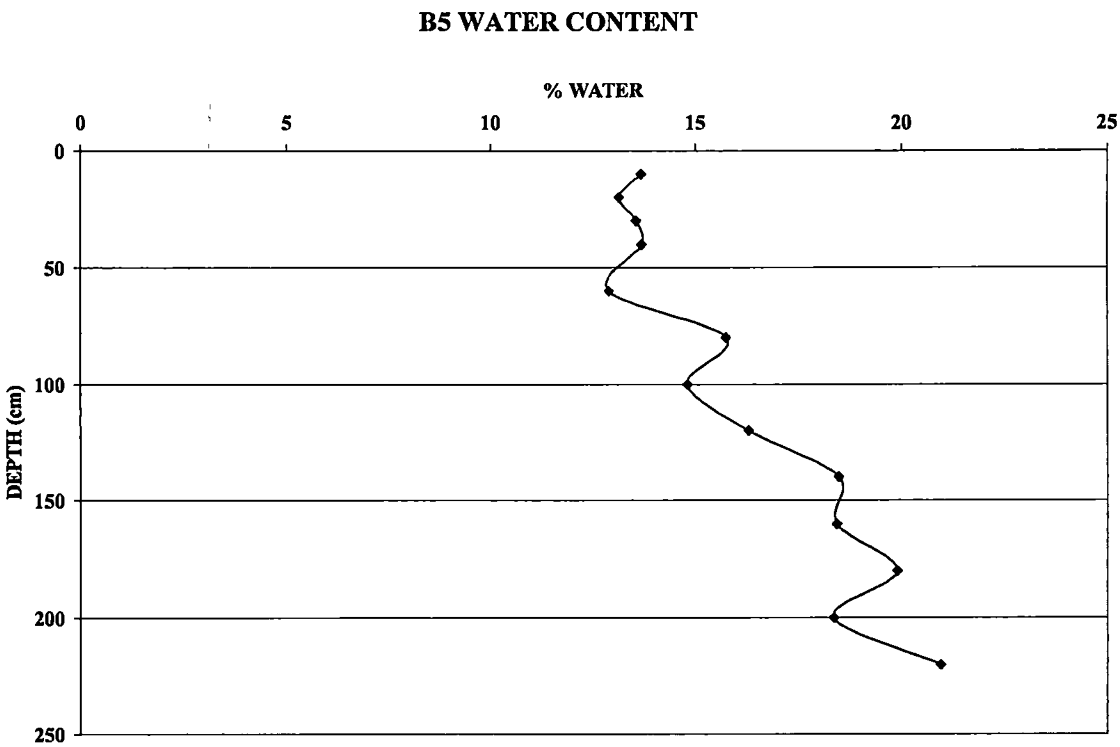
B5 WATER CONTENT
% WATER
0
5
10
15
20
25
DEPTH (cm)
0
50
100
150
200
250

B7 WATER CONTENT

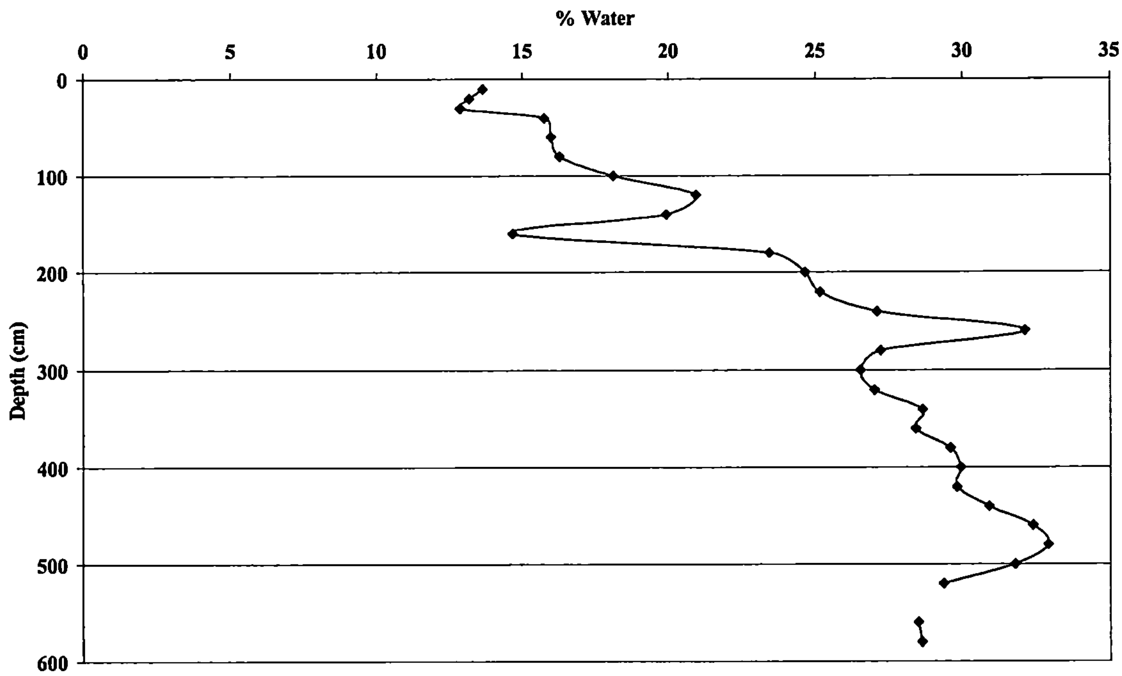

Appendix C: Thin-section Micrographs

All thin-sections are 7.5 cm by 5 cm, images shown below are approximately 1:1.
Up orientation is towards the top of the page.
All images were scanned using a flat-bed scanner with transparency attachment.

Borehole 1

43-51 cm depth
Thin-section showing gradational boundary between BE and Bt1 soil horizons.
Note common, large multigenerational Fe-oxide concretions.

233-239 cm depth
Highly oxidized clay with loamy interbed possibly representing surficial (A or BE) sandy loam infillings within a decayed root pore.

367-373 cm depth, Soil Horizon Bt1, silty clay
Possible loamy infilling within root pore, pedogenic clay coloration and mottling clearly showing active macropores.

554-562 cm depth, Soil Horizon Bt4, clay
Well-developed, Fe-rich pedogenic clay coatings. Note weathering rim around perimeter of dolostone fragments.

595-602 cm depth, Soil horizon ?, silty sand. Heavily mottled horizon composed largely of fine to med.-grained Qtz. sands and dolomite silts. Sands are sub. to well-rounded, as are common pedogenic clay papules. Note the subrounded calcareous siltstone lithorelicts toward the bottom left.

671-678 cm depth, Soil horizon Bt5, gravelly sandy clay. Large fragments of moderately weathered dolostone (similar to Mascot) that grades downward into well-rounded f/mg sands. Note the lighter colored, deeply weathered sandstone lithorelicts directly above large dolostone fragment in the middle.

707-714 cm depth, Soil horizon Cr
Gravelly sandy clay.
Prominent features include many deeply weathered sandstone lithorelicts, zones of silt infillings and redox. mottling.

796-803 cm depth, Soil horizon Bt6
Gravelly silty clay. All RF and sand grains are angular. Heavily mottled and convoluted bands of multigenerational pedogenic clays and Fe-oxide coats. Angular ped. clay papules and vfg -sandstone lithorelicts.

979-986 cm depth, Soil horizon Cr2
Gravelly silty clay.
Note the horizontal relict bedding of deeply weathered shale and siltstone lithorelicts.
Deeply weathered plant material / root traces.
RF include coarse-equant dolostone and oolitic/pelloidal dolostone.

1023-1030 cm depth, Soil horizon Bt7
Clay
This may represent BE horizon (toward top) and transition into Bt1 of the true soil residuum.
Very clay-rich, common RF, few root traces and burrows with dolomite silt + silt/vfg- Qtz. infillings, presence of fecal material

Borehole 2

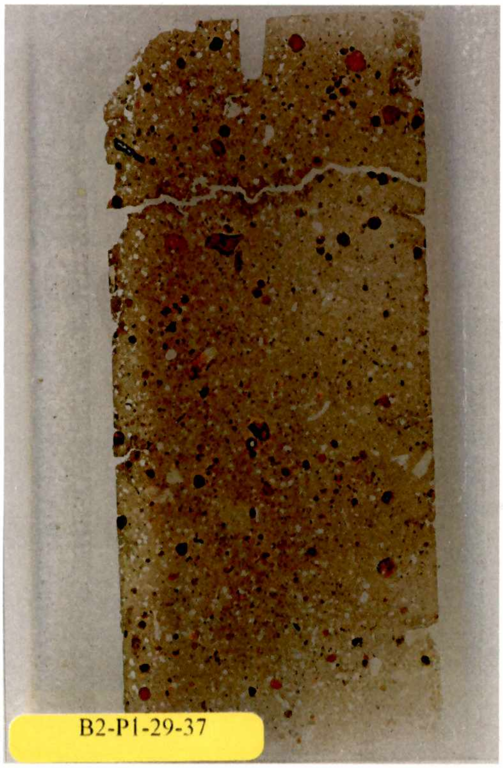

29-37 cm depth, Soil horizon Ae
Clay loam
Fine and very fine roots and common, large multigeneration Fe-oxide concretions.

412-417 cm depth, Soil horizon Bt4
Clay
Dense homogenous clay with some near horizontal bands of very deeply weathered siltstone lithorelicts and thick bands of pedogenic clay.

Borehole 4

3-10 cm depth, Soil horizon A
Loam
Abundent vermiform and insect fecal material near top of slide.

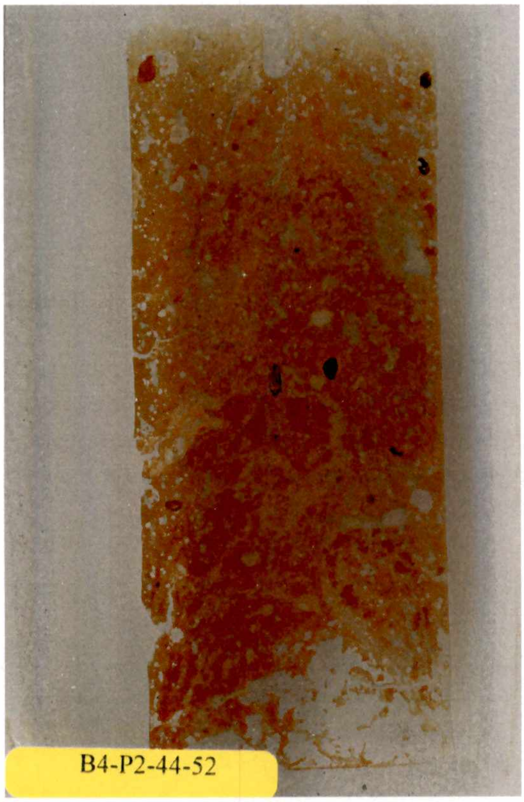

44-52 cm depth, Soil horizon BE + Bt1
Silty clay
Very few very fine roots near top, common dessication cracks, macropores quickly become occluded with pedogenic clay below contact.

572-580 cm depth, Soil horizon Bt5
Gravelly sandy clay
Common dessication cracks, extensive multi-generation pedogenic clay coats on pore walls, ped & grain faces. Note deeply weathered sandstone saprorelict near top.

598-606 cm depth, Soil horizon Bt6
Sandy clay
Slightly convoluted layering (relict bedding ?), RF include deeply weathered shale lithorelicts and Mascot-like dolostone.

813-820 cm depth, Soil horizon Bt8
Gravelly clay
Significant RF's that include deeply weathered shale lithorelicts and Mascot-like dolostone, some pores/grains/shale lithorelicts coated w/ kaolinitic cement, ped. clay coats, and thick Fe-oxide coats.

873-880 cm depth, Soil horizon Bt10 + Bt11
Clayey sand
Overall greener, drab coloration of clays, sands are med.-coarse grained, moderately to well-sorted, and well-rounded, sharp contact b/w Bt10 and Bt11 (gravelly clay).

Borehole 5

235-243 cm depth, Soil horizon Bt3 + Cr
Gravelly clay
Heavily mottled with common dissication cracks, Fe-oxide coats, hypocoats and small concretions, sharp contact with basal (fine-med. grained) Mascot Dolostone bedrock with thick multigeneration pedogenic clays directly above.

Mascot Bedrock

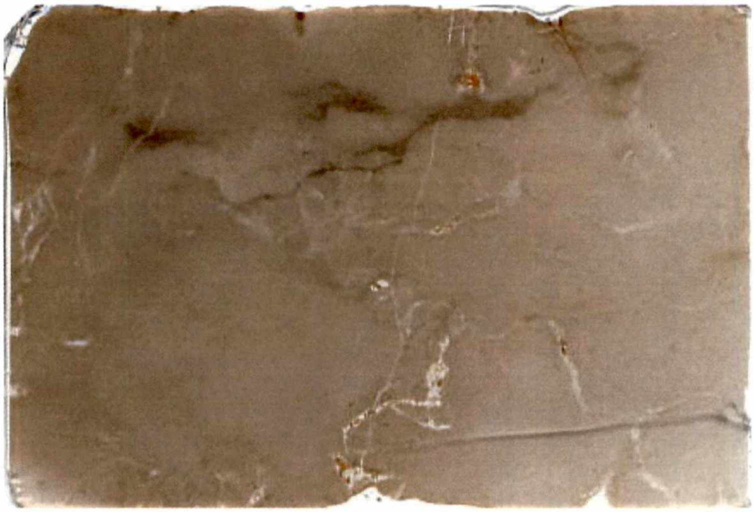

Fine to medium grained dolostone w/ some coarse-grained dolomite spar-filled cements, minor pedogenic clays filling macropores, few Fe-oxide cements along intergranular grain faces and pore walls.

Appendix D: Particle Size Analysis

I.D.	DEPTH (cm)	HORIZON	Ps (g/cm3)	Total Sample Wt. (g)	Sand Fraction Wt. (g)	Silt & Clay Frac. Wt. (g)	Clay % of XDC Solution	Clay % * 0.01
B1-1	10	A	2.67	14.998	5.192	9.806	67.75	0.6775
B1-4	40	Be	2.73	15.006	3.11	11.896	50.35	0.5035
B1-5	58	Sandy Interbed	2.63	15.008	2.92	12.088	64.4	0.644
B1-9	140	Bt_2	2.72	14.992	0.528	14.464	90.3	0.903
B1-17	305	Bt_3	2.78	15.002	0.406	14.596	94.1	0.941
B1-22	407	Bt_4	2.77	15.001	0.205	14.796	81.75	0.8175
B1-28	527	Bt_5	2.74	15	2.016	12.984	83	0.83
B1-31	595	Sandy Interbed	2.56	15.003	8.199	6.804	59.9	0.599
B1-34	655	Bt_6	2.71	14.995	1.562	13.433	89.6	0.896
B1-41	815	Bt_7	2.90	14.996	0.16	14.836	77.6	0.776
B1-50	1050	Bt_8	2.69	15.003	1.045	13.958	68.75	0.6875
B4-1	10	A	2.64	15.005	3.93	11.075	45.7	0.457
B4-3	30	Be	2.91	14.1874	3.27	10.9174	47.5	0.475
B4-5	60	Sandy silt int. w/ Bt_2	2.65	14.993	1.573	13.42	76.5	0.765
B4-11	180	Bt_3	2.72	14.998	0.207	14.791	71.1	0.711
B4-23	425	Bt_4	3.09	14.913	0.671	14.242	73	0.73
B4-27	510	Bt_5	2.67	15.005	0.116	14.889	68.5	0.685
B4-32	610	Bt_6	2.94	12.711	1.922	10.789	68.85	0.6885
B4-36	690	Bt_7	2.75	15.004	0.21	14.794	86	0.86
B4-42	810	Bt_8	3.12	14.948	0.523	14.425	55	0.55
B4-44	850	Bt_9	2.81	15.08	0.209	14.871	74.9	0.749
B4-45	870	Clayey sand	2.74	15.017	5.186	9.831	61	0.61
B4-46	880	Bt_{10}	2.66	14.997	4.454	10.543	44.75	0.4475

after 2mm sieve

Silt Fraction Wt. (g)	Clay Fraction Wt. (g)	Sand Fraction %	Silt Fraction %	Clay Fraction %	Total	Cum Clay	Cum Silt + Clay	Cum Sand + Silt + Clay
3.162435	6.643565	34.62	21.09	44.30	100.00	44.30	65.38	100.00
5.906364	5.989636	20.73	39.36	39.91	100.00	39.91	79.27	100.00
4.303328	7.784672	19.46	28.67	51.87	100.00	51.87	80.54	100.00
1.403008	13.060992	3.52	9.36	87.12	100.00	87.12	96.48	100.00
0.861164	13.734836	2.71	5.74	91.55	100.00	91.55	97.29	100.00
2.70027	12.09573	1.37	18.00	80.63	100.00	80.63	98.63	100.00
2.20728	10.77672	13.44	14.72	71.84	100.00	71.84	86.56	100.00
2.728404	4.075596	54.65	18.19	27.17	100.00	27.17	45.35	100.00
1.397032	12.035968	10.42	9.32	80.27	100.00	80.27	89.58	100.00
3.323264	11.512736	1.07	22.16	76.77	100.00	76.77	98.93	100.00
4.361875	9.596125	6.97	29.07	63.96	100.00	63.96	93.03	100.00
6.013725	5.061275	26.19	40.08	33.73	100.00	33.73	73.81	100.00
5.731635	5.185765	23.05	40.40	36.55	100.00	36.55	76.95	100.00
3.1537	10.2663	10.49	21.03	68.47	100.00	68.47	89.51	100.00
4.274599	10.516401	1.38	28.50	70.12	100.00	70.12	98.62	100.00
3.84534	10.39666	4.50	25.79	69.72	100.00	69.72	95.50	100.00
4.690035	10.198965	0.77	31.26	67.97	100.00	67.97	99.23	100.00
3.3607735	7.4282265	15.12	26.44	58.44	100.00	58.44	84.88	100.00
2.07116	12.72284	1.40	13.80	84.80	100.00	84.80	98.60	100.00
6.49125	7.93375	3.50	43.43	53.08	100.00	53.08	96.50	100.00
3.732621	11.138379	1.39	24.75	73.86	100.00	73.86	98.61	100.00
3.83409	5.99691	34.53	25.53	39.93	100.00	39.93	65.47	100.00
5.8250075	4.7179925	29.70	38.84	31.46	100.00	31.46	70.30	100.00

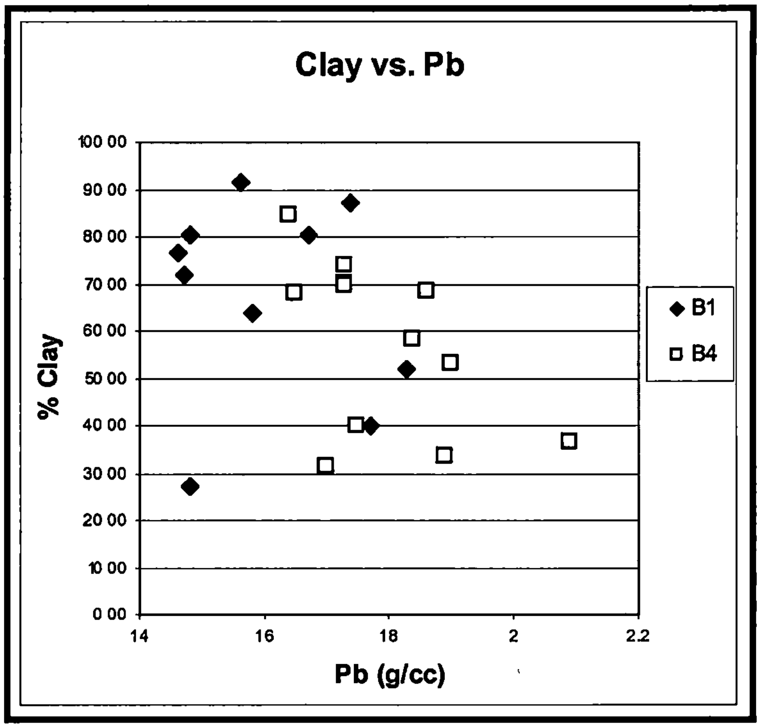

Clay vs. Pb
% Clay
Pb (g/cc)
B1
B4

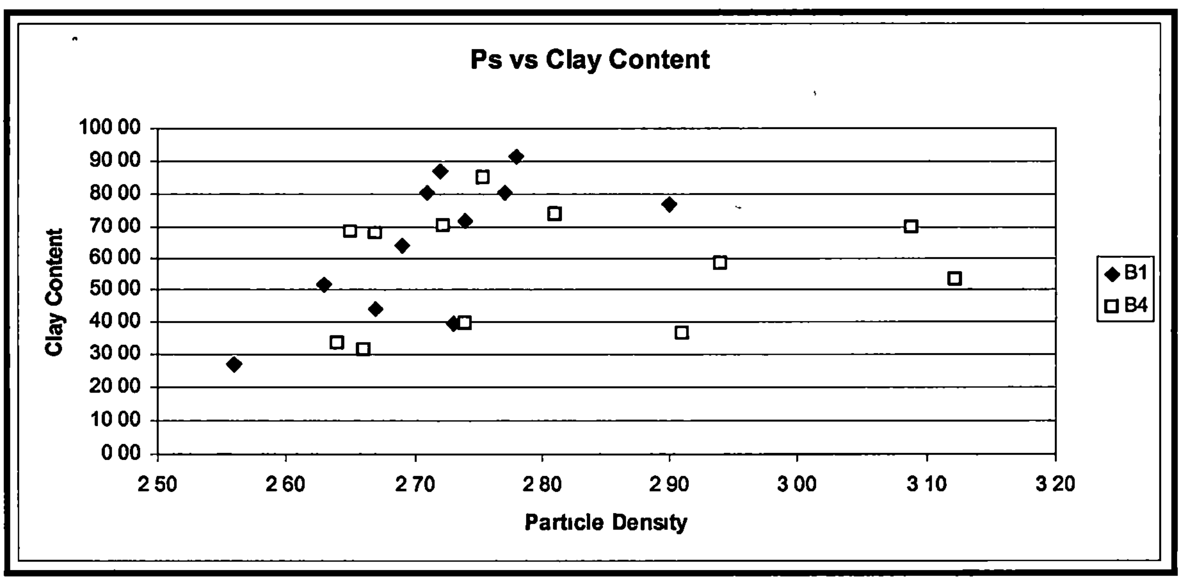

Ps vs Clay Content
Clay Content
Particle Density
B1
B4

Particle Size Analysis Method and Protocol

[Schultz's Handy-Dandy Guide for a Detailed Particle Size Analysis Using an X-Ray Disc Centrifuge (XDC)]

MATERIALS NEEDED (after preparation of samples):

1) Pipette with Tygon tubing attachment
2) Kimwipes for proper disk cleaning and drying (do not use abrasive paper! This will scratch and damage the disk)
3) 2 beakers for flushing/cleaning out disk between sample runs
4) Geiger counter and clip-on dosimeter
5) Zip disk for recording data

PREPARATION OF SAMPLES:

1) Mortar and Pestle sample; weigh total (standard 15 g)
2) Pass through 2 mm sieve; weigh retained material
3) Material passing through:
   -Add chemical dispersant, i.e. Na-hexametaphosphate (0.75 g for 15 g sample) and 150 mL DI water
   -Physical dispersion (Sonification) for 2 ½ min. at 33%
4) Wet sieve using 53 µm and distilled water
5) Oven dry and weigh retained material (sand fraction)
6) Dry sieve sand fractions if desire detailed sand distributions
7) Subsample at least 30 mL of suspension for PSD using BI-XDC
8) Oven dry remainder of suspension for measurement of Particle Density (~10g needed using Pycnometer method)
9) Record Ps

- **Note**- No two samples are the same!!! The XDC requires 25 mL sample solutions at concentrations of 0.5-5.0 % by volume. Samples containing greater Fe, Ti, Mn will require more dilution (~0.5%) than those containing lesser amounts (~5.0%). This is because Fe-enriched soils/samples typically have higher Ps than Fe-poor samples; samples with higher Ps have greater attenuation of the X-rays, thereby requiring lesser concentration levels to achieve an ideal 0.3 Volt separation between the upper and lower baselines measured on the XDC.

RUNNING A SAMPLE ON THE XDC:

1) An ideal protocol for running samples on the XDC involves 2 sets of measurements in X-mode (centrifugal mode):
-Set 1: X-mode running for 5 min. @ 1000 rpm yields range ~ 4.3-0.27 μm
-Set 2: X-mode running for 80 min. @ 7000 rpm yields range ~0.6-0.01 μm

   - Note- this protocol is good for samples having Ps ranging from 2.40-5.00
(Increase in Ps = Increase in Lower Diameter range & Decrease in High Diameter range)

2) Double-click on Brookhaven desktop icon to begin software
3) Power on XDC (switch in back)
4) If first run of day, inject 10 mL of distilled water in disk for Upper Baseline measurement
5) Press "Head" button with left and right arrows to slide X-ray detectors into place
6) Turn on X-ray tube by turning key on panel from "off" to "on" position and let warm up for 30-45 min. (always make sure distilled water is present in disk before powering on X-rays)
7) Press "clear" on the window for the PSD software (this ensures a new sample will be run)
8) Click on "Parameters" and set the appropriate sample I.D., mode, Ps, etc. and click "save"
9) Click "start" to begin measurement
10) A window will pop-up with instructions for loading the sample

   - Click "start" to measure upper baseline (10 mL of distilled water should already be loaded)
   - If multiple samples are to be run in the same day, you can save the upper baseline and load it for the additional samples
   - Click "continue"; a new window appears = remove 10 mL distilled water with pipette and dry disk
   - Next load 25 mL of sample after thoroughly shaking/mixing and press "mix" on the XDC panel
   - After mixing for about a minute, press "start" to begin measurement of lower baseline (Note- there should be roughly 0.3 V difference between the upper and lower baselines)
   - The window will inform you to press "mix" again to stop mixing; as soon as disk stops turning press "start" on either the XDC panel or on the current window to begin measurement

11) When sample measurement is complete, press "motor" to stop disk

12) Press "head" to move X-ray detectors back in to allow for sample removal

- Note- when running a second mode (i.e. 5 min. first, then 80 min. second), do NOT remove sample; Instead, press "clear" on the main software window and update the parameter settings such as run time, RPM, I.D. #, etc.

13) Open door on XDC front panel and remove disk plug; using pipette suck out sample (this "used" sample may be retained for future analyses if desired)
14) Flush out the disk with a series of distilled water blanks and press "mix" on panel; when disk is completely clean, use Kimwipes and dry thoroughly
15) Close door on panel and turn key from "on" to "off" position to power off x-rays
16) Power off instrument (switch in back) and software, and return Geiger counter and dosimeter

<u>MERGING DATA FROM TWO RUNS</u>:

1) On main software window, click "merge" and select the desired files for merging (while holding down the "Ctrl" button, you may select up to two files to merge)
2) A new window will open asking for "auto-merge" or "manual-merge"; I use the auto-merge to combine data from the two runs
3) On main software window, click "file", "database" to view the merged data

<u>EXPORTING DATA TO EXCEL</u>:

1) Clear any present PSD data if you have just finished running a sample
2) On main window, click "file" and then "database"
3) When new window pops up, highlight sample of interest and click "export files" and save file to zip disk or hard drive
4) Open Microsoft Excel
5) Click "open" and select sample file (file saved as .dat)
6) In Text Import Wizard window, select "delimited" and click next; use a comma as the delimiter and click "finish" (data is now delimited and in excel file format)
7) Compare data in excel with data in Brookhaven software to identify any unknown numbers and ensure successful exportation of data

HELPFUL HINTS:

1) The XDC provides a very accurate method for acquiring particle size data. By providing detailed results that include cumulative distribution graphs, one can determine the percentage of clay in the suspension and then back-calculate to attain the overall sand/silt/clay fractions.
2) Although this method works well for my carbonate derived clay-rich samples, there are other protocols to be explored that may be more effective for other soil types. For example, different modes (i.e. gravitational) and combinations of parameters (i.e. RPMs, duration of time interval, etc.) can allow for different ranges of results. You can play around with different parameters and use the "modeling utility" button on the main window to estimate the range of particles sizes to be measured.
3) Do not discard your solutions!!! The solutions can be saved and re-used for later investigations if desired.
4) Although this guide should help first time users, it should be used in conjunction with the owner's manual to ensure that no damage is done to the instrument.
5) If you have any questions feel free to contact author at: bschultz@utk.edu

Appendix E: BULK DENSITY (Pb), PARTICLE DENSITY (Ps) and BULK POROSITY DATA

Bulk density calculated using the wax clod method. Particle density calculated using the pycnometer method.

Equations (Blake and Hartge, 1986):

Bulk Density [Pb] = Ws / ((Wsww - Wbw) - (Wsw – Ws))

Where:

Ws = Weight (g) of oven-dried clod in air
Wsww = Weight (g) of sample + paraffin in water
Wbw = Weight (g) of beaker w/ 550 mL water
Wsw = Weight (g) of sample + paraffin

B1	**Sample + String Wt. (g)**	**Sample + String + Wax Wt. (g)**	**Wt. (g) (In Water)**	**Beaker wt. (g) w/ 550 mL**	**Pb**
B1-4	13 36	16.67	784 56	773.7	1.77
B1-5	45.26	52.27	805.44	773 7	1 83
B1-9	59 82	70 87	819 18	773.7	1 74
B1-17	37.73	47.55	807.69	773.7	1 56
B1-22	19 65	24.37	790.22	773 7	1 67
B1-28	20 86	29.22	796.24	773.7	1 47
B1-31	29 52	36	800.1	773.7	1 48
B1-34	11 45	15.87	785.86	773.7	1 48
B1-41	28 52	34 55	799.33	773.7	1 46
B1-50	16 65	21 93	789 49	773.7	1.58
B4					
B4-1	48 47	53.57	804 43	773.7	1.89
B4-3	30 55	34 66	792 46	773.7	2.09
B4-5	19 91	24.13	788 64	773.7	1 86
B4-11	24.87	31.6	794.84	773.7	1.73
B4-23	34 66	40 16	799.21	773.7	1.73
B4-27	45 64	52 55	808.21	773.7	1.65
B4-32	7.29	9.2	779.57	773.7	1 84
B4-36	41 77	47.72	805.06	773 7	1 64
B4-42	15 08	17 87	784.41	773.7	1.90
B4-44	17 88	21.18	787.35	773.7	1.73
B4-45	21.83	29 96	794.33	773.7	1 75
B4-46	26.02	31.71	794 74	773.7	1.70
M D.	40.49	50 31	797 57	773.7	2.88

Bulk porosity calculated using bulk density (Pb) and particle density (Ps) data, whereby:

100*(1-(Pb/Ps)) = Bulk Porosity

Sample I.D.	Depth (cm)	Pb	Ps	% Clay	Bulk Porosity (%)
B1-4	40	1 77	2 73	40	35
B1-5	58	1.83	2.63	52	30
B1-9	140	1.74	2.72	87	36
B1-17	305	1.56	2.78	92	44
B1-22	407	1.67	2.77	81	40
B1-28	527	1.47	2 74	72	46
B1-31	595	1 48	2.56	27	42
B1-34	655	1.48	2.71	80	45
B1-41	815	1 46	2.90	77	50
B1-50	1050	1.58	2.69	64	41
B4-1	10	1 89	2 64	34	28
B4-3	30	2.09	2 91	37	28
B4-5	60	1.86	2.65	68	30
B4-11	180	1.73	2.72	70	36
B4-23	425	1.73	3.09	70	44
B4-27	510	1.65	2.67	68	38
B4-32	610	1.84	2.94	58	37
B4-36	690	1.64	2.75	85	40
B4-42	810	1.9	3.12	53	39
B4-44	850	1.73	2 81	74	38
B4-45	870	1.75	2.74	40	36
B4-46	880	1 70	2 66	31	36

Appendix F: Raw bulk geochemical data

Geochemical data are expressed as weight % for major elements and oxides and in ppm for trace elements and oxides

Dewey (Ultisol) Strong Farm																							
Sample I D	Horizon	Depth (cm)	Na2O	MgO	Al2O3	SiO2	P2O5	K2O	CaO	TiO2	Cr	MnO	Fe2O3	Co	Ni	Pb	As	Rb	Sr	Zr	Ba	Cu	Total
B1-1	Ap	-10																					
B1-4	Be	-40	0.084	0.325	7.912	82.670	0.109	0.677	0.074	1.294	0.0046	0.479	3.034	0.0006	0.0016	0.0028	0.0015	0.0049	0.0031	0.054	0.0363	0.0014	96.77
B1-5	Bt2	-60	0.054	0.456	11.389	76.985	0.067	0.765	0.056	1.242	0.0058	0.113	4.514	0.0012	0.0024	0.0027	0.0014	0.0064	0.0031	0.0497	0.0297	0.0017	95.75
B1-9	Bt2	-140	0.052	1.041	21.794	57.622	0.073	1.599	0.143	0.790	0.0087	0.033	8.531	0.0026	0.005	0.0032	0.0019	0.00109	0.0025	0.022	0.0247	0.0038	91.75
B1-17	Bt3	-305	0.035	1.051	28.055	47.929	0.103	1.690	0.000	0.766	0.0091	0.051	10.288	0.0033	0.008	0.0043	0.0029	0.00138	0.0022	0.0154	0.0251	0.0049	90.05
B1-22	Bt4	-407	0.042	1.107	24.567	54.234	0.100	1.951	0.000	0.763	0.0085	0.049	8.600	0.0027	0.0061	0.0035	0.0023	0.00121	0.0021	0.0145	0.0269	0.0043	91.49
B1-28	Bt5	527	0.041	1.013	23.161	52.160	0.137	1.863	0.003	0.726	0.0074	0.582	10.735	0.0032	0.0104	0.0054	0.0041	0.0012	0.0023	0.0132	0.0284	0.0049	90.50
B1-31	? vfs	-595	0.827	0.536	20.315	63.225	0.092	0.816	0.375	0.447	0.0044	0.141	6.766	0.0017	0.0035	0.0025	0.0012	0.0048	0.0032	0.0101	0.0227	0.0035	93.60
B1-34	Bt6	-655	0.038	0.734	20.690	61.046	0.108	1.173	0.003	0.538	0.0052	0.440	7.839	0.0024	0.015	0.0034	0.0021	0.0093	0.0021	0.0104	0.0243	0.0038	92.69
B1-41	Bt7	-815	0.047	0.939	23.389	54.279	0.130	3.344	0.036	0.820	0.0079	0.294	8.465	0.0026	0.0074	0.0041	0.0028	0.00113	0.0033	0.0154	0.0313	0.0042	91.82
B1-50	Bt8	-1050	0.072	2.079	17.578	53.890	0.125	6.245	2.269	0.643	0.0062	0.278	7.689	0.0023	0.0067	0.0038	0.0025	0.0097	0.0031	0.0125	0.0308	0.0035	90.95
B4-1	Ae	-10	0.065	0.334	6.664	84.698	0.099	0.649	0.236	0.903	0.0047	0.151	2.822	0.0006	0.0015	0.0023	0.0009	0.0041	0.0029	0.0423	0.0282	0.0011	96.71
B4-3	Be	-30	0.062	0.395	7.816	83.226	0.057	0.682	0.068	0.987	0.0049	0.055	3.317	0.0009	0.0015	0.0022	0.0009	0.0052	0.0029	0.0435	0.0279	0.0012	96.76
B4-5	Bt1	-60	0.041	0.895	17.823	64.742	0.062	1.313	0.037	1.016	0.0075	0.017	6.292	0.0019	0.0031	0.0023	0.0009	0.00108	0.0025	0.0356	0.0259	0.0021	92.32
B4-11	Bt3	-180	0.046	1.618	26.297	50.600	0.078	2.709	0.000	0.852	0.00101	0.027	8.821	0.0028	0.0046	0.0023	0.0009	0.0016	0.0022	0.0182	0.0263	0.0031	91.11
B4-23	Bt4	-425	0.038	1.273	23.094	56.625	0.082	2.046	0.000	0.750	0.0081	0.034	7.548	0.0023	0.0051	0.0026	0.0012	0.00111	0.0018	0.0197	0.024	0.004	91.56
B4-27	Bt5	-510	0.051	2.002	25.890	55.421	0.061	3.887	0.000	0.865	0.0098	0.058	4.613	0.0013	0.0033	0.0023	0.0009	0.00136	0.0017	0.0212	0.0259	0.003	92.92
B4-32	Bt7	-610	0.052	1.006	14.686	69.353	0.071	2.098	0.000	0.582	0.0055	0.050	4.347	0.0012	0.0024	0.0021	0.0007	0.0076	0.0024	0.0268	0.0277	0.0025	92.33
B4-36	Bt8	-690	0.039	1.142	25.365	53.277	0.100	2.156	0.000	0.773	0.0075	0.196	7.904	0.0025	0.0076	0.0028	0.0014	0.00131	0.0027	0.016	0.0289	0.0032	91.03
B4-42	Bt9	-810	0.056	0.976	12.138	72.148	0.092	6.295	0.000	0.447	0.0041	0.275	4.843	0.0014	0.0033	0.0015	0	0.0098	0.0024	0.0072	0.0279	0.001	97.33
B4-44	Bt10	-850	0.056	1.064	17.852	62.975	0.108	4.970	0.126	0.532	0.0057	0.112	5.807	0.0018	0.0054	0.002	0.0006	0.00119	0.0029	0.0134	0.0293	0.0027	93.67
B4-45	? med s	-870	0.063	1.363	11.812	74.568	0.083	5.513	0.000	0.368	0.0034	0.045	2.867	0.0007	0.0036	0.0015	0.0001	0.00101	0.0029	0.0156	0.0296	0.0021	96.74
B4-46	Bt11	-880	0.134	7.618	6.886	52.217	0.115	4.354	11.628	0.321	0.0027	0.149	2.404	0.0006	0.0075	0.0015	0	0.0071	0.0054	0.0116	0.0277	0.0014	85.89
M D -1	-1100	-890	0.027	0.116	0.910	100.336	0.033	0.482	0.022	0.044	0	0.000	0.000	0	0	0.0012	0	0.005	0.0016	0.0012	0.0155	0	101.99
M D -2	-1100	-890	0.043	0.142	1.670	97.314	0.037	0.961	0.022	0.084	0	0.000	0.000	0	0	0.0012	0	0.001	0.0017	0.0022	0.0171	0.0008	100.30
M D -3	-1100	-890	0.215	16.846	0.389	15.977	0.039	0.237	26.186	0.026	0	0.020	0.381	0	0.001	0.0012	0	0.003	0.0067	0.0005	0.0144	0.0002	60.34
N D S	-1100	-1100	0.206	16.367	2.338	14.784	0.048	0.682	26.548	0.119	0.003	0.005	1.066	0.001	0.0017	0.0012	0	0.0023	0.00107	0.0027	0.0161	0.0007	62.19

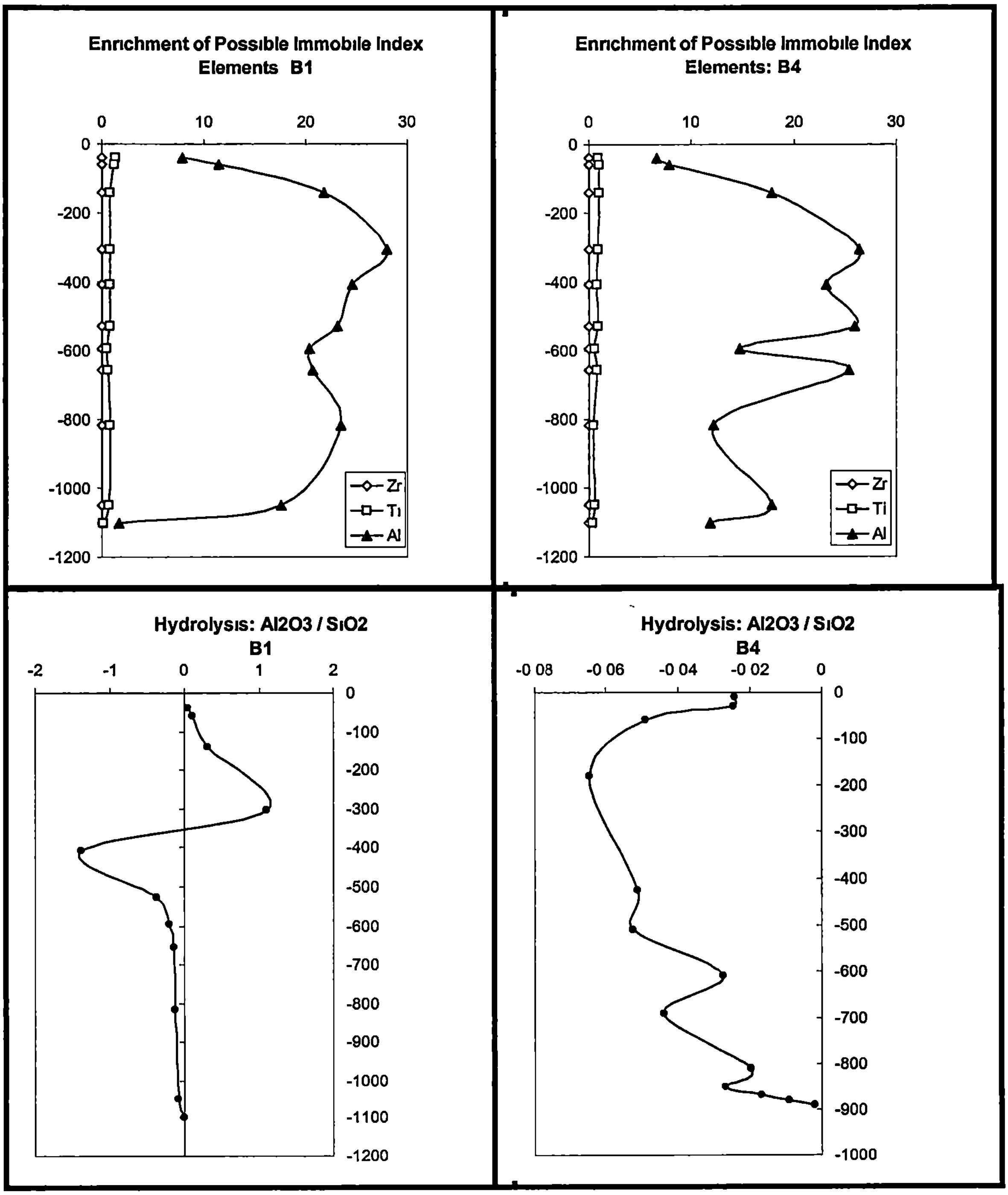
Enrichment of Possible Immobile Index Elements B1
Enrichment of Possible Immobile Index Elements: B4
0 10 20 30
0 -200 -400 -600 -800 -1000 -1200
Zr
Ti
Al
Hydrolysis: Al2O3 / SiO2 B1
-2 -1 0 1 2
0 -100 -200 -300 -400 -500 -600 -700 -800 -900 -1000 -1100 -1200
Hydrolysis: Al2O3 / SiO2 B4
-0 08 -0 06 -0 04 -0 02 0
0 -100 -200 -300 -400 -500 -600 -700 -800 -900 -1000

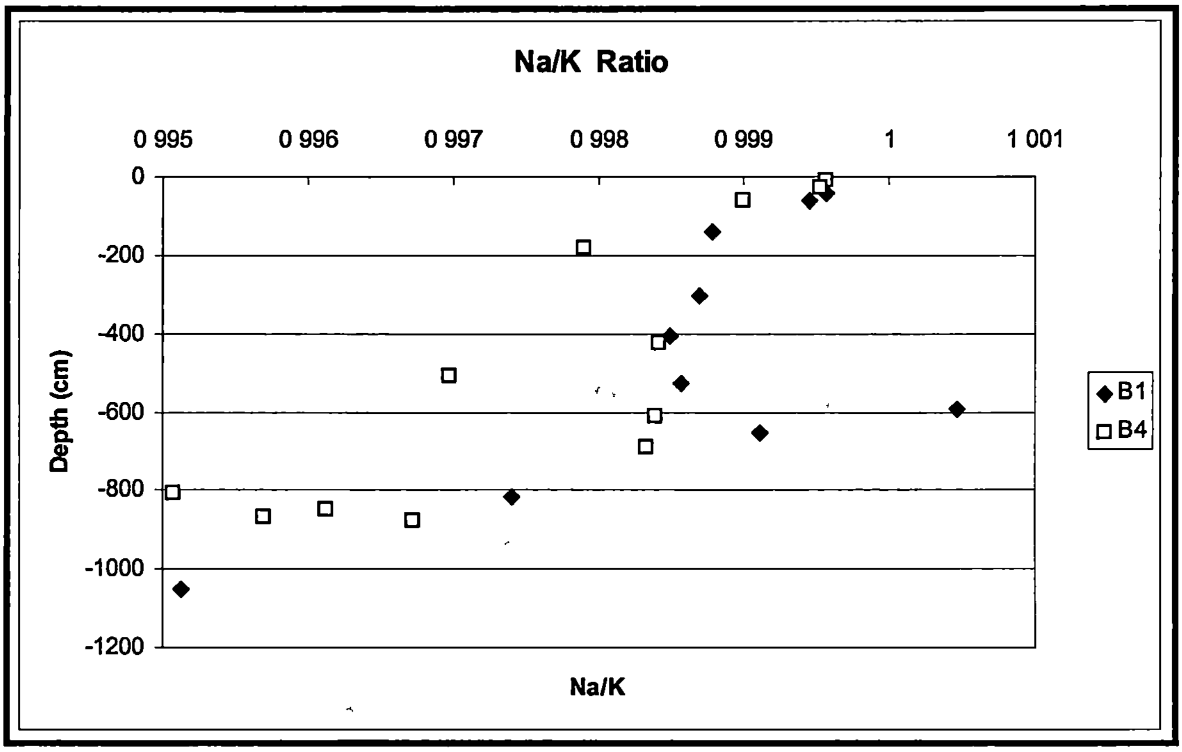
Na/K Ratio
0 995
0 996
0 997
0 998
0 999
1
1 001
0
-200
-400
-600
-800
-1000
-1200
Depth (cm)
Na/K
B1
B4

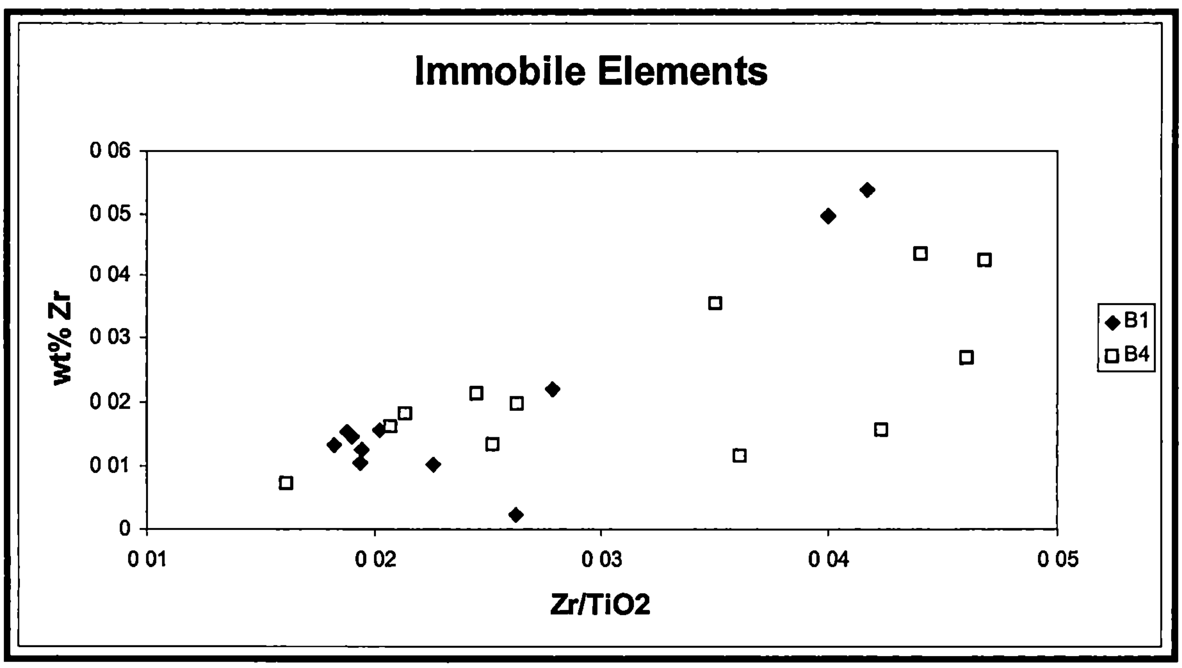
Immobile Elements
0 06
0 05
0 04
0 03
0 02
0 01
0
wt% Zr
0 01
0 02
0 03
0 04
0 05
Zr/TiO2
B1
B4

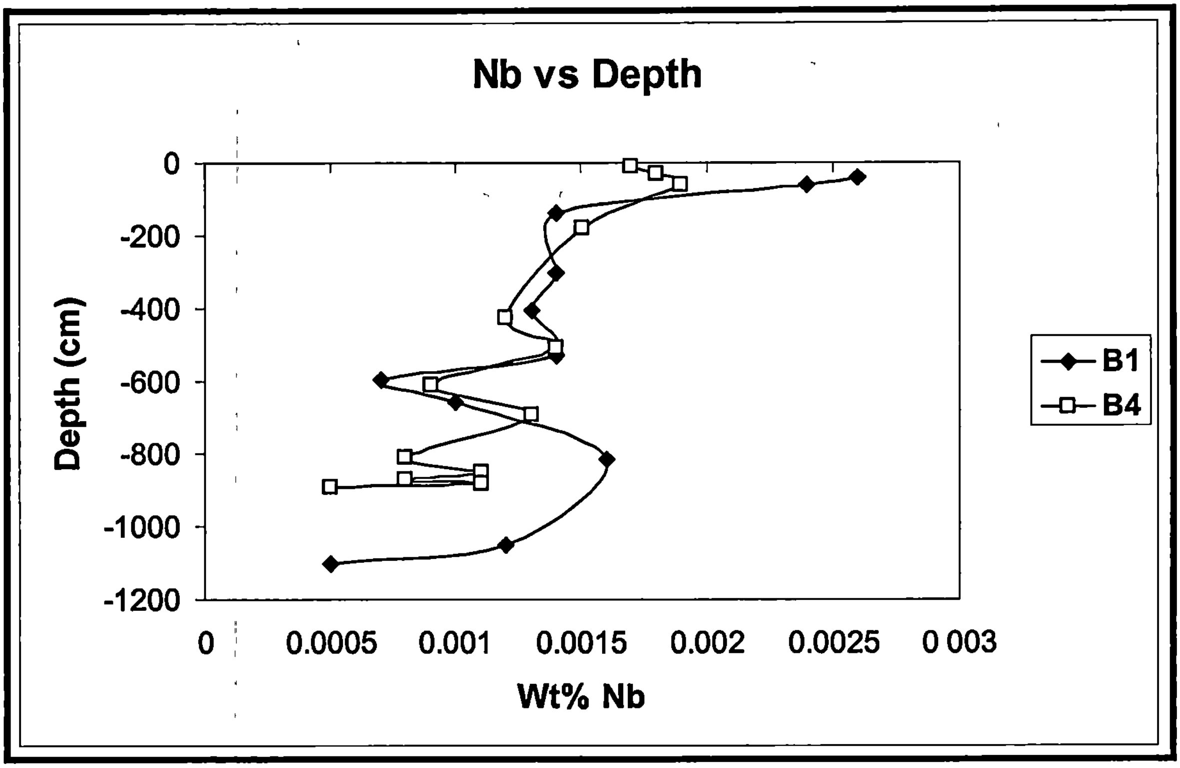
Nb vs Depth
0
-200
-400
-600
-800
-1000
-1200
Depth (cm)
0
0.0005
0.001
0.0015
0.002
0.0025
0 003
Wt% Nb
B1
B4

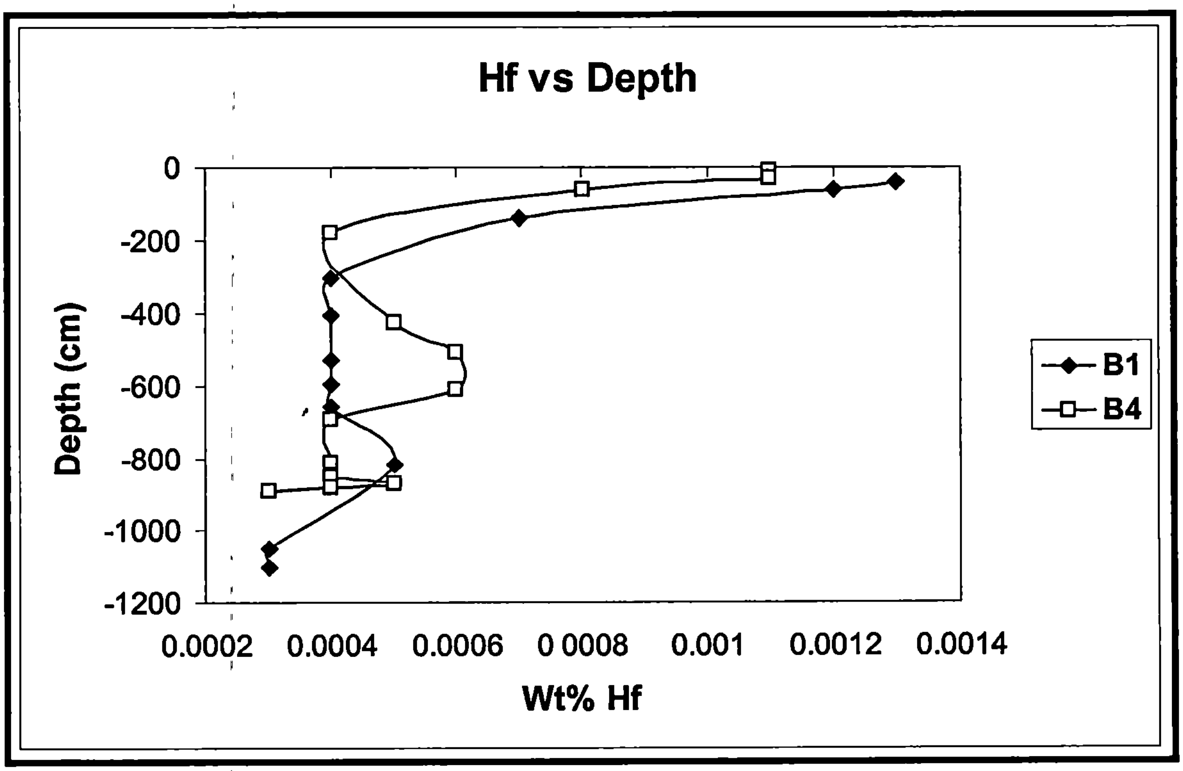
Hf vs Depth
0
-200
-400
-600
-800
-1000
-1200
Depth (cm)
0.0002
0.0004
0.0006
0 0008
0.001
0.0012
0.0014
Wt% Hf
B1
B4

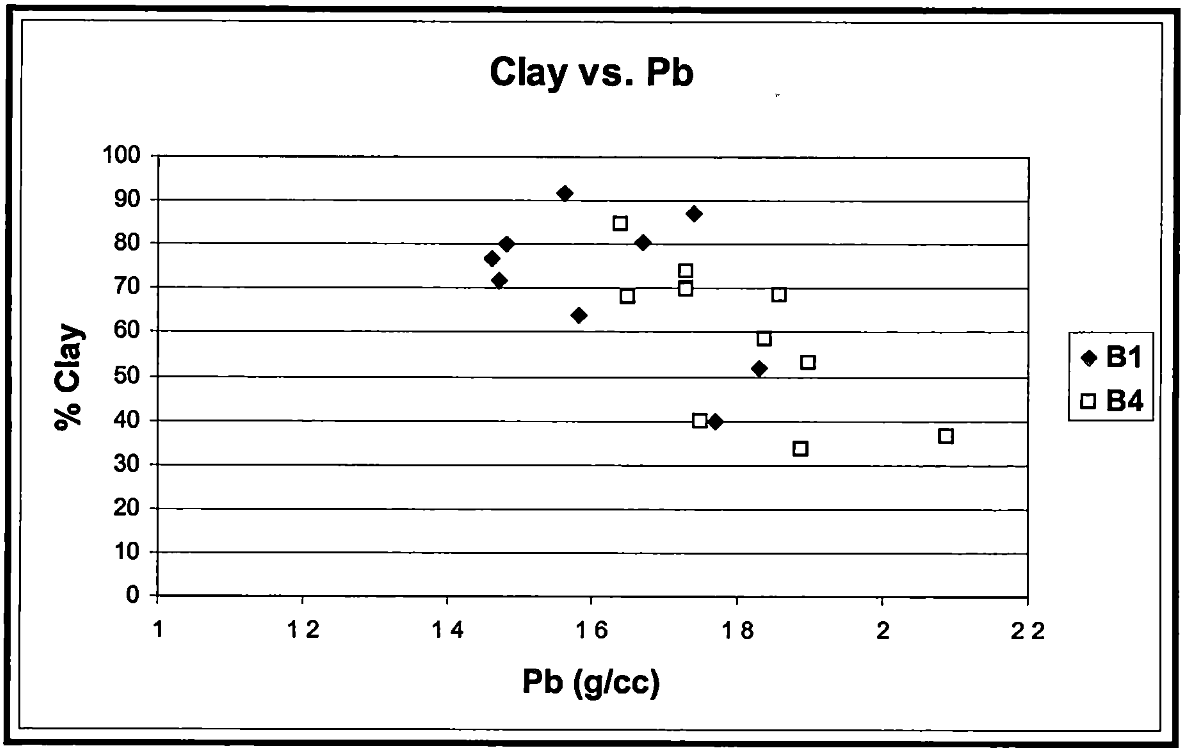

Clay vs. Pb
100
90
80
70
60
50
40
30
20
10
0
% Clay
1
1 2
1 4
1 6
1 8
2
2 2
Pb (g/cc)
B1
B4

Appendix G: Raw clay mineralogical data

University of Tennessee

Terra Rosa Soil Samples
Estimated mineralogical composition

Sample I.D.	Depth (cm)	Size (mm)	Hydroxy-Smectite %	Smectite %	Illite %	Chlorite %	Kaolinite %
B4	30	2-0.5	12	0	20	10	15
B4	30	0.5-0.1	9	0	20	12	35
B4	30	<0.1	14	0	15	10	45
B1	305	2-0.5	0	0	40	0	12
B1	305	0.5-0.1	3	0	20	0	66
B1	305	<0.1	4	0	20	0	50
B4	610	2-0.5	3	0	35	1	12
B4	610	0.5-0.1	3	0	45	3	25
B4	610	<0.1	4	0	45	0	20
B4	810	2-0.5	2	0	55	0	0
B4	810	0.5-0.1	1	0	68	0	12
B4	810	<0.1	1	0	78	0	10
B1	1050	2-0.5	2	0	40	0	17
B1	1050	0.5-0 1	5	0	30	2	47
B1	1050	<0.1	2	0	25	2	55

Halloysite %	K/S %	Quartz %	K-feldspar %	Anatase %	Goethite %	Total %
0	0	35	2	3	3	100
5	0	8	0	1	10	100
5	0	1	0	0	10	100
3.5	0	38	0.5	2	4	100
3	0	1	0	0	7	100
10	0	1	0	0	15	100
8	?	34.5	0 5	1	5	100
10	?	8	0	1	5	100
15	5	1	0	0	10	100
0	0	34	2	2	5	100
3	0	10	0	1	5	100
3	0	1	0	0	7	100
5	0	25	3	1	7	100
5	0	4	0	0	7	100
5	0	1	0	0	10	100

Appendix H: Borehole Drilling Notes

Strong Farm Core Log
Logged by: Bryan Schultz
Date: 7/18/03
Drilling began at 9:00am and finished at 6:45pm

Borehole #	Depth (ft)	Recovery (in / %)	Description / Comments
1	0-4'	43"/90%	
1	4-8'	45"/94%	
1	8-12'	44"/100%	greater difficulty penetrating
1	12-15'	48"/133%	>100% recovery (clay swelling)
1	15-19'	48"/100%	
1	19-23'	45"/94%	
1	23-27'	48"/100%	
1	28-32'	31"/65%	< 100% recovery (compaction)
1	32-36'	17"/35%	<< 100% recovery
1	36-38.8'	15"/45%	< 100% recovery; refusal at 38.8'
2	0-4'	35"/73%	< 100% recovery
2	4-8'	48"/100%	
2	8-12'	47"/98%	
2	12-13.7'	47"/230%	refusal at 13.7'
3	0-4'	42.5"/89%	
3	4-8'	48"/100%	
3	8-10.4'	48"/163%	>>100% recovery (sig. swelling)
3	10.4-12.5'	48"/185%	drillers claim refusal @ 12.5' but I encouraged them to continue
3	12.5'-14.5'	48"/200%	>>100%
3	14.5-18.5'	48"/100%	
3	18.5-18.7'	5"/208%	drillers claim refusal at 18.7'
4	0-4'	37"/77%	<100% recovery (compaction)
4	4-7'	48"/133%	>100% recovery (swelling)
4	7-10'	48"/133%	>100% recovery
4	10-13.4'	48"/118%	>100% recovery
4	13.4-16.6'	48"/125%	>100% recovery
4	16.6-20'	47"/118%	mild swelling
4	20-24'	48"/100%	
4	24-25.4'	23"/136%	refusal at 25.4'

Borehole #	Depth (ft)	Recovery (in)	Description / Comments
5	0-4’	35”/73%	<100% recovery (compaction)
5	4-8’	38”/79%	<100% recovery
5	8-12’	23”/48%	<<100% recovery
5	12-16’	27”/56%	<<100% recovery
5	16-19.5’	22”/52%	<<100% recovery; refusal @ 19.5’
7	0-4’	23”/48%	<<100% recovery
7	4-8’	47”/98%	
7	8-12’	48”/100%	
7	12-16’	48”/100%	
7	16-20’	48”/100%	
7	20-22’	48”/200%	>>100% recovery (sig. swelling)

Summary of core samples and their respective recoveries >100%

Borehole	# of Core Samples	# >100% Recovery
1	10	1
2	4	1
3	7	4
4	8	6
5	5	0
7	6	0

Appendix I: Pedological Terminology

Because this research overlaps both geology and soil science (each with different approaches concerning classification systems), this section is included to define and clarify some of the terminology used herein this thesis. Definitions of terminology are supplemented from:
Becker, 1895
Fanning and Fanning, 1989
Fitzpatrick, 1993
Soil Survey Staff, 1994
Buol et al., 1997
Driese et al., 2001

Saprolite = rotten, friable, isovolumetrically weathered bedrock, having characteristics of both soil and rock. Saprolite has been found to retain original structure and sedimentary layering, while also containing soil features such as high matrix porosity, translocation or illuviation of clays, precipitation of Fe/Mn oxides, and bioturbation

Residuum = unconsolidated and weathered mineral materials accumulated by disintegration of consolidated rock in place

Regolith = the unconsolidated mantle of weathered rock, soil and superficial deposits overlying solid rock

Soil = 1) the natural space-time continuum occurring at the surface of the earth and supporting plant life; 2) collection of natural bodies on the earth's surface containing living matter and supporting or capable of supporting plants out-of-doors. Its upper limit is air or shallow water. Its lower limit is usually hard rock or earthy materials devoid of roots, animals, or marks of biologic activity. Horizonation in soils that differ from the underlying rock material, result from the interaction of time, climate, biology, parent materials, and relief.

Colluvium = relocated soil materials with or without rock fragments that accumulate at the base of slopes by gravitational action

Alluvium = sediment deposited by streams and sometimes varying widely in particle size

VITA

Bryan Scott Schultz was born on October 19, 1978 and raised in Buford Georgia, were he spent most of his life. At an early age, curiosity in the geosciences were sparked by observations of highly deformed metamorphic rocks of the Piedmont physiographic province, and in particular, the bizarre looking rocks of the Brevard Fault Zone (that later became known in proper terms as "mylonites") that literally cropped out in his back yard. After graduating from Buford High School in 1997, Bryan attended Georgia Perimeter College after being awarded a scholarship to play baseball. After one year at G.P.C., he transferred to Gainesville College and declared geology as a major. In December of 1999, Bryan obtained an Associate of Science at G.C. and transferred once again to the State University of West Georgia in Carrollton, GA. While majoring in geology at S.U.W.G. many independent research opportunities were made possible, which included hydrological, coastal sedimentological, satellite imagery processing, and geochemical projects. These projects served to provide experience in various sub-fields of geology, which in turn continued to generate interest in science. After receiving a BS in Geology at S.U.W.G. in 2002, Bryan continued in academia by attending graduate school at the University of Tennessee in August of 2002.

Bryan is a member of the Geological Society of America, National Groundwater Association, and the American Association of Petroleum Geologists. He continues to have an interest in multi-discipline geoscience and plans to pursue employment as a hydrogeologist in Asheville, N.C.